

# The Development of RAPTA Compounds for the Treatment of Tumors

Benjamin S. Murray,<sup>‡</sup> Maria V. Babak,<sup>#</sup> Christian G. Hartinger,<sup>#</sup> Paul J. Dyson<sup>†</sup>

<sup>‡</sup> Department of Chemistry, University of Hull, Cottingham Road, Hull, HU6 7RX, UK.

<sup>#</sup> School of Chemical Sciences, University of Auckland, Private Bag 92019, Auckland 1142, New Zealand.

<sup>†</sup> Institut des Sciences et Ingénierie Chimiques, Ecole Polytechnique Fédérale de Lausanne (EPFL), CH-1015 Lausanne, Switzerland.

## Table of Contents

1. Introduction
2. The basic RAPTA structure: prototypical RAPTA compounds
3. Anticancer Activity of RAPTA compounds
  - 3.1. Activity in cell lines and in *in vivo* models
  - 3.2. Antimetastatic activity
4. Structure-activity relationships
  - 4.1 Systematic modulation and development of the RAPTA structure
  - 4.2. Development of RAPTA compounds for conjugation and macromolecular RAPTA conjugates
  - 4.3. Modulation of the labile chlorido ligands of the RAPTA structure with chelating ligands.

- 4.4. Introduction of additional phosphine ligands into the RAPTA framework
- 4.5. RAPTA-type compounds with  $\eta^5$ -coordinated cyclopentadienyl rings
- 5. Mechanistic studies
  - 5.1. Plasma protein interaction of RAPTA compounds
  - 5.2. Subcellular localization
  - 5.3. Reactions with potential intracellular targets
    - 5.3.1. DNA as a suggested target
    - 5.3.2. RAPTA and protein interactions
      - 5.3.2.1. Interaction with model proteins
      - 5.3.2.2. Histone proteins as targets and target identification from cell extracts
- 6. Concluding remarks
- 7. Acknowledgements
- 8. References

## **Abstract**

Ruthenium(II)-arene RAPTA-type compounds have been extensively explored for their medicinal properties. Herein a comprehensive review of this class of compounds is provided. A discussion of the basic RAPTA structure is given together with the ways it has been modified to elucidate the key role of each part and to afford targeted derivatives. The various mechanistic studies conducted on RAPTA compounds are described and these are linked to the observed macroscopic biological properties. Ultimately, the review shows that certain RAPTA compounds display quite unique properties that point towards a clinical investigation.

## Keywords

RAPTA, bioorganometallic chemistry, cancer, metastasis, angiogenesis

## Abbreviations

[9]aneS<sub>3</sub>, 1,4,7-trithiacyclononane ligand; acac, acetylacetonate; apo-Tf, apo-transferrin; BCN, bicyclo[6.1.0]non-4-yn-9-ylmethanol; BRCA1, human breast cancer suppressor gene 1; CAM, chicken chorioallantoic membrane; carbo-RAPTA, [Ru( $\eta^6$ -*p*-cymene)(C<sub>6</sub>H<sub>6</sub>O<sub>4</sub>)(PTA)]; CEMA, 2-chloroethyl methacrylate; CORM, carbon monoxide releasing molecule; CP, conjugated peptide; ct-DNA, calf thymus DNA; CZE, capillary zone electrophoresis; cod, 1,5-cyclooctadiene; cyt, cytochrome-c; DAPTA, 3,7-diacetyl-1,3,7-triaza-5-phosphabicyclo[3.3.1]nonane; DFT, density functional theory; dGMP, 2'-deoxyguanosine 5'-monophosphate; DLS, dynamic light scattering; DNA, 2'-deoxynucleic acid; donq, 5,8-dioxido-1,4-naphthoquinonato; en, ethylenediamine; ESI-MS, electrospray ionization mass spectrometry; EtG, 9-ethylguanine; EPR, enhanced permeability and retention; FDA, Food and Drug Administration; GSH, glutathione; GST, glutathione S-transferase; hmb, hexamethylbenzene; hA<sub>3</sub>AR, human A<sub>3</sub> adenosine receptor; HSA, human serum albumin; IC<sub>50</sub>, half maximal inhibitory concentration; ICP, inductively coupled plasma; KP1019, indazolium *trans*-[tetrachloridobis(1*H*-indazole)ruthenate(III)]; LA-ICP-MS, laser ablation inductively coupled mass spectrometry; log P<sub>ow</sub>, octanol-water partition coefficient; MALDI-TOF, matrix-assisted laser desorption/ionization time-of-flight; mPTA, *N*-methyl-1,3,5-triaza-7-phosphaadamantane; MS, mass spectrometry; mTPPMS, (*m*-sulfonatophenyl)diphenylphosphine; MudPIT, multidimensional protein

identification technology; NAMI-A, imidazolium *trans*-[tetrachlorido(1*H*-imidazole)(*S*-dimethyl sulfoxide)ruthenate(III)]; NCP, nucleosome core particle; nESI-FT-ICR, nanoelectrospray ionization Fourier transform ion cyclotron resonance; NKP1339, sodium *trans*-[tetrachloridobis(1*H*-imidazole)ruthenate(III)]; NMR, nuclear magnetic resonance; OTf, trifluoromethanesulfonate; oxali-RAPTA, [Ru( $\eta^6$ -*p*-cymene)(C<sub>2</sub>O<sub>4</sub>)(PTA)]; PARPs, poly(adenosine diphosphate (ADP)-ribose) polymerases; pHEA, poly(2-hydroxyethyl acrylate); P(HPMA-CEMA), *N*-(2-hydroxypropyl)methacrylamide/2-chloroethyl methacrylate; PLA, polylactide; PTA, 1,3,7-triaza-5-phosphabicyclo[3.3.1]nonane; PTN, 3,7-dimethyl-7-phospha-1,3,5-triazabicyclo[3.3.1]nonane; QM/MM, quantum mechanics/molecular mechanics; RAED, [Ru( $\eta^6$ -arene)(en)Cl]<sup>+</sup>; RAFT, reversible addition-fragmentation chain-transfer; RAPTA, [Ru( $\eta^6$ -arene)(PTA)X<sub>2</sub>]; RAPTA-B, [Ru( $\eta^6$ -benzene)Cl<sub>2</sub>(PTA)]; RAPTA-C, [Ru( $\eta^6$ -*p*-cymene)Cl<sub>2</sub>(PTA)]; RAPTA-Im, [Ru( $\eta^6$ -1,2-dimethyl-3-(4-methylphenethyl)-1*H*-3 $\lambda^4$ -imidazole)Cl<sub>2</sub>(PTA)][BF<sub>4</sub>]; RAPTA-T, [Ru( $\eta^6$ -toluene)Cl<sub>2</sub>(PTA)]; rHSA, recombinant human serum albumin; scDNA, supercoiled DNA; ssDNA, single-stranded DNA; tpt = 2,4,6-tri-(pyridin-4-yl)-1,3,5-triazine; ub, ubiquitin; VEGFR, vascular endothelial growth factor receptor;

## 1. Introduction

Platinum-based drugs comprise some of the most important chemotherapeutics in cancer treatments. The prototype, cisplatin, was approved by the FDA in 1978 and is now widely used to treat testicular, bladder and ovarian cancers [1]. Despite the success of cisplatin in the clinic it is not without serious problems, including severe side-effects such as nephrotoxicity, ototoxicity and neurotoxicity and problems associated with intrinsic or acquired tumor resistance [2].

Efforts to circumvent/mitigate these toxicity and resistance issues led to the development of several approved cisplatin analogues, including carboplatin and oxaliplatin, that exhibit lower toxicity and a wider spectrum of activity compared to cisplatin. A macromolecular formulation of cisplatin, termed lipoplatin, that appears to selectively accumulate in the tumor environment [3] is also progressing through clinical trials and could lead to more selective treatments with reduced side-effects [4]. Many other types of macromolecular systems are also under development [5]. However, there is still room for further improvements and an increased understanding of the mechanism of action of cisplatin, including resistance mechanisms, continues to spur research in this field [6].

The search for more efficacious and less toxic anticancer drugs has also embraced non-platinum compounds. Among many other metals, the ruthenium-based anticancer agents show considerable promise [7, 8]. The two lead ruthenium compounds are NAMI-A (imidazolium *trans*-[tetrachlorido(1*H*-imidazole)(*S*-dimethyl sulfoxide)ruthenate(III)]) and KP1019 (indazolium *trans*-[tetrachloridobis(1*H*-indazole)ruthenate(III)]) (also studied as its more water soluble sodium salt NKP1339), which have been evaluated in clinical trials. NAMI-A is active against solid metastatic tumors and shows a remarkable degree of selectivity [9]. A phase I clinical study performed with NAMI-A reported disease stabilization in a non-small cell lung carcinoma patient but also revealed dose-limiting toxicity in the form of blistering [10]. A phase I/II trial combining NAMI-A with gemcitabine for the treatment of non-small cell lung cancer was recently undertaken with the results showing that the combination is less active than gemcitabine treatment alone [11]. However, at low NAMI-A doses the combination treatment appears to be very promising, which conflicts with usual clinical practices to administer the maximum tolerated doses. In contrast to the

selective antimetastatic activity of NAMI-A, the structurally similar *trans*-[tetrachloridobis(1*H*-indazole)ruthenate(III)] complex exhibits particularly good activity in preclinical studies on the autochthonous colorectal tumor model of the rat in the absence of severe side effects. Phase I clinical studies with KP1019 and NKP1339 revealed promising anticancer activity accompanied by only modest side-effects [12, 13]. Despite the differences in their antitumor activities a common feature of these Ru(III) coordination compounds is believed to be that they are activated by reduction to more active Ru(II) species in the low oxygen environment of solid tumors. Additionally, there is also evidence to suggest that these compounds may be (selectively) delivered to tumors by protein-mediated pathways [14, 15].

More recently, the development of organometallic ruthenium(II)-arene compounds, stabilized in the +2 oxidation state by the  $\eta^6$ -coordinated arene ligand, have introduced a completely different metallodrug scaffold to that of the coordination compounds that have entered clinical studies. Of these ruthenium(II)-arene compounds two sub-families of compounds have been studied in detail; the RAPTA family ( $[\text{Ru}(\eta^6\text{-arene})(\text{PTA})\text{X}_2]$ , PTA = 1,3,5-triaza-7-phosphaadamantane; Figure 1), which are the focus of this review, and the  $[\text{Ru}(\eta^6\text{-arene})(\text{en})\text{Cl}]^+$  (en = ethylenediamine, RAED) family of compounds (Figure 1) [16]. The RAED series of compounds, which were first reported in 2001 [17], are able to coordinate to DNA through the N7 of guanine residues and, when bearing an extended arene ligand such as biphenyl, dihydroanthracene, and tetrahydroanthracene, may concomitantly intercalate DNA. These compounds are cytotoxic to a range of cancer cell lines [16], including cisplatin-resistant strains, and an *in vivo* study [18] established that  $[\text{Ru}(\eta^6\text{-biphenyl})(\text{en})\text{Cl}]^+$  possesses activity against the MCa mammary carcinoma, reducing both the growth of the primary tumor and the development and growth of lung metastases.

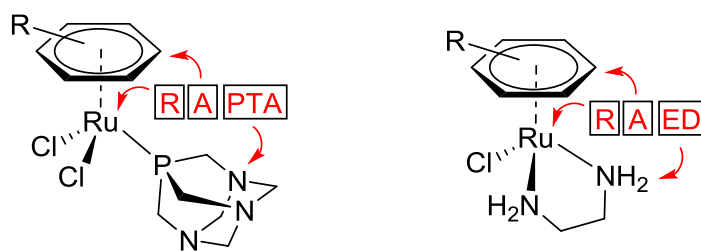


Figure 1. Generic structures of RAPTA and RAED anticancer agents.

In addition, a myriad of structurally related organometallic Ru(II) compounds have been prepared and their cytotoxicity to cancer cells examined [19-24]. The wealth of organometallic ruthenium structures devised to date has been surveyed in several excellent reviews where further insights into this field may be found [24-28].

This review focuses on compounds featuring the RAPTA core structure that have been evaluated for biological activity relevant to antitumor activity. The development of the prototypical RAPTA structure (Figure 1) is reviewed, charting the modulation of the individual structural elements (examples are shown in Figure 2) and relating these changes to biological activity, through to the development of more complex RAPTA compounds bearing biologically active ligands and those conjugated to macromolecular carriers. Closely related RAPTA-type compounds are also described including the rapidly evolving ruthenium cyclopentadienyl family of complexes and compounds bearing other face-capping groups and phosphine ligands derived from PTA. In addition, the wealth of bioanalytical, biochemical and biophysical studies performed to uncover and explain the biological activities of the RAPTA compounds are discussed together with all the pre-clinical data currently available.

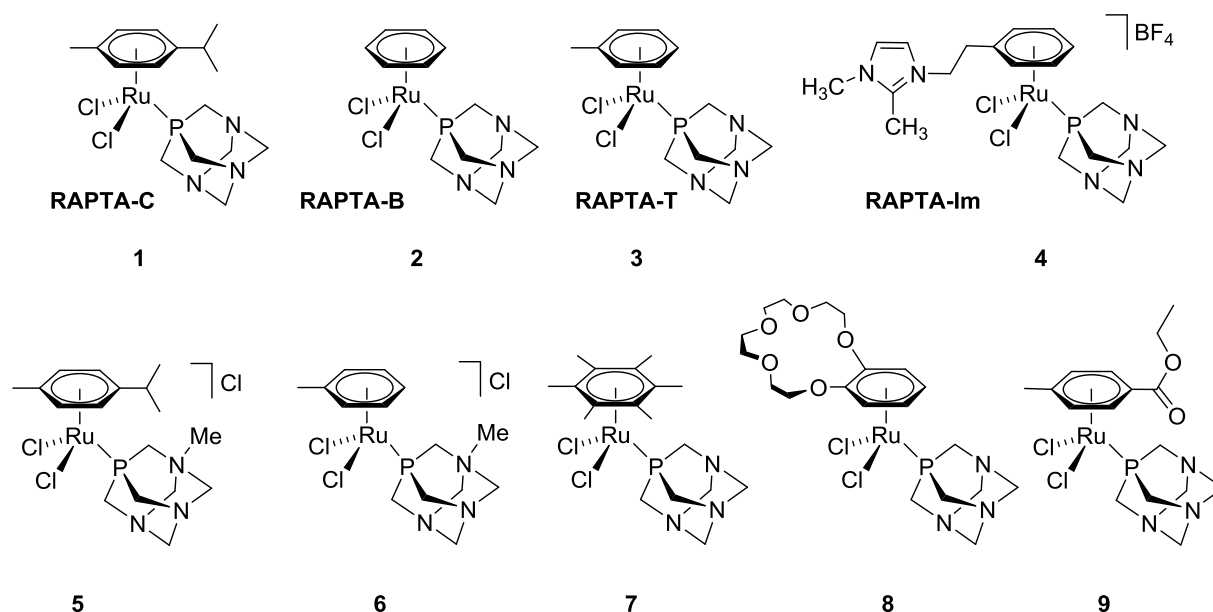


Figure 2. Examples of some early RAPTA compounds [29, 30].

## 2. The basic RAPTA structure: prototypical RAPTA compounds

The RAPTA compounds are characterized by their piano-stool structure (Figure 1) where three of the ruthenium coordination sites are occupied by a  $\eta^6$ -coordinated arene ligand which serves to stabilize the Ru(II) oxidation state. A further coordination site is occupied by the amphiphilic PTA ligand to leave two remaining coordination sites that are usually occupied by relatively labile chlorido ligands. The monodentate PTA ligand may be seen as the distinguishing feature of the RAPTA structure that differentiates this family of complexes from other ruthenium(II)-arene complexes evaluated for their anticancer activity. PTA is a sterically undemanding ligand relative to other phosphines (cone angle of  $103^\circ$ ) [31] and may confer a degree of water solubility to the RAPTA complexes depending on the nature of the co-ligands.

The first RAPTA structure to be reported was  $[\text{Ru}(\eta^6\text{-}p\text{-cymene})\text{Cl}_2(\text{PTA})]$  (**1**) [29], later abbreviated to RAPTA-C (Figure 2). This early report hinted at the potentially interesting biological activity of RAPTA-C in that when it was incubated with



supercoiled pBR322 DNA, pH-dependent DNA damage was observed. DNA damage was observed at pH 7.0 and below but not at physiological pH (pH  $\geq 7.5$ ), indicating the potential of using RAPTA-C to damage DNA selectively in diseased hypoxic cells (which have a reduced pH).

The antibiotic and antiviral properties of RAPTA-C and three close analogues,  $[\text{Ru}(\eta^6\text{-}p\text{-cymene})\text{X}_2(\text{PTA})]$  ( $\text{X} = \text{Cl}, \text{Br}, \text{I}, \text{NCS}$ ), were evaluated shortly after the initial report of the DNA damaging properties of RAPTA-C [32]. Although none of the RAPTA compounds possessed antiviral activity, a degree of antibiotic activity was observed. The level of activity against a particular microbe was observed to be related to the nature of the leaving group ( $\text{X}$ ) ligand. The *in vitro* DNA-damaging ability of a particular RAPTA complex did not correlate with the observed antimicrobial activity, suggesting a non-DNA-based mechanism of cytotoxicity. A study of RAPTA-C incubated with *E. Coli*, followed by the extraction and separation of intracellular proteins, that were then examined by laser ablation inductively coupled mass spectrometry (LA-ICP-MS), indicated the formation of specific protein-ruthenium interactions, implying protein-binding may be a major factor in the activity of these compounds.

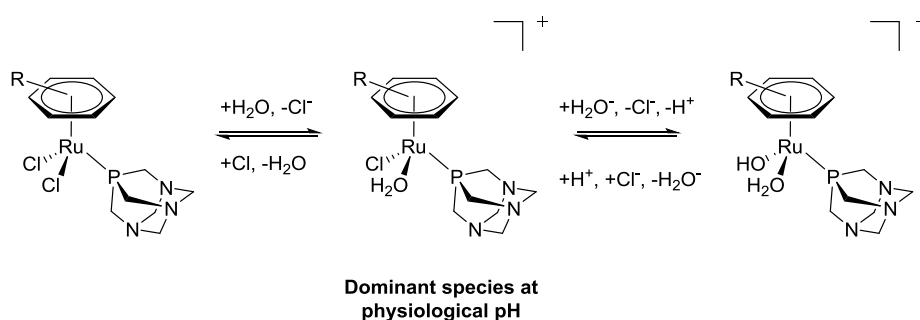


Figure 3. Aquation of the prototypical RAPTA structure (e.g. RAPTA-B **(2)**/RAPTA-C **(1)**) at physiological pH. The first step is the displacement of a chlorido ligand by an aqua ligand to yield the mono-aquated product which dominates at physiological pH (middle); further ligand exchange leads to a minor quantity of  $[\text{Ru}(\eta^6\text{-arene})(\text{OH})(\text{H}_2\text{O})(\text{PTA})]^+$ .

A later study reported the *in vitro* anticancer activity of several new RAPTA structures [30]. Simple variations of the arene ligand and the use of Me-PTA in place of the PTA ligand were used to expand the structural diversity of the RAPTA skeleton. In the same study the hydrolysis profile was explored, with RAPTA-C shown to undergo rapid hydrolysis in aqueous solution containing 4 mM NaCl [30], whereas at a NaCl concentration of 100 mM, i.e. that present in blood, hydrolysis is suppressed. More in-depth studies on the hydrolysis of RAPTA-C [33, 34] and RAPTA-B ( $[\text{Ru}(\eta^6\text{-benzene})\text{Cl}_2(\text{PTA})]$  (**2**); Figure 2) [35] revealed that under physiological conditions of low chloride concentration (5 mM) the most abundant species in solution is the mono-aquated form of the RAPTA complex,  $[\text{Ru}(\eta^6\text{-arene})\text{Cl}(\text{H}_2\text{O})(\text{PTA})]^+$ , with lesser amounts of  $[\text{Ru}(\eta^6\text{-arene})(\text{OH})(\text{H}_2\text{O})(\text{PTA})]^+$  and  $[\text{Ru}(\eta^6\text{-arene})\text{Cl}_2(\text{PTA})]$  also present with equilibrium reached within 20 min (1 mM RAPTA-C, 298 K, 150 mM  $\text{NaClO}_4$ , pH 7.8 at  $\tau = 0$ ; Figure 3). Hence, it may be assumed that *in vivo* the RAPTA compounds, like cisplatin, are likely to be activated to the more reactive aqua form only in a low chloride environment, such as that found in an intracellular environment. It would therefore appear that RAPTA-C is transported in the less active chlorido form in blood plasma and can be considered as a prodrug. Note that the  $\text{pK}_a$  values of the PTA ligand of several RAPTA compounds, in 0.1 M NaCl solution (used to preserve the dichlorido form), were in the range 2.99–3.31 [30], implying that the PTA ligand is unlikely to be protonated under physiological conditions *in vivo*. These  $\text{pK}_a$  values are likely to be modulated as the complexes are aquated on dissolution in aqueous media.

### 3. Anticancer Activity of RAPTA compounds

#### 3.1. Activity in cell lines and in *in vivo* models

The *in vitro* anticancer activity of the RAPTA compounds was initially evaluated against the TS/A adenocarcinoma and HBL-100 epithelial (non-cancerous) cell lines using the MTT assay (72 h exposure). Compounds possessing a PTA ligand exhibited no cytotoxicity towards the non-tumorigenic HBL-100 cell line ( $IC_{50} > 300 \mu\text{M}$ ) and only mild or no cytotoxicity towards the TS/A cell line (66 to  $> 300 \mu\text{M}$ ) [30]. Two compounds, RAPTA-T ( $[\text{Ru}(\eta^6\text{-toluene})\text{Cl}_2(\text{PTA})]$ ) (**3**) and RAPTA-Im ( $[\text{Ru}(\eta^6\text{-1,2-dimethyl-3-(4-methylphenethyl)-1H-3\lambda^4\text{-imidazole})Cl}_2(\text{PTA})][\text{BF}_4]$ ) (**4**) (Figure 2), exhibited good cytotoxic selectivity towards the TS/A cell line over the HBL-100 cell line (74 and 66  $\mu\text{M}$  *versus*  $> 300 \mu\text{M}$ , respectively). In contrast, the Me-PTA-containing compounds (**5**, **6**) were more cytotoxic towards the HBL-100 cell line than the TS/A cell line. An *in vivo* study of RAPTA-B and RAPTA-C was performed in mice bearing the MCa mammary carcinoma [30]. Neither compound was active against the primary tumors, but both were effective in reducing the number and weight of solid lung metastases that originate from the primary tumor. These promising *in vivo* results established RAPTA compounds as potential antimetastatic agents.

### 3.2. Antimetastatic activity

Since RAPTA-T (**3**) showed the highest selectivity with respect to cytotoxicity towards cancerous cell lines over normal cell lines a detailed evaluation of the antimetastatic activity of RAPTA-T in a series of *in vitro* and *in vivo* experiments was undertaken. Non-cancerous HBL-100, non-invasive MCF-7 human breast cancer and highly invasive MDA-MB-231 breast cancer cell lines were used in a series of *in vitro* experiments simulating aspects of metastatic progression, namely detachment, motility, invasion and adhesion experiments [36]. It was found that following treatment with RAPTA-T the MDA-MB-231 cell line was more resistant to detachment from

fibronectin or collagen IV substrates whilst remaining relatively unaffected on a poly-L-lysine substrate relative to control cells. No effect was seen with the MCF-7 and HBL-100 cell lines (Figure 4) [36].

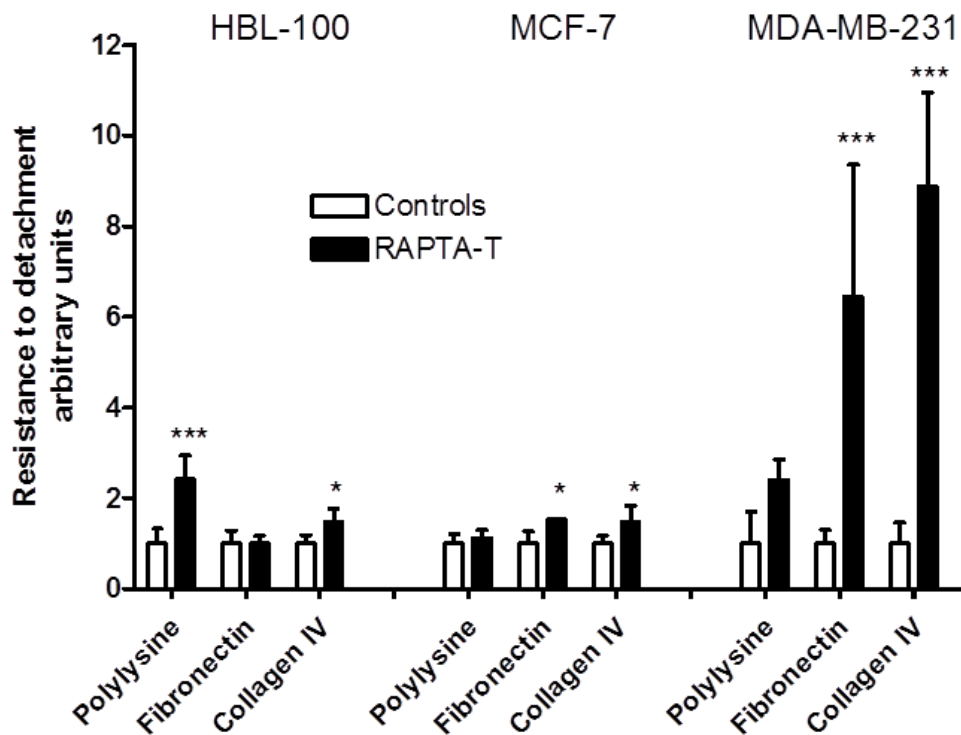


Figure 4. Effect of RAPTA-T on resistance to detachment. HBL-100, MCF-7 and MDA-MB-231 cells showing that the compound is selectively active against the highly invasive MDA-MB-231 cell line. Adapted from ref. [36].

The ability of the MDA-MB-231 cell line to adhere to various extra cellular matrix components following treatment with RAPTA-T was also reduced. In contrast, the ability of the HBL-100 cell line to adhere to the various substrates was unaffected by treatment with RAPTA-T and the MCF-7 cells showed a reduced tendency to adhere to collagen IV and matrigel, but this effect was less than that observed with the MDA-

MB-231 cell line. In addition, treatment with RAPTA-T reduced the ability of MDA-MB-231 cells to migrate (~50% relative to control cells). Reduced migration was also observed with the MCF-7 cell line but was unchanged with the HBL-100 cell line. *In vivo* experiments comprising RAPTA-T treatment (80 mg kg<sup>-1</sup> per day on days 8, 9 and 12 following tumor implant) of a CBA mouse model bearing murine mammary carcinoma led to a negligible reduction in primary tumor growth but led to a 35% reduction in the weight of lung metastases, notably with a reduction in the number of metastases of large dimensions [36].

Overall, RAPTA-T exerts a degree of selectivity to invasive cancer cells and metastatic tumors. It was suggested that treatment with RAPTA-T leads to the cell body becoming more rigid through changes to the cytoskeleton, which leads to the cell losing the flexibility required for detachment and reattachment processes. The selective antimetastatic activity *in vivo* could be rationalized from the *in vitro* effects and points towards the biological activity of the RAPTA compounds being due, at least in part, to their action on cell surface molecules.

A later study [37] evaluated the effect of RAPTA-C on primary tumor growth in preclinical models using different dosing protocols compared to those in previous studies. When evaluated against human A2780 ovarian carcinoma transplanted onto the chicken chorioallantoic membrane (CAM) model, RAPTA-C was found to inhibit tumor growth by approx. 75% at a dose of 0.2 mg kg<sup>-1</sup> per day for 5 days (starting 4 days after tumor inoculation of the CAM). Examination of tissue sections from the treated tumor revealed large areas of non-proliferating tumor cells and a significantly reduced microvessel density in treated tissue compared to the well-vascularized viable tumor tissue found in controls. RAPTA-C was also evaluated in athymic mice bearing a LS174T colorectal adenocarcinoma on the right flank. In mice treated with RAPTA-

C at 100 mg kg<sup>-1</sup> per day for 11 days tumor growth was inhibited by 50% relative to controls whilst doses of 10 and 40 mg kg<sup>-1</sup> per day did not lead to tumor growth inhibition. Analysis of the treated tumor tissue revealed a strong anti-angiogenic activity of RAPTA-C exemplified by a decrease in microvessel density (Figure 5), consistent with related earlier studies which described the antiangiogenic activity of RAPTA-C and RAPTA-T in a series of cell-based assays and in the CAM model [38].

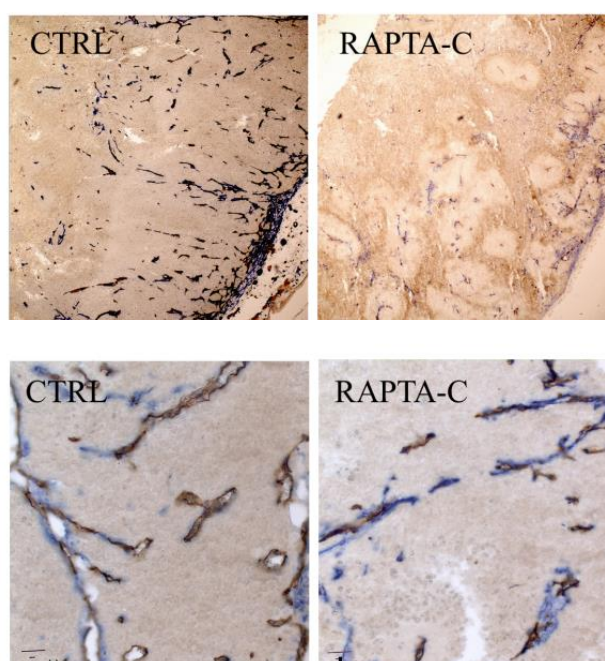


Figure 5. Immunohistochemical sections of tumors taken from RAPTA-C treated athymic mice with human LS174T colorectal carcinoma; (top) images of CD31 positive immunohistochemical sections and (bottom) images of SMA and CD31 positive immunohistochemical sections, both indicative of fewer mature blood vessels in the RAPTA-C treated tumors. Adapted from ref. [37] – with permission of The Royal Society of Chemistry © 2014.

No toxicity was associated with RAPTA-C treatment in the mouse model, even at the highest doses, and a biodistribution study of ruthenium 2 hours post-treatment

revealed fast renal excretion of ruthenium with no significant accumulation in vital organs. In contrast to earlier *in vivo* studies with RAPTA-C, this work indicates that with appropriate dosing protocols RAPTA-C can be extremely effective in reducing the volume of primary tumors – an effect that may be partly explained by the anti-angiogenic effects demonstrated by the complex – whilst remaining essentially non-toxic.

The most promising *in vivo* data for RAPTA-C has been obtained in combination studies with other approved and developmental drugs. A high throughput screening approach commencing with nine angiostatic drugs, including RAPTA-C, was used to determine optimal low-dose drug combinations [39]. The optimal synergistic drug combination found comprises erlotinib (an endothelial growth factor receptor inhibitor [40]), BEZ-235 (a dual PI3K/mTOR inhibitor [41]) and RAPTA-C. This drug combination showed enhanced endothelial cell specificity and synergistically inhibited proliferation of endothelial cells. The drug combination was evaluated in two *in vivo* tumor models (A2780 tumor grown in the CAM and LS174T tumor growth in athymic mice) and was found to inhibit tumor growth synergistically using drug doses that were reduced by up to 11-fold compared to optimal single drug concentrations. Indeed, the single drug monotherapies displayed, at best, negligible activity in the animal models. In the mouse model, when used in combination with erlotinib and BEZ-235, a single dose of RAPTA-C at 40 mg/kg was sufficient to afford a ca. 80% reduction in tumor growth. In the absence of RAPTA-C no effective drug combination could be found from the starting drugs used in the study.

In a different type of combination therapy, RAPTA-C was used following treatment with axitinib, a VEGFR targeting tyrosine kinase inhibitor [42]. The role of axitinib is to induce a transient period of increased tumor oxygenation which simultaneously

reduces vascular permeability, reducing interstitial fluid pressure in the tumor and improving uptake of small molecule drugs. It was found that when doxorubicin, a nanomolar cytotoxic drug [43], was applied during the period of increased tumor oxygenation (known as the normalization window), its efficacy improved (A2780 tumor grown in the CAM). However, the improvement was small compared to that of RAPTA-C applied during the normalization window. In the *in vivo* model doxorubicin applied at a dose of 3 mg/kg led to a reduction in tumor growth of 78%, whereas RAPTA-C, which is essentially not cytotoxic, led to almost 90% inhibition in tumor growth at a dose of only 400  $\mu$ g/kg (both applied after pretreatment with axitinib during tumor normalization). This study shows that under the right conditions extremely low doses of RAPTA-C can be applied *in vivo* without the observation of any side-effects (note that RAPTA-C is well tolerated at 100 mg/kg).

#### 4. Structure-activity relationships

The promising antitumor activity and low general toxicity displayed by some of the original RAPTA structures, in particular RAPTA-B (**2**), RAPTA-C (**1**) and RAPTA-T (**3**) (Figure 2), prompted further investigations on the effect of modulating individual structural elements of the RAPTA scaffold to ascertain structure-activity relationships in order to obtain more efficacious compounds. This work in turn led to the development of more complex RAPTA structures including dinuclear analogues and macromolecular RAPTA conjugates. In addition, the relatively uncommon antimetastatic activity observed led to detailed analytical studies of their interactions with potential biomolecular targets, and studies on their cellular uptake and localization, in order to unravel their molecular mechanisms of action.



#### 4.1 Systematic modulation and development of the RAPTA structure

The  $\eta^6$ -bound arene ligand of the piano-stool RAPTA structure may be readily modulated and it has been extensively varied and derivatized to introduce more complex functionality. The introduction of hydrogen-bonding substituents to the arene ligand of the RAPTA structure was investigated as a route by which hydrogen-bonding interactions with potential biomolecular targets could be increased alongside metal coordination [44]. A range of complexes were developed utilizing  $\eta^6$ -arene ligands incorporating alcohol and amine functionalities, including amines able to form intermolecular tethers through coordination to the ruthenium center, and in some cases the PTA analogue, DAPTA (3,7-diacetyl-1,3,7-triaza-5-phospha-bicyclo[3.3.1]nonane), was employed in place of the PTA ligand (see complexes **11** and **16**, Figure 6). In each case the functionalized complexes were less cytotoxic towards the TS/A cell line relative to the unfunctionalized analogues RAPTA-C, RAPTA-B and RAPTA-T, and essentially non-cytotoxic towards the HBL-100 cell line ( $IC_{50} > 600 \mu M$  in each case). In addition, for compounds with increased hydrogen-bonding functionality lower ruthenium uptake into TS/A cells relative to RAPTA-C, RAPTA-B and RAPTA-T was observed after 24 h treatment – most likely explaining the decrease in cytotoxicity for these compounds. Interestingly, in oligonucleotide binding studies monitored by ESI-MS, apart from the arene-substituted RAPTA derivatives bearing primary amine ligands and the intramolecularly chelated derivative, these complexes exhibited increased reactivity towards a 14-mer oligonucleotide sequence relative to RAPTA-C and RAPTA-T, principally forming adducts through loss of the arene ligand. The lack of correlation between the reactivity of the complexes with the oligonucleotide and their  $IC_{50}$  values aligns with the observation of their reduced cellular uptake.

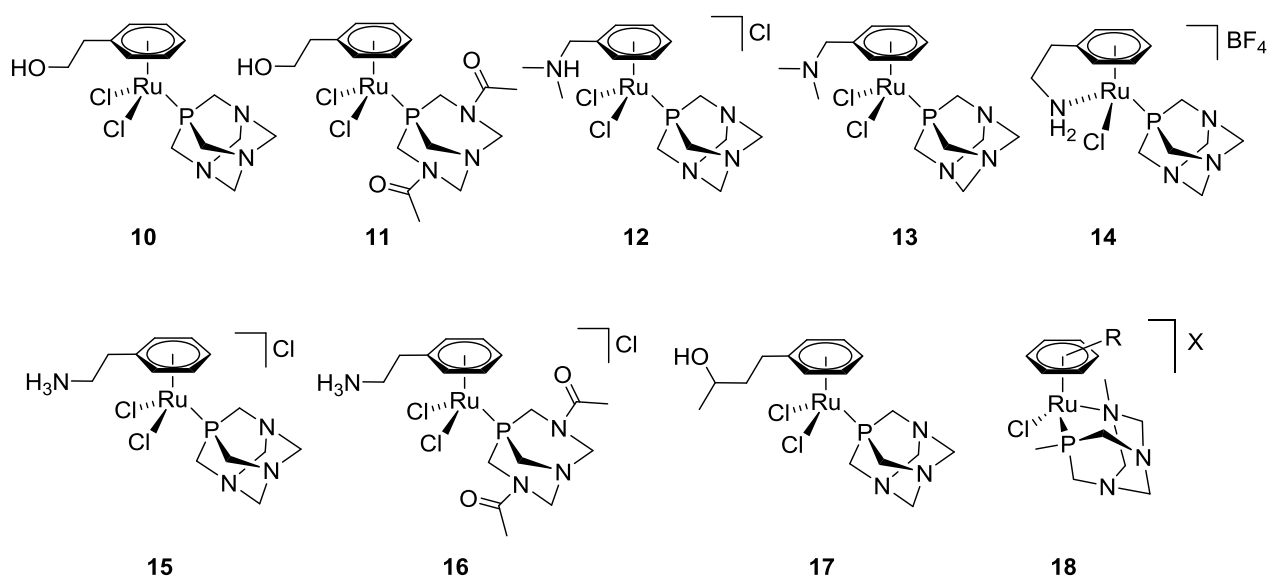


Figure 6. Structures of RAPTA derivatives with functionalized arene ligands and the general RAPTN structure (bottom right) [44, 45].

A related study examined a series of RAPTA analogues with a chelating PTN (3,7-dimethyl-7-phospha-1,3,5-triazabicyclo[3.3.1]nonane) ligand in place of the PTA ligand to yield complexes of the general formula  $[\text{Ru}(\eta^6\text{-arene})\text{Cl}(\text{PTN})]\text{X}$  (arene = *p*-cymene, benzene, toluene, hexamethylbenzene; X = Cl<sup>-</sup>, BF<sub>4</sub><sup>-</sup>; Figure 6 – structure **18**, bottom right) [45]. These complexes, containing a *P,N* chelate courtesy of the PTN ligand, were highly water soluble (with the sole exception of the *p*-cymene analogue). These complexes were less reactive than their  $[\text{Ru}(\eta^6\text{-arene})\text{Cl}_2(\text{PTA})]$  analogues in water. The *p*-cymene/benzene PTN complexes showed no evidence of ligand exchange in H<sub>2</sub>O over 7 days whilst the toluene analogue appeared to undergo aquation over 24 h with <5% of free arene observed at 72 h. The hexamethylbenzene analogue decomposed completely in H<sub>2</sub>O over 72 h as evidenced by loss of the arene ligand. It was observed that upon reaction with ubiquitin the *p*-cymene PTN complex

and RAPTA-C formed identical adducts after 72 h incubation although adduct formation was observed to be faster with the PTN complex. The  $[\text{Ru}(\eta^6\text{-}p\text{-cymene})\text{Cl}(\text{PTN})]^+$  complex was unreactive towards guanosine 5'-monophosphate over 72 h and was found only to react with a single-stranded 14-mer oligonucleotide when present in a 5-fold excess (ca. 10% relative intensity of adducts in nESI-FT-ICR mass spectra at 24 h). The cytotoxicity of the complexes against the A2780 cell line was assessed, with modest  $\text{IC}_{50}$  values of 154-278  $\mu\text{M}$  observed and the toluene analogue being the most cytotoxic. All these complexes were more cytotoxic than RAPTA-C against A2780 cells. The reactivity of the complex may be mediated through ring-opening of the *P,N* chelate, in particular in the  $[\text{Ru}(\eta^6\text{-}p\text{-cymene/benzene})\text{Cl}(\text{PTN})]^+$  complexes, where aquation is not observed.

Computational studies predicted the introduction of electron-withdrawing substituents to arene ligands of the RAPTA structure would modulate the equilibrium between the hydroxido- and aqua forms of the mono-hydrolyzed complexes at physiologically relevant pH [35]. The introduction of fluoroarene ligands was predicted to lower the  $\text{pK}_a$  sufficiently that pH differences between healthy tissue and cancerous tissue could be exploited. In the more acidic cancer tissue, the more active aqua-form of fluoro-RAPTA would dominate whereas in healthy cells the more inert hydroxo-form should dominate, thus enhancing selectivity. Three RAPTA complexes,  $[\text{Ru}(\eta^6\text{-fluoroarene})\text{Cl}_2(\text{PTA})]$  (fluoroarene =  $\text{C}_6\text{H}_5\text{F}$  (**19**),  $\text{C}_6\text{H}_5\text{CF}_3$  (**20**) and 1,4- $\text{C}_6\text{H}_4\text{CH}_3\text{F}$  (**21**); Figure 7), were prepared to evaluate this hypothesis and were accessed through an atypical route involving fluoroarene exchange with a  $[\text{Ru}^0(\eta^6\text{-naphthalene})(\eta^4\text{-cod})]$  intermediate due to safety issues associated with Birch reductions of halogenated arenes [46].

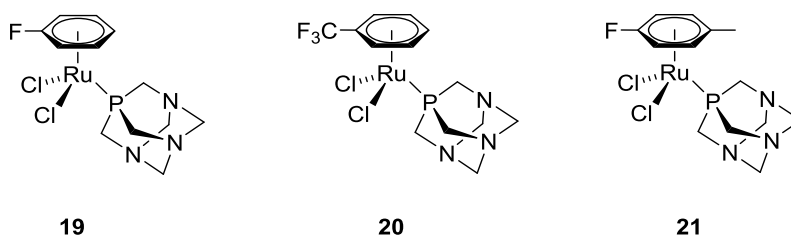


Figure 7. Structures of fluoro-RAPTA derivatives [46].

In aqueous solution the three complexes were found to hydrolyze slowly relative to non-fluorinated RAPTA analogues, with equilibrium states being reached after 2 h in the cases of  $[\text{Ru}(\eta^6\text{-C}_6\text{H}_5\text{F})\text{Cl}_2(\text{PTA})]$  (**19**) and  $[\text{Ru}(\eta^6\text{-1,4-C}_6\text{H}_5\text{CH}_3\text{F})\text{Cl}_2(\text{PTA})]$  (**21**) and after 1 day in the case of  $[\text{Ru}(\eta^6\text{-C}_6\text{H}_5\text{CF}_3)\text{Cl}_2(\text{PTA})]$  (**20**). A 5-fold increase in the rate of hydrolysis of  $[\text{Ru}(\eta^6\text{-C}_6\text{H}_5\text{CF}_3)\text{Cl}_2(\text{PTA})]$  was observed at pH 4.7 compared to 5.7. It was suggested this increased reactivity may enable selective targeting of more acidic cancerous tissue through increased rates of complex activation by hydrolysis. After 3 days in 100 mM NaCl solution, free arene ligand is detected to varying extents for  $[\text{Ru}(\eta^6\text{-1,4-C}_6\text{H}_5\text{CH}_3\text{F})\text{Cl}_2(\text{PTA})]$  (**21**) and  $[\text{Ru}(\eta^6\text{-C}_6\text{H}_5\text{CF}_3)\text{Cl}_2(\text{PTA})]$  (**20**), highlighting the comparatively weak Ru–arene bond as the fluoroarene ligands are electron-poor. The  $\text{pK}_a$  values for the protonation of the three  $[\text{Ru}(\eta^6\text{-fluoroarene})\text{Cl}(\text{OH})(\text{PTA})]$  complexes were calculated to be 8.3 for  $[\text{Ru}(\eta^6\text{-C}_6\text{H}_5\text{F})\text{Cl}(\text{OH})(\text{PTA})]$ , 5.5 for  $[\text{Ru}(\eta^6\text{-C}_6\text{H}_5\text{CF}_3)\text{Cl}(\text{OH})(\text{PTA})]$  and 8.9 for  $[\text{Ru}(\eta^6\text{-1,4-C}_6\text{H}_5\text{CH}_3\text{F})\text{Cl}(\text{OH})(\text{PTA})]$  compared to 8.7 calculated for  $[\text{Ru}(\eta^6\text{-cymene})\text{Cl}(\text{OH})(\text{PTA})]$ , thus highlighting the importance of the choice of arene ligand in the design of these complexes. The cytotoxicity of the compounds was screened (72 h) against the A2780 cell line revealing a significantly higher cytotoxicity for  $[\text{Ru}(\eta^6\text{-1,4-C}_6\text{H}_5\text{CH}_3\text{F})\text{Cl}_2(\text{PTA})]$  (**21**) and  $[\text{Ru}(\eta^6\text{-C}_6\text{H}_5\text{CF}_3)\text{Cl}_2(\text{PTA})]$  (**20**) ( $\text{IC}_{50} = 78$  and  $38$   $\mu\text{M}$  respectively) relative to  $[\text{Ru}(\eta^6\text{-C}_6\text{H}_5\text{F})\text{Cl}_2(\text{PTA})]$  (**19**) and RAPTA-C (**1**) ( $\text{IC}_{50} = 507$  and  $353$   $\mu\text{M}$ , respectively). The cytotoxicity of  $[\text{Ru}(\eta^6\text{-C}_6\text{H}_5\text{CF}_3)\text{Cl}_2(\text{PTA})]$  (**20**) and

$[\text{Ru}(\eta^6\text{-1,4-C}_6\text{H}_5\text{CH}_3\text{F})\text{Cl}_2(\text{PTA})]$  (**21**) is likely related to the increased lability of the fluoroarene ligands in these two complexes, as this would lead to increased reactivity with biomolecular targets and potentially stronger binding. The lability of the trifluorotoluene ligand present in  $[\text{Ru}(\eta^6\text{-C}_6\text{H}_5\text{CF}_3)\text{Cl}_2(\text{PTA})]$  (**20**) was further established in a subsequent study that showed on binding to ubiquitin and a double-stranded oligonucleotide the arene ligand of the complex was readily lost [47]. This process resulted in the formation of different biomolecular adducts to those observed for RAPTA-C, largely as a result of multidentate binding of the resulting fragment to the biomolecular target.

In related work, examining the necessity of a face-capping aromatic component for anticancer activity in RAPTA compounds and other organometallics, a RAPTA analogue was prepared with a 1,4,7-trithiacyclononane ligand ( $[\text{9}]\text{aneS}_3$ ) in place of the arene, *i.e.*  $[\text{Ru}([\text{9}]\text{aneS}_3)\text{Cl}_2(\text{PTA})]$  (**22**) (Figure 8) [48].

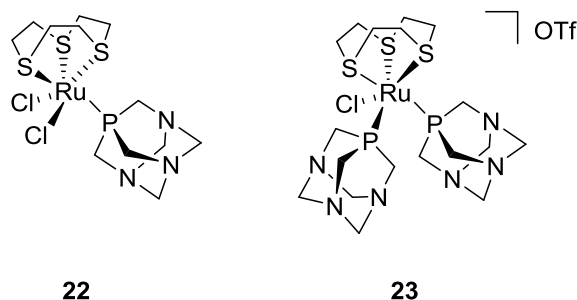


Figure 8. RAPTA-derived complexes with the  $[\text{9}]\text{aneS}_3$  ligand replacing the arene [48].

In aqueous solution the complex behaved in a similar manner to the other compounds in the RAPTA series with exchange of a chlorido ligand by a water ligand. This product was stable over prolonged periods with no loss/exchange of the other ligands. The hydrolysis reaction was reversed in the presence of 100 mM NaCl [48]. The impact of the complex on cell viability was studied against TS/A and HBL-100 cell lines. Like the

original RAPTA series, the complex was only slightly cytotoxic with  $IC_{50}$  values  $>600$   $\mu\text{M}$  against the TS/A and HBL-100 cell lines. A further analogue containing two coordinated PTA ligands,  $[\text{Ru}([\text{9}]ane\text{S}_3)\text{Cl}(\text{PTA})_2][\text{OTf}]$  (**23**) (Figure 8), was inert in aqueous solution at physiological pH. However, it exhibited a selective mild cytotoxicity towards the TS/A cell line ( $IC_{50}$  388  $\mu\text{M}$ ) whilst being inactive against the HBL-100 cell line ( $IC_{50}$   $>1000$   $\mu\text{M}$ ). This study indicates that the arene ligand may be effectively replaced by other face-capping ligands of similar steric demand without significantly changing the *in vitro* activity.

The RAPTA structure was used as the base for the rational design of two novel glutathione transferase P1-1 inhibitors where ethacrynic acid, an effective glutathione transferase inhibitor, was tethered with the arene unit of a RAPTA complex [49]. The complexes were designed so that upon binding of the ethacrynic acid moiety to the H-site of the human GST P1-1 enzyme, which is expressed in certain chemoresistant tumors, the RAPTA moiety is directed towards the interface of the dimeric protein where it could potentially bind to cysteine residues resulting in distortion and deactivation of the enzyme. Through competitive inhibition studies it was found both complexes are competitive inhibitors of the substrate 1-chloro-2,4-dinitrobenzene. Studies showed that both complexes (see Figure 9 for their structures) bind at the enzyme H-site and that the ruthenium center plays a major role in inhibition. Through mass spectrometric analysis of the GST P1-1 enzyme incubated with the ethacrynic acid-RAPTA complex it was found that 1:1 adducts were formed with the enzyme, with loss of both Cl ligands, alongside lower mass adducts where the ruthenium fragment had been lost (only observed after longer incubation times) leaving an ethacrynic acid-GST P1-1 adduct. This data was supported by crystal structures of GST P1-1 incubated with the ethacrynic acid-RAPTA complex (Figure 10). The crystal structure

showed that the ruthenium ion was bound to the cysteine residues at the interface of the dimer following loss of the chlorido ligands alongside further van der Waal's interactions between the RAPTA arene and PTA ligands with amino acid side chains in the vicinity of the dimer interface. The ethacrynic acid moiety was directed into the H-site of the enzyme and in a second structure collected after a prolonged incubation time, ethacrynic acid was found to bind to the H-site of the enzyme with the metal absent. It was postulated that this mechanism could potentially be exploited to simultaneously inactivate glutathione transferase P1-1 resistance and release a cytotoxic organometallic fragment into the sensitized cell. Subsequent biological studies indicated that this two-step process takes place also *in vitro* [50, 51].

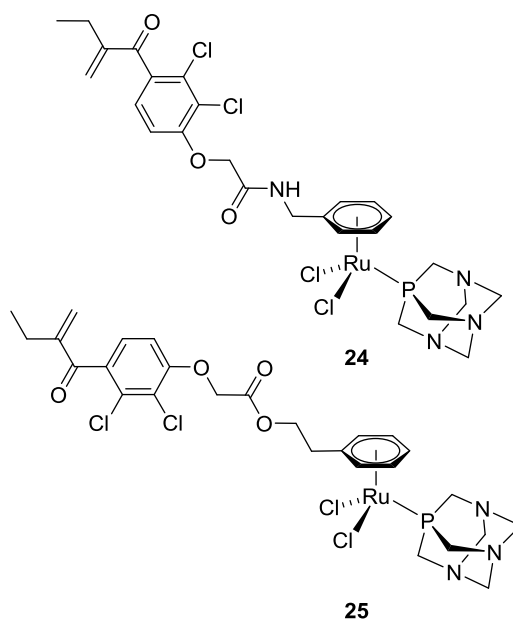


Figure 9. Structures of ethacrynic acid-functionalised RAPTA derivatives [49].

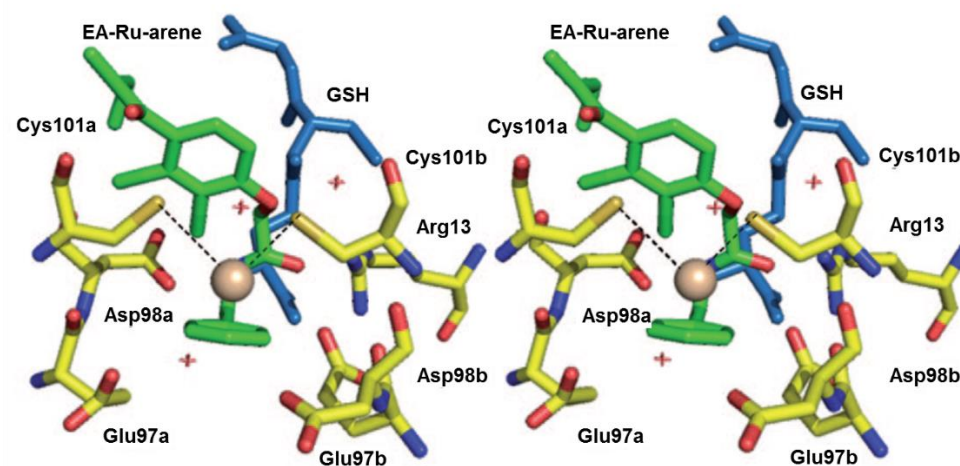


Figure 10. Stereo picture highlighting the interaction between GST P1-1 and the amide-linked ethacrynic acid-RAPTA complex at the GST P1-1 dimer interface. Adapted from ref. [49] © 2009 John Wiley and Sons.

A range of planar aromatic substituents have been tethered to the arene ring of the RAPTA structure (Figure 11), thus introducing a potential DNA intercalator with fluorescent properties that may conveniently be utilized to track intracellular localization, the first of these comprised of anthracene derivatives linked to the arene ring (Figure 11, structure **(26)**) [52]. The complexes were found to undergo aquation in aqueous solution and were assessed for cytotoxicity towards 12 cell lines (72 h). It was found that both compounds possessed very low toxicity towards each cell line ( $IC_{50} > 200 \mu M$ ), in keeping with the low toxicities observed for the parent RAPTA analogues. Intracellular localization was monitored in the A549 lung carcinoma cell line (24 h incubation,  $50 \mu M$ ,  $\lambda_{ex}$  365 nm), however only weak fluorescence was observed which precluded identification of precise intracellular localization of the complex.



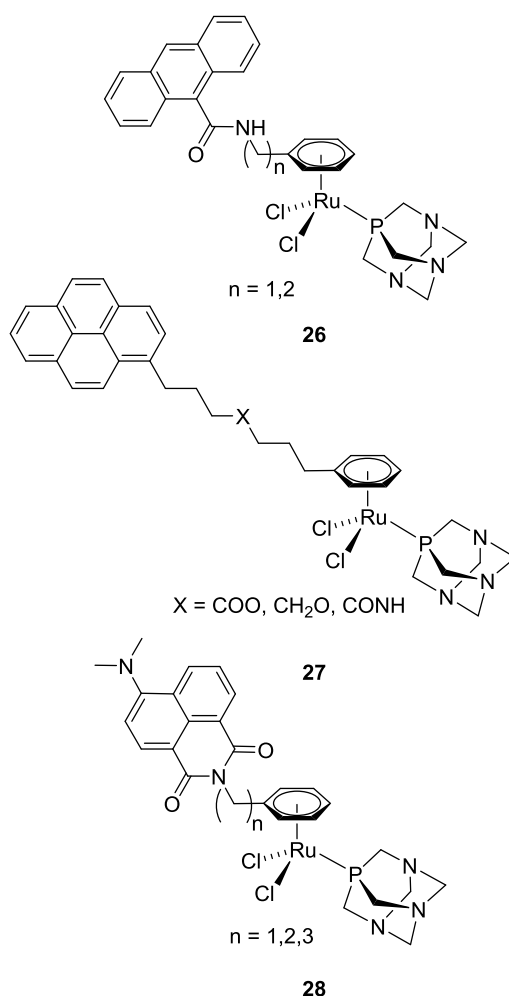


Figure 11. Functionalization of the arene ligand of RAPTA compounds with anthracene (top) [52], pyrene (center) [53] and naphthalimide (bottom) [54].

A similar series of compounds was developed with pyrene moieties tethered to the RAPTA arene ligand (Figure 11, structure **(27)**). These were then encapsulated into a water-soluble metalla-cage ( $[\text{Ru}_6(\eta^6\text{-}p\text{-cymene})_6(\text{tpt})_2(\text{donq})_3]^{6+}$ ) (tpt = 2,4,6-tri-(pyridin-4-yl)-1,3,5-triazine; donq = 5,8-dioxido-1,4-naphthoquinonato) to circumvent the reduced water solubility of the novel RAPTA-pyrene complexes [53]. In cytotoxicity assays against the A549, A2780, A2780cisR, Me300 and HeLa cell lines (72 h) the three complexes alone were not cytotoxic towards the cell lines at the maximum concentration tested (25  $\mu\text{M}$ ), with the sole exception of the ether-tethered pyrene complex which possessed  $\text{IC}_{50}$  values of 15.8, 17.7 and 19.7  $\mu\text{M}$  against the

A2780cisR, Me300 and A2780 cell lines, respectively. The host-guest systems were significantly more cytotoxic towards all cell lines ( $IC_{50}$  values of 2.0–7.7  $\mu\text{M}$ ), however, the cage itself also exhibited considerable cytotoxicity towards the cell lines on which it was examined ( $IC_{50}$  3.1–4.6  $\mu\text{M}$ ). This work illustrated that the introduction of a planar aromatic moiety to the arene ligand of the RAPTA structure *via* a stable tether may result in an increase in cytotoxic activity. However, it is unclear whether this effect is as a result of modulation of complex lipophilicity, DNA intercalation by the pyrene functionality [55], or a combination of both. The formation of the host-guest complex with the metalla-cage did result in an increase in cytotoxicity, but this effect is dominated by the inherent cytotoxicity of the metalla-cage.

The naphthalimide functionality, a known DNA intercalator [56], was introduced to the arene ligand of the RAPTA structure *via* short alkyl-chain tethers (Figure 11, structure **(28)**) [54]. These complexes were found to undergo aquation on the same timeframe as RAPTA-C and they exhibited high cytotoxicity (72 h) towards the A2780 and A2780cisR cell lines ( $IC_{50}$  2.3–9.1  $\mu\text{M}$ ). In addition, the compounds were moderately more cytotoxic (2- to 3-fold) towards the A2780/A2780cisR cell lines than the non-cancerous HEK293 cell line. Incubation of the complex with the ethyl-linker between the  $\eta^6$ -bound arene ring and naphthalimide moiety with ubiquitin led to the formation of 1:1 adducts within 1 h (established by ESI MS) and in separate experiments the interaction of the naphthalimide group of this complex with ct-DNA was tentatively confirmed. Given the known intercalation properties of the naphthalimide group and the rapid coordination of the ruthenium center to ubiquitin, it was postulated that the high cytotoxicity of these compounds could be related to simultaneous intercalation of the naphthalimide moiety with DNA and coordination of the ruthenium ion to protein – essentially forming DNA-protein crosslinks.

The compounds described above highlight that the cytotoxicity of a RAPTA structure may be modulated through the introduction of a planar aromatic moiety tethered to the arene ligand. These aromatic systems have the potential to intercalate with DNA, but they also result in an increase in lipophilicity of the complex that may also modulate their cellular uptake and localization relative to the parent RAPTA complexes. Although it is unclear whether the increased cytotoxicity of these compounds is due to modified mechanisms of action such as DNA intercalation or due to increased cellular uptake and/or modulated intracellular localization, since other very hydrophobic RAPTA derivatives such as  $[\text{Ru}(\eta^6\text{-}p\text{-cymene})(\text{PPh}_3)(\text{PTA})\text{Cl}]^+$  (**56**) display limited cytotoxicity (see below) [57], it is tempting to correlate the higher levels of cytotoxicity with mechanisms related to the intercalating moiety.

In a further study that modulated the ability of a RAPTA complex to covalently modify biological targets, the DNA-alkylating agent chlorambucil was conjugated with the RAPTA scaffold (Figure 12, structure (**29**)), yielding complexes capable of simultaneous DNA alkylation and coordination to proteins [58]. These complexes exhibited cytotoxicity in the low to medium  $\mu\text{M}$  range towards the A2780, A2780cisR and MCF7 cell lines ( $\text{IC}_{50}$  8.3–45  $\mu\text{M}$ ) and one example was more active in cisplatin-resistant cell lines than chlorambucil, RAPTA-T or a mixture of both. To test the ability of the complex to crosslink DNA and protein, model experiments with EtG (EtG = 9-ethylguanine) and amino acids revealed that coordination of EtG following hydrolysis of the complexes was faster than alkylation of EtG by the chlorambucil moiety, but there were also signals detected in the mass spectra that were assigned to species featuring both EtG and amino acids, demonstrating the feasibility of the approach.

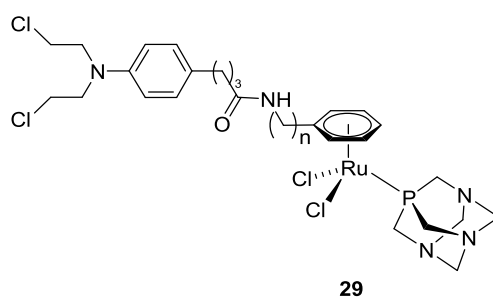


Figure 12. Chlorambucil-functionalized RAPTA complexes capable of crosslinking DNA and proteins [58].

The effect of introducing enantiomerically pure chiral groups to the arene ligand of the RAPTA structure was investigated through the introduction of (*R*)- or (*S*)-methylbenzylamine (Figure 13, structures **(30)** and **(31)**) [59]. Two sets of complexes were developed – chlorido analogues that readily undergo aquation in aqueous solution and oxalato analogues that are more resistant towards ligand substitution in water [59]. The cytotoxicity of the complexes was determined against the A2780, A2780cisR and HEK293 cell lines (72 h). All complexes were cytotoxic towards the A2780 cell line ( $IC_{50}$  8.7–44  $\mu$ M) and for the oxalato **(31)** complexes a similar level of cytotoxicity was also observed against the A2780cisR and HEK293 cell lines ( $IC_{50}$  21–33  $\mu$ M). For the chlorido analogues **(30)** both enantiomers were essentially non-toxic towards the A2780cisR cell line ( $IC_{50}$  396 and 228  $\mu$ M), however, the *R*-enantiomer was significantly less cytotoxic towards the HEK293 cell line than the *S*-enantiomer ( $IC_{50}$  >1000  $\mu$ M *versus* 255  $\mu$ M), i.e. displaying selectivity cytotoxicity towards the cancerous cell lines. Thus, the introduction of the chiral appendage tethered to the  $\eta^6$ -arene ligand, in these examples, dramatically increases cytotoxicity towards cancerous A2780 cell lines relative to RAPTA-C and oxaloRAPTA-C as the parent analogues that are essentially inactive towards these cell lines. Notably, with the chlorido **(30)** analogues there are cytotoxic differences between the two enantiomers

that can only be attributed to differences in chirality at the arene ring that presumably influences binding to biomolecular targets. From this work it is apparent that the introduction of chiral substituents represents a promising route to modulate activity/selectivity of RAPTA complexes and potentially other classes of ruthenium(II)-arene compounds; however, it should be noted that on aquation of a chiral RAPTA complex, where only one of the chlorido ligands is replaced, diastereomers are formed which may react differently with biomolecular targets.

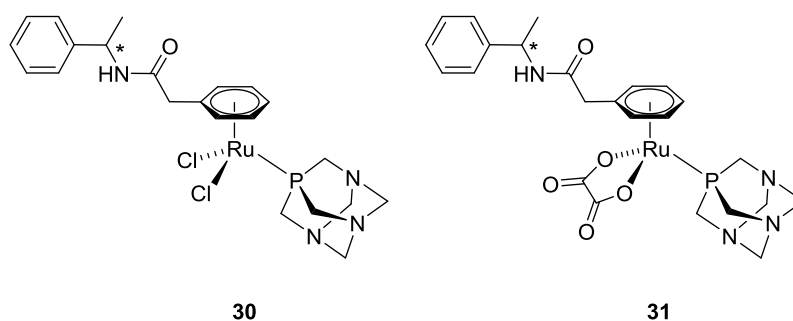


Figure 13. Structures of RAPTA compounds with chiral substituents at the arene ligand [59].

The arene ligand of the RAPTA structure has been used as a tethering point to form arene-linked dinuclear RAPTA analogues (Figure 14, structures **(32)** and **(33)**) [60]. These dinuclear compounds were formed using rigid diphenylethylenediamine-based linkers to fix the position of the metal centers relative to each other to investigate how the conformation of the ruthenium complexes influences their interactions with biomolecular targets and subsequent cytotoxicity profiles. Binding studies between the chlorido complexes and 5'-GMP or a 13-mer single-stranded oligonucleotide revealed facile coordination *via* chloride-loss and, significantly, arene loss resulting in cleavage of the dinuclear complex. In contrast, binding studies with the peptide H-Asp-Ala-Glu-Phe-Arg-His-Asp-Ser-Gly-Tyr-Glu-Val-His-His-Gln-Lys-OH containing three histidine residues resulted in 1:1 adducts formed through loss of the chlorido and PTA ligands

from the complexes. Electron-transfer dissociation fragmentation MS studies of adducts were performed to elucidate the ruthenium ion binding sites. Using this technique it was found that very different adducts were formed by the dinuclear complexes compared to the mononuclear analogues, with each ruthenium ion of the former simultaneously coordinating to one or more histidine residues of the peptide whereas for the latter a single ruthenium ion was found to coordinate to one or more histidine residues. However, no differences were found in coordination sites or size (ion mobility mass spectrometry) of the peptide adducts of the isomeric dinuclear complexes. Despite the lack of discrimination observed in analytical studies, an assessment of the cytotoxicity of the complexes against the A2780, A2780cisR and HEK293 cell lines revealed differences between the activities of these complexes (72 h). Both mononuclear analogues ((**34**) and (**35**)) were essentially non-toxic ( $IC_{50} > 300 \mu M$ ). The dinuclear complexes with the more closed (*S,S*)- or (*R,R*)-configuration were highly active against all three cell lines ( $IC_{50}$  values (complex concentrations) for oxalato analogues of 6–15  $\mu M$  and for chlorido analogues of 3.7–8.0  $\mu M$ ), whereas those with the open (*R,S*)-configuration were less cytotoxic ( $IC_{50}$  values (complex concentrations) for oxalato analogues 19–74  $\mu M$ , chlorido analogues 20–95  $\mu M$ ). The flexible ethylenediamine-linked complex possessed a similar activity to the complex of (*R,S*)-configuration ( $IC_{50}$  values (complex concentrations) oxalato analogues 23–88  $\mu M$ , chlorido analogues 35 to  $> 300 \mu M$ ). This study demonstrated that modulation of biological activity is possible through the tethering of two RAPTA complexes, with the two ruthenium centers able to simultaneously coordinate to suitable biological targets to crosslink and distort their structure leading to novel adducts and increased cytotoxicity. The choice of linker is important and may play a crucial role in the type of intracellular adducts formed.

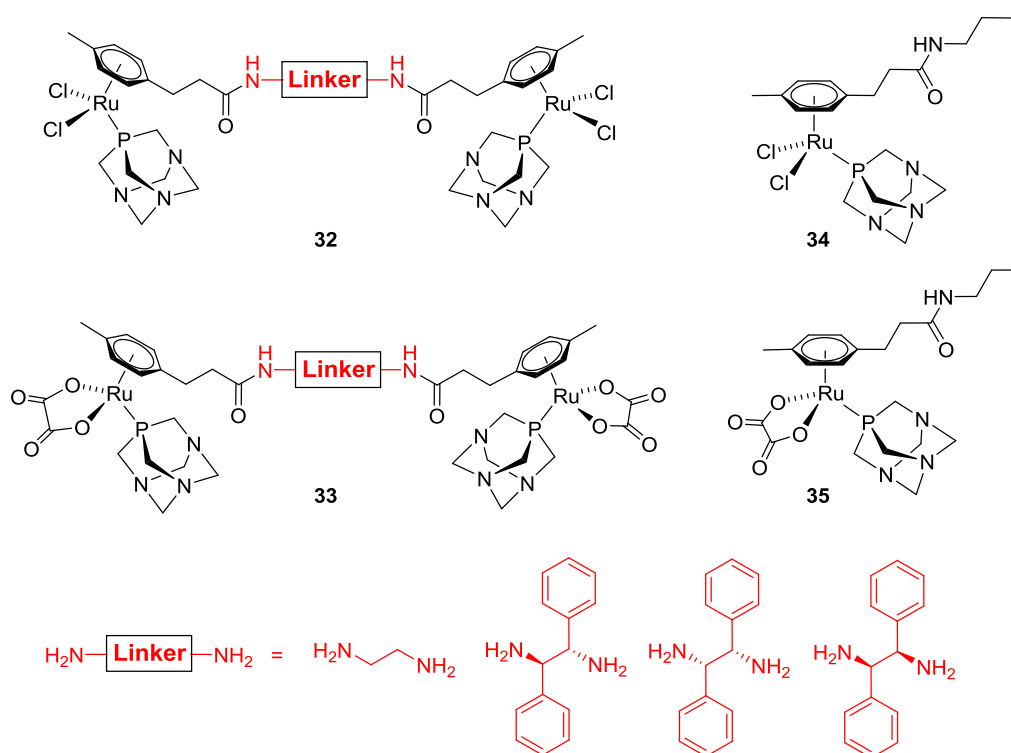


Figure 14. Arene-linked dinuclear RAPTA derivatives and their mononuclear analogues [60].

Since dinuclear RAPTA compounds tend to be more cytotoxic than related mononuclear species a strategy to generate dinuclear species inside cancer cells was explored as a route to enhance selectivity [61]. This approach involved the development of a RAPTA complex bearing an arene ligand functionalized with a bicyclo[6.1.0]non-4-yn-9-ylmethanol moiety (BCN-RAPTA (**36**); Figure 15). BCN can participate in strain-promoted cycloaddition reactions with tetrazines [62], and it was found that the combination of a ditetrazine (**37**) and the BCN-RAPTA derivative in biological media resulted in the *in situ* formation of a dinuclear RAPTA complex (**38**). Combining the ditetrazine and BCN-RAPTA components *in vitro* in A2780 cells resulted in an  $\text{IC}_{50}$  value (complex concentrations) of 2.6  $\mu\text{M}$  (72 h), compared to an  $\text{IC}_{50}$  value of 5.7  $\mu\text{M}$  for a mononuclear tetrazine conjugate analogue formed *in situ* and 12  $\mu\text{M}$  for BCN-RAPTA and >400  $\mu\text{M}$  for the tetrazines. This approach

demonstrates that the developing field of strain-promoted cycloaddition reactions may offer scope for modification and activation of metal complexes in a biological environment.

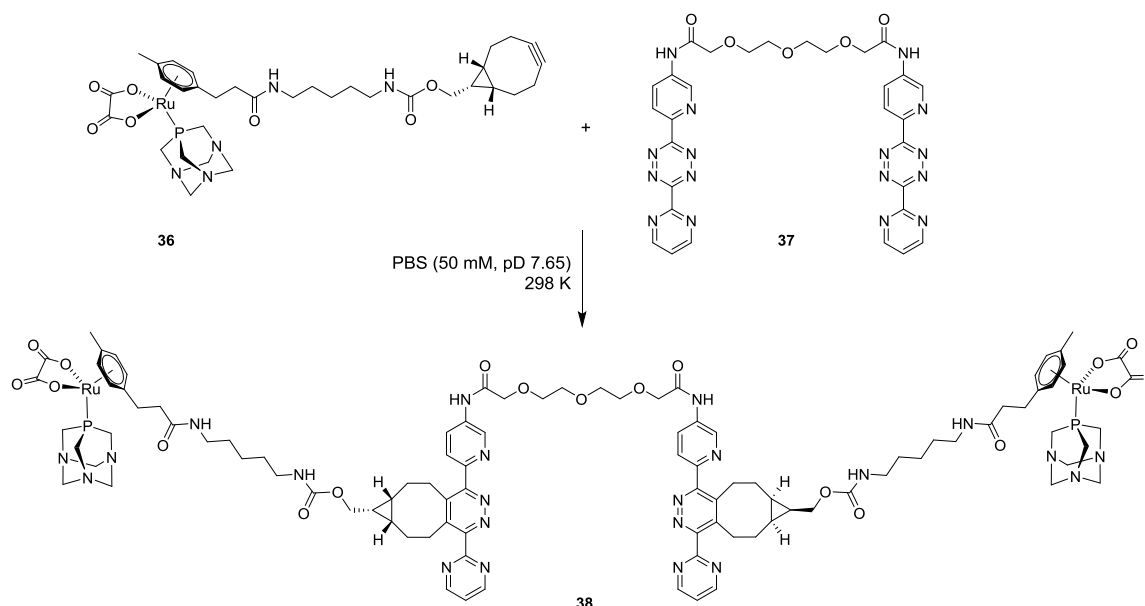


Figure 15. Preparation of a binuclear RAPTA derivative from a tetrazine and BCN-RAPTA bearing a bicyclononyne functional group [61].

#### 4.2. Development of RAPTA compounds for conjugation and macromolecular RAPTA conjugates

Modulation of the arene ligand of the RAPTA compounds has been exploited for the development of drug targeting/delivery strategies. The first carrier system to be developed for the RAPTA compounds is based on human serum albumin (HSA) [63]. HSA is known to accumulate in tumors relative to normal tissue, due to the enhanced permeability and retention (EPR) effect [64], and previously, it has been shown that chlorambucil [65] and paclitaxel [66] tethered to HSA can improve its activity while simultaneously reducing toxic side effects. Hydrazine-functionalized recombinant human serum albumin (rHSA) allowed a novel RAPTA compound (Figure 16, **(39)**) to



be conjugated through an aldehyde functionality tethered to the arene ligand. The resulting RAPTA-rHSA conjugates carry 3 to 4 RAPTA moieties per HSA molecule. When screened against the A2780 cell line the hydrazine-functionalized rHSA was not cytotoxic at the highest concentration tested (75  $\mu\text{M}$ ) and the aldehyde-functionalized RAPTA exhibited an  $\text{IC}_{50}$  value of 288  $\mu\text{M}$ . In contrast, the rHSA-RAPTA conjugate was found to have an  $\text{IC}_{50}$  value of 11  $\mu\text{M}$ , significantly more cytotoxic than the constituent protein and RAPTA components alone. This increase in cytotoxicity was attributed to a combination of facilitated cellular uptake of the conjugate and targeted release of the RAPTA compound through cleavage of the hydrazone linkers, possibly in the acidic conditions of lysosomes. This targeted-delivery approach does appear to offer clear benefits in enhancing the cytotoxicity of a RAPTA compound, with potential for *in vivo* tumor accumulation and targeted cellular release of the cytotoxic drug. Indeed, a similar approach has recently been reported for a Ru-based carbon monoxide releasing molecule (CORM) with high tumor accumulation observed *in vivo* [67]. The concept of a RAPTA complex able to participate in conjugation/labelling reactions was further extended in the development of acetal-containing RAPTA structures [68]. The idea was to allow access to a water-soluble RAPTA structure with a less bulky aldehyde functionality (Figure 16, **(41)**) than the water insoluble benzaldehyde-based RAPTA **(39)**. Chlorido and oxalato analogues of the acetal-containing RAPTA structures were obtained. The chlorido-analogue was reactive in aqueous solution as per the parent RAPTA structures, including rapid aquation and reactivity with GSH, whereas the oxalato analogue was essentially inert under the same conditions. The acetal group **(40)** may be converted to an aldehyde **(41)** in 10 mM HCl which was found to react readily with an oxime group under mild conditions (pH 6), however, ESI-MS analysis of the reaction products revealed the concomitant

loss of the oxalato group. In addition, model healthy HEK293 cells were treated with the chlorido analogue of the acetal complex and fixed by treatment with HCl to form the aldehyde functionality. Treatment of the fixed cells with a hydroxylamine-bearing fluorophore resulted in elevated levels of fluorescence relative to control cells, indicating the intracellular localization of these complexes may be probed by fluorescence microscopy.

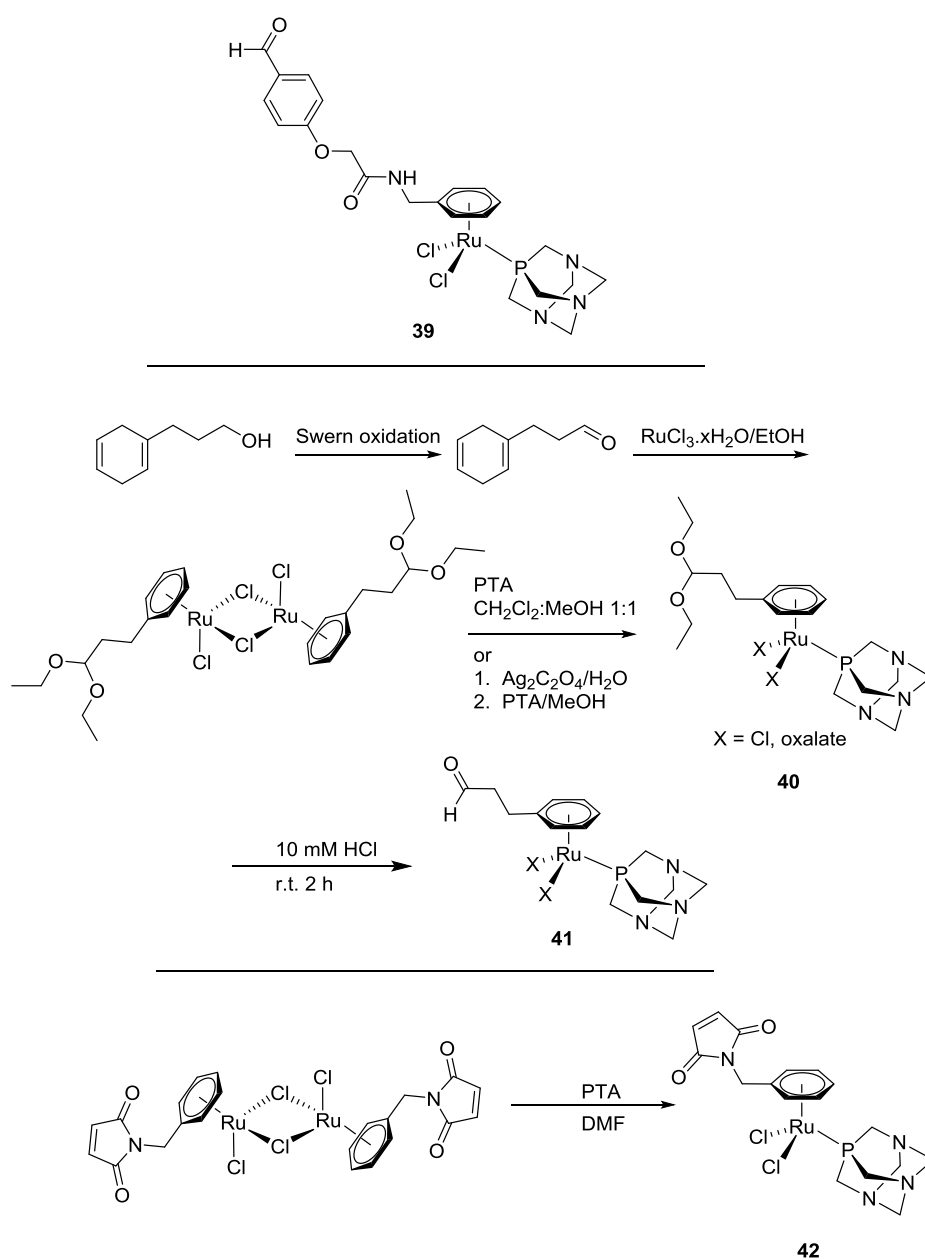


Figure 16. Protein conjugation strategies of RAPTA compounds [63, 68, 69].

A similar strategy exploited a maleimide-functionalized RAPTA compound (Figure 16, **(42)**) to enable covalent binding to thiol-containing biomolecules [69]. The maleimide-RAPTA species was found to react rapidly with cysteine, glutathione, *N*-acetylcysteine and *N*-acetylcysteine methyl ester under physiological conditions (phosphate buffer, pH 7.4, 100 mM NaCl, 310 K), with the thiol functionalities reacting selectively *via* nucleophilic addition to the maleimide and not by coordination to the ruthenium center (evidenced by NMR spectroscopy and mass spectrometry). The complex was found to react with HSA although noticeably slower than with the small molecules. An assessment of the cytotoxicity of the complex was performed with CH1 human ovarian, SW480 colon and A549 non-small cell lung cancer cells (96 h exposure) and was very similar to that observed with RAPTA-C. Consequently, targeting thiol functionalities in biomacromolecules represents another viable strategy for the preparation of RAPTA-bioconjugates for drug delivery.

Macromolecular ruthenium conjugates have also been developed that are based on synthetic dendrimers and polymers in order to exploit the EPR effect for selective tumor accumulation [70]. Dendrimer-based RAPTA delivery systems have been devised based on salicylaldimine dendritic ligands where RAPTA moieties with *p*-cymene and hexamethylbenzene (hmb) arene ligands were coordinated to dendrimers with 4, 8, 16 and 32 coordination points (Figure 17, conjugate **(43)**), resulting in polycationic metallodendrimers with ruthenium centers [71]. The cytotoxicity of the dendrimers was evaluated against the A2780, A2780cisR and HEK293 cell lines (72 h) and compared to mononuclear analogues (Figure 17 **(44)**). It was found that the cytotoxicity of the dendrimers increases as the generation number increases. For example, against the A2780 cell line the metallodendrimers with the *p*-cymene arene ligands possessed IC<sub>50</sub> values of 174, 9.3, 1.4 and 0.8 μM and for the

hexamethylbenzene analogues the values were 8.9, 6.2, 2.9 and 2.0  $\mu\text{M}$  for dendrimers with 4, 8, 16 and 32 RAPTA moieties, respectively. When expressing the  $\text{IC}_{50}$  values as concentration per metal center, the dendrimers with *p*-cymene ligands are more cytotoxic than the mononuclear analogue for dendrimers with 32 RAPTA molecules while for lower generations there seems to be only an additive effect. For the hexamethylbenzene analogues, the correlation of the  $\text{IC}_{50}$  value with the number of metal centers is less clear as only small increments in cytotoxicity are observed as the generation number increases and the cytotoxicity of the mononuclear analogue is relatively high ( $\text{IC}_{50}$  of 38, 93 and 60  $\mu\text{M}$  for A2780, A2780cisR and HEK293 cell lines, respectively). However, both dendrimer systems were more cytotoxic towards the A2780/A2780cisR cell lines than the HEK293 cell line (up to one order of magnitude) indicative of a certain level of selectivity whereas the mononuclear species are not selective. Incubation of the positively charged dendrimers with pBR322 plasmid DNA followed by analysis with gel electrophoresis revealed that incubations with dendrimers with 8 or more metal centers resulted in DNA aggregation. The positive charge of these dendrimers appears to be important in this aggregation process as related neutral metallodendrimers did not significantly aggregate DNA. These results show that, like the micellar systems above, the use of macromolecular metallodrug delivery systems can lead to increased cytotoxicity and also increased selectivity towards cancerous cell lines, and can also potentially alter the mechanism of action of the RAPTA structure, especially when release of the RAPTA fragment does not easily take place following cellular uptake.

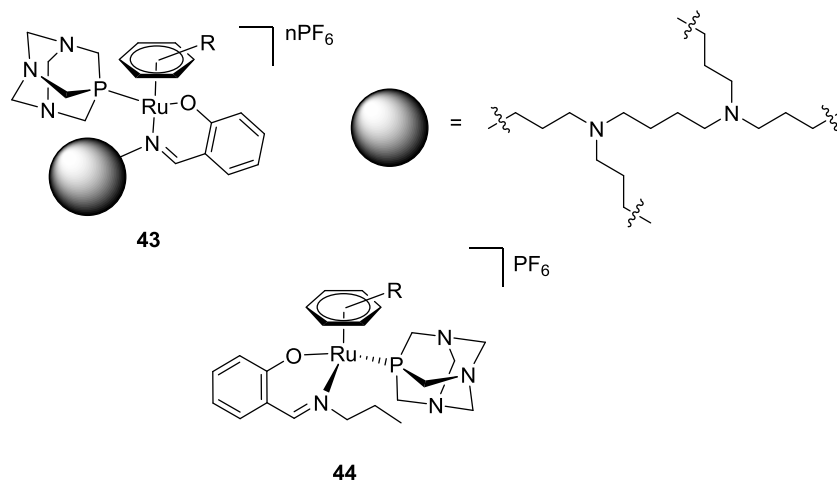


Figure 17. Generic structure of dendrimer-based polynuclear RAPTA derivatives and the mononuclear reference compound ( $n = 4, 8, 16, 32$ ; arene = *p*-cymene, hexamethylbenzene) [71].

RAPTA-C conjugation to a synthetic polymer has been achieved *via* the reaction of the PTA ligands with halogenides to form quaternary ammonium cations [72]. Synthetic routes were used to access a linear water-soluble *N*-(2-hydroxypropyl)methacrylamide/2-chloroethyl methacrylate (P(HPMA-CEMA)) copolymer that could be conjugated to RAPTA complexes. The P(HPMA-CEMA) copolymer was accessed through RAFT polymerisation and then modified through cleavage of the RAFT end-group. The chloride end-groups were then converted to iodide end-groups using the Finkelstein method to yield the modified P(HPMA-IEMA) copolymer. This was then reacted with PTA followed by  $[\text{RuCl}_2(\eta^6\text{-}p\text{-cymene})]_2$  to yield the water soluble RAPTA-C-containing copolymer, P(HPMA<sub>172</sub>-IEMA<sub>44</sub>-(RAPTA-C-EMA)<sub>44</sub>) (Figure 18; **(45)**). Assessment of the cytotoxicity of the RAPTA-C copolymer and RAPTA-C was performed against the OVCAR-3 human ovarian cancer cell line (SRB assay, 72 h exposure). Both exhibited very low cytotoxicity although the RAPTA co-polymer was less cytotoxic than RAPTA-C at equivalent concentrations of

ruthenium, postulated to be due to slow diffusion of the polymer across the cell membrane and the hydrodynamic diameter of the RAPTA co-polymer being too small to activate endocytosis. To improve on the P(HPMA<sub>172</sub>-IEMA<sub>44</sub>-(RAPTA-C-EMA)<sub>44</sub>) delivery system, degradable polymeric micelles were used to generate a degradable macromolecular drug that undergoes fast endocytosis [73]. An amphiphilic block copolymer was obtained from 2-chloroethyl methacrylate and 2-hydroxyethyl acrylate (with 1% fluorescein *O*-methacrylate as a fluorescent tag) as the hydrophilic RAPTA-bearing block and a biodegradable polylactide (PLA) hydrophobic block (Figure 18; bottom right). RAPTA-C was again incorporated into the polymer structure *via* conversion of the polymer chloride groups to iodide groups using the Finkelstein reaction, followed by reaction of the polymer with PTA and then addition of the dimer [RuCl<sub>2</sub>( $\eta^6$ -*p*-cymene)]<sub>2</sub>. Two RAPTA-containing polymers were obtained, PLA<sub>347</sub>-*b*-P(HEA<sub>74</sub>-(RAPTA-C-EMA)<sub>25</sub>) and PLA<sub>347</sub>-*b*-P(HEA<sub>140</sub>-(RAPTA-C-EMA)<sub>45</sub>) (Figure 18; **(46)**), from which self-assembled micelles were produced [diameter (DLS) 252 nm (PDI 0.332) and 555 nm (PDI 0.370), respectively]. It was found that the micelles disassembled when incubated with a hydrolase enzyme, indicating that in a cellular environment the micelles should degrade to release water-soluble RAPTA-C containing polymer fragments. The micelles were evaluated for cytotoxicity against the A2780, A2780cisR and OVCAR-3 cell lines (WST-1 assay, 72 h). Both RAPTA-containing micelles were more cytotoxic than RAPTA-C towards all cell lines. For example, IC<sub>50</sub> values of 15 and 51  $\mu$ M were observed against the A2780 cell line relative to 271  $\mu$ M for RAPTA-C. Fluorescence microscopy indicated that the micelles co-localized within the lysosomes (A2780 cell line, 3 h incubation) and ICP-MS revealed higher intracellular ruthenium concentrations in cells incubated with the micelles compared to RAPTA-C (up to a 12-fold increase in uptake).

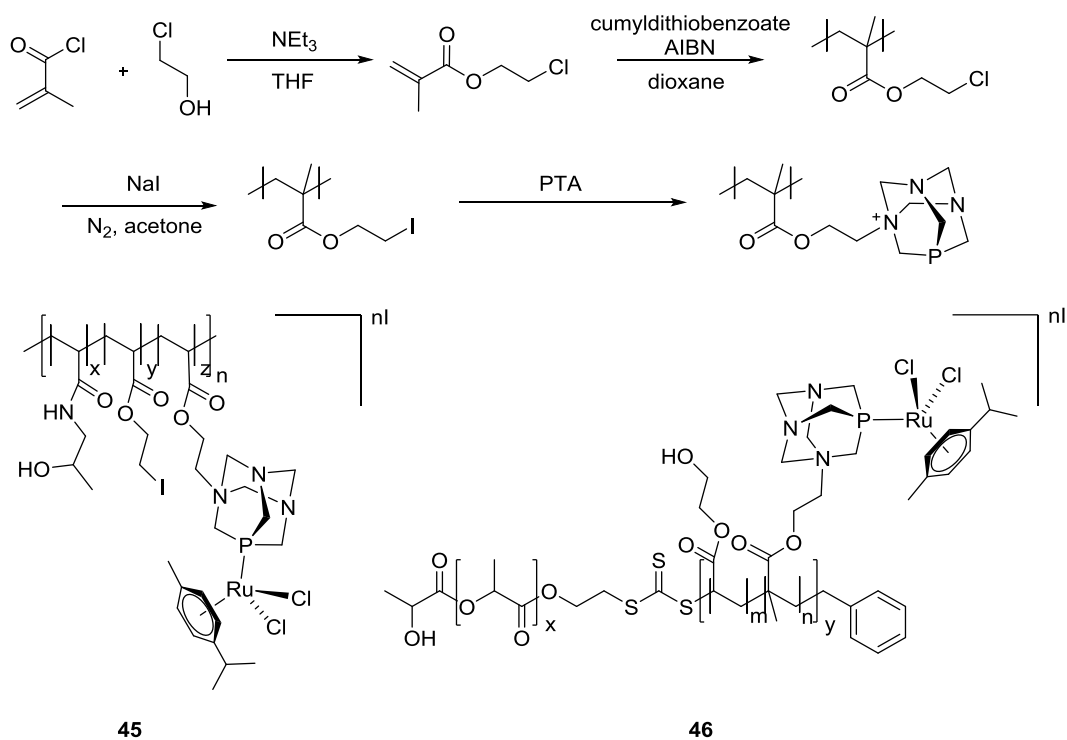


Figure 18. Synthetic route to PTA-containing polymers and polymers loaded with the RAPTA unit via the PTA ligand [72, 73].

Further studies resulted in the development of cyclic peptide-polymer nanotubes as carrier systems of RAPTA-C [74]. Two  $p(\text{HEA}_{58}\text{-co-CEMA}_{10})$  polymers were coupled to a cyclic peptide via an alkyne end-group, followed by exchange of the chloride groups of the CEMA side chains to iodide groups using the Finkelstein reaction. RAPTA-C was then covalently attached to the polymer via reaction of PTA with the iodide side-chains followed by addition of  $[\text{RuCl}_2(\eta^6\text{-}p\text{-cymene})]_2$ . The self-assembly of the RAPTA-C conjugates into nanotubes, via stacking of the cyclic peptides, was confirmed by static and dynamic light scattering and also transmission electron microscopy, with the hydrodynamic diameter of the observed aggregates being reported as between 500 and 1000 nm in solution. The activity of the assembled

nanotubes was assessed against the A2780 and A2780cisR cell lines. A [CP-p(HEA<sub>58</sub>-co-CEMA<sub>10</sub>)<sub>2</sub>] reference assembly, containing no RAPTA-C, was non-toxic (up to 590 µg mL<sup>-1</sup>) whilst the NT-RAPTA-C conjugate ((**47**) – structure not shown) was significantly more active against both cell lines (IC<sub>50</sub> of 15 µM (A2780) and 22 µM (A2780cisR)) compared to RAPTA-C (IC<sub>50</sub> of 271 µM (A2780) and 266 µM (A2780cisR)). These results likely reflect increased and/or a modulated uptake profile of the ruthenium complex when conjugated to the polymer compared to the free species.

Hence, incorporation of RAPTA-C into a suitably sized macromolecular carrier can result in increased cellular uptake of ruthenium leading to increased cytotoxicity. Such carrier systems should also facilitate the selective targeting of RAPTA to tumors, but to date *in vivo* studies demonstrating enhanced targeting of RAPTA-modified macromolecules have not been reported.

#### 4.3. Modulation of the lability of the anionic co-ligands of the RAPTA structure with chelating ligands

The incorporation of chelating ligands in place of the chlorido ligands in the RAPTA structure has been used to develop complexes resistant to decomposition in aqueous solution (Figure 19). In addition, further chelating ligands have been incorporated to modulate the lipophilicity of the complex.



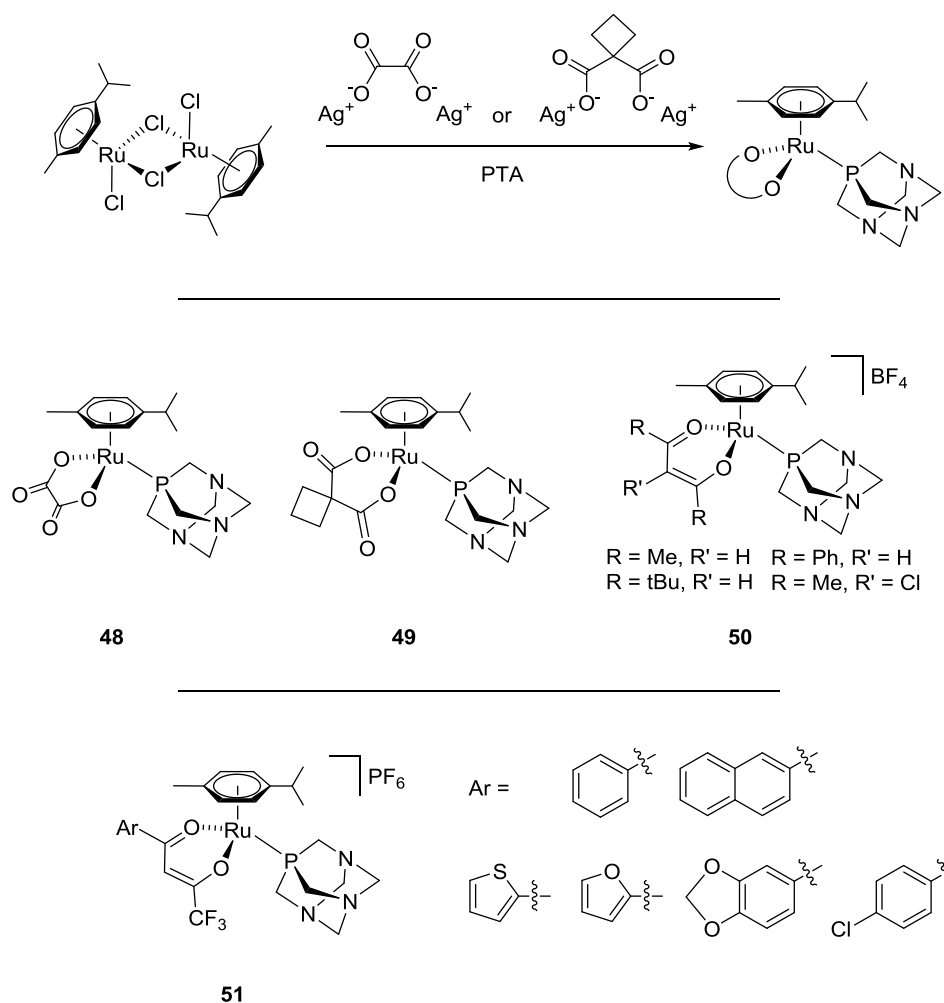


Figure 19. General scheme highlighting the synthetic route towards RAPTA compounds incorporating oxalato or 1,1-cyclobutanecarboxylato ligands (top) [75]. RAPTA compounds with chelating oxalato (oxali-RAPTA), 1,1-cyclobutyldicarboxylato (carbo-RAPTA) (middle) and acetylacetonato-derived co-ligands (middle and bottom) [76, 77].

The development of water-stable RAPTA analogues was approached as a route by which to circumvent the often difficult problems of identification and characterization of aquation products, and thus identification of the active solution species of the RAPTA complexes [75]. Reaction of  $[(\eta^6\text{-}p\text{-cymene})\text{RuCl}(\mu\text{-Cl})_2]$  with silver oxalate or 1,1-cyclobutanedicarboxylate followed by PTA addition (Figure 19, top) yielded the complexes  $[\text{Ru}(\eta^6\text{-}p\text{-cymene})(\text{C}_2\text{O}_4)(\text{PTA})]$  and  $[\text{Ru}(\eta^6\text{-}p\text{-cymene})(\text{C}_6\text{H}_6\text{O}_4)(\text{PTA})]$  (Figure 19, **(48)** and **(49)**, respectively). These complexes were 5- to 10-times more

soluble than RAPTA-C in water, and in aqueous solution both complexes were found to resist aquation, with no significant ligand exchange occurring in water compared to rapid aquation of RAPTA-C. On incubation of both complexes with single-stranded DNA for 24 h, followed by analysis with MALDI-TOF, multiple adducts were observed, formed largely through loss of the carboxylate ligand with a minor proportion of adducts formed through loss of the arene and/or PTA ligands. The  $pK_a$  of  $[\text{Ru}(\eta^6\text{-}p\text{-cymene})(\text{C}_2\text{O}_4)(\text{PTA})]$  and  $[\text{Ru}(\eta^6\text{-}p\text{-cymene})(\text{C}_6\text{H}_6\text{O}_4)(\text{PTA})]$  were estimated to be 2.35 and 2.64, respectively, compared to a value of 3.13 for RAPTA-C, indicating that like in RAPTA-C the PTA ligands of both complexes are not protonated under physiological conditions. Given the similar reactivity of both complexes with chelating ligands as RAPTA-C towards ssDNA, it is not surprising that they possess similar cytotoxicity profiles as RAPTA-C towards HT29, A549, T47D and MCF7 cell lines (72 h). Both compounds and RAPTA-C are mildly cytotoxic towards the HT29 cell line ( $\text{IC}_{50}$  values of 267, 265 and 436  $\mu\text{M}$ , respectively), and virtually non-toxic towards the other three cell lines ( $\text{IC}_{50} > 1000 \mu\text{M}$  in each case).

A further strategy employed to modulate the lipophilicity of the RAPTA structure, to increase cell uptake and hence cytotoxicity, involved the introduction of 1,3-diketonato ligands ( $\text{R}_2\text{acac}$ ,  $\text{R} = \text{Me}, \text{tBu}, \text{Ph}$ ; Figure 19, structure **(50)**) of varying lipophilicity, at the sites normally occupied by the labile chlorido ligands [76]. The monocationic complexes, *i.e.*  $[\text{Ru}(\eta^6\text{-}p\text{-cymene})(\text{R}_2\text{acac}/\text{R}_2\text{acac}\text{-Cl})(\text{PTA})][\text{BF}_4]$ , slowly undergo aquation in 5 mM NaCl aqueous solution and form RAPTA-C in 100 mM NaCl solution. The cytotoxicity of the compounds against A2780 human ovarian cancer and A549 lung carcinoma cell lines (72 h) revealed good activity against the A2780 cell line ( $\text{IC}_{50}$  7–15  $\mu\text{M}$ ) and moderate activity against the A549 cell line (50–97  $\mu\text{M}$ ), with the exception of  $[\text{Ru}(\eta^6\text{-}p\text{-cymene})(\text{Me}_2\text{acac})(\text{PTA})][\text{BF}_4]$  ( $\text{IC}_{50} > 2000 \mu\text{M}$ ).

A related series of compounds was later reported which incorporated an asymmetrically functionalised diketonato ligand ( $F_3C$ -acac-Ar) within the RAPTA structure (Figure 19, **(51)**); with the  $CF_3$  substituent remaining constant whilst the aromatic substituent was modulated [77]. This series of compounds was relatively stable (<5% conversion to secondary species) for up to 48 h in aqueous solution (3% DMSO). The activity of the complexes was assessed (MTT assay, 72 h) against CH1 ovarian cancer ( $IC_{50}$  8–46  $\mu M$ ), MG63 osteosarcoma ( $IC_{50}$  17–41  $\mu M$ ) and HaCaT nonmalignant keratinocytes-derived ( $IC_{50}$  >100  $\mu M$  except the 4-chlorophenyl-substituted acac-containing complex (72  $\mu M$ )) cell lines, with selected examples also equally active towards the A2780 and A2780cisR cell lines. These results indicate a certain level of selectivity between the cell lines with relatively small differences in activity being observed as the structure of the diketonate ligand was modulated. These complexes were found, in general, to act via a cytostatic mode of action as indicated by selected examples inducing cellular accumulation in the  $G_0/G_1$  phase, although the 4-chlorophenyl-substituted acac-containing complex was found to induce apoptosis to significant extent. The cytotoxicity of these complexes was not related to the generation of reactive oxygen species.

These studies demonstrate that the labile chlorido ligands of the RAPTA structure may be readily exchanged for chelating ligands without loss of reactivity towards model substrates, while increasing water solubility and cellular cytotoxicity relative to parent RAPTA analogues. It may be envisaged that careful choice of substituents of the chelating ligand will allow the ligand exchange rates to be tuned to a cellular environment. Moreover, the complex may be endowed with dual functionality through the release of the chelating ligand containing a bioactive organic moiety able to interact with biomolecular targets. In this regard RAPTA derivatives containing chelating

curcuminoid ligands (Figure 20, **(52)**), where curcumin itself exhibits antitumoral effects, have been evaluated for chemotherapeutic properties [78].

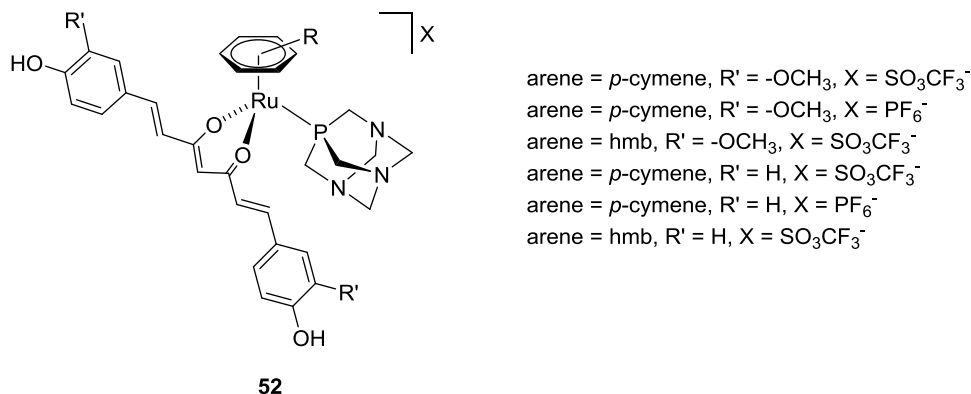


Figure 20. Curcuminato complexes derived from the RAPTA structure [78].

A comparison of the aqueous stability of two curcuminato complexes (arene = *p*-cymene, R' = OCH<sub>3</sub> or H, X = SO<sub>3</sub>CF<sub>3</sub>) was performed in 5 and 100 mM NaCl solutions. Whereas the curcuminato complex (R' = OCH<sub>3</sub>) was inert to ligand substitution in both conditions over 7 days, the curcuminoid ligand of the complex with R' = H was labile, being replaced by two chlorido ligands in 100 mM NaCl after 24 hours. Despite this difference in behavior with respect to ligand substitution, all complexes were highly cytotoxic towards the A2780 and A2780cisR cell lines (IC<sub>50</sub> 0.14–1.15 and 0.27–1.18 μM, respectively) and all the complexes were more active than cisplatin and, importantly, curcumin (IC<sub>50</sub> in A2780 = 8 μM and in A2780cisR = 11 μM). Interestingly, all complexes were up to 70-fold less active towards the HEK293 cell line (IC<sub>50</sub> 4.5–30 μM), indicative of selectivity for cancer cells.

Two RAPTA analogues with β-ketoamine ligands coordinated in place of the labile chlorido ligands of the RAPTA structure were reported as part of a wider study into the biological activity of β-ketoamine ligands coordinated to ruthenium (Figure 21, **(53)**)

[79]. The cytotoxicity of the two RAPTA derivatives, which were sparingly soluble in aqueous solution, and the  $\beta$ -ketoamine ligands was determined against the A2780 and A2780cisR cell lines (72 h). The  $\beta$ -ketoamine ligand containing a naphthyl-substituent was cytotoxic towards both cell lines ( $IC_{50}$  values of 14.4 and 14.0  $\mu$ M in A2780 and A2780cisR cell lines, respectively), whereas the ligand with the phenyl-substituent was comparatively non-toxic ( $IC_{50}$  values of 275 and 271  $\mu$ M in A2780 and A2780cisR cell lines, respectively). The complex with the coordinated naphthyl-substituted  $\beta$ -ketoamine ligand yielded  $IC_{50}$  values of 6.0 and 6.1  $\mu$ M against the A2780 and A2780cisR cell lines, respectively, whereas the complex with the coordinated phenyl-substituted  $\beta$ -ketoamine ligand yielded  $IC_{50}$  values of 18.9 and 19.5  $\mu$ M. These complexes are equally active in the A2780 parent cell line and the cisplatin-resistant strain, indicating they are unaffected by cisplatin-resistance mechanisms. The bulky  $\beta$ -ketoamine ligands appear to increase complex lipophilicity relative to RAPTA-C and this likely plays a role in their high activity through increased cellular uptake and modulation of cellular localization. However, for the complex with the naphthyl-substituted  $\beta$ -ketoamine ligand the high cytotoxicity of the ligand itself probably contributes to the observed cytotoxicity of the complex whereas the complex with the phenyl-derived  $\beta$ -ketoamine ligand possesses a high cytotoxicity not apparently related to the ligand.

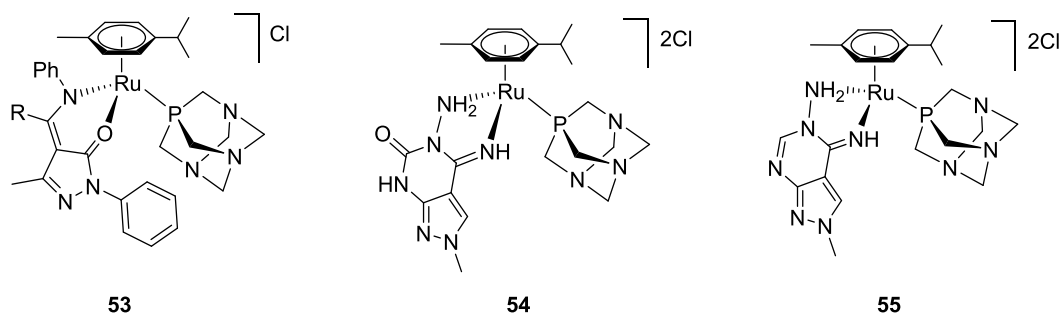


Figure 21. RAPTA compounds with chelating  $N,O$   $\beta$ -ketoamine (R = phenyl, naphthyl) [79] and  $N,N$  pyrazolo-[3,4-*d*]pyrimidine co-ligands [80].

Two RAPTA analogues were also reported as members of a wider series in a study developing organometallic inhibitors of the human A<sub>3</sub> adenosine receptor (hA<sub>3</sub>AR), which is a prospective chemotherapeutic target in the treatment of cancer and is overexpressed in various tumors [80]. The complexes incorporated chelating pyrazolo-[3,4-*d*]pyrimidine ligands (Figure 21, **(54)** and **(55)**) in place of the chlorido ligands of the RAPTA structure to create novel organometallic inhibitors based on the pyrazolo[4,3-*e*]-1,2,4-triazolo-[1,5-*c*]pyrimidine scaffold, examples of which are known to inhibit the hA<sub>3</sub> receptor in the nM range. The binding affinities of the complexes were assessed against human hA<sub>1</sub>, hA<sub>2</sub> and hA<sub>3</sub> adenosine receptors expressed in Chinese hamster ovary (CHO) cells. The RAPTA-based inhibitors displays slightly lower binding affinities towards the receptors relative to analogues bearing a chlorido ligand in place of the PTA ligand, attributed to the increased steric bulk of the inhibitor due to the PTA ligand. However, these RAPTA-based inhibitors display selective inhibition towards the hA<sub>3</sub> receptor highlighting the value in modulating the ligands around the ruthenium ion to tune selectivity for a receptor of interest.

#### 4.4. Introduction of additional phosphine ligands into the RAPTA framework

Other studies focusing on the development of more hydrophobic RAPTA analogues based on the substitution of one chloride ligand by a phosphine ligand have been undertaken in an attempt to increase their uptake into cancer cells and thus modulate their cytotoxicity [57]. Two chiral-at-metal center RAPTA complexes were reported as racemic mixtures, *i.e.*, analogues of RAPTA-C and [Ru( $\eta^6$ -C<sub>6</sub>H<sub>5</sub>CH<sub>2</sub>CH<sub>2</sub>OH)Cl<sub>2</sub>(PTA)] with a PPh<sub>3</sub> ligand in place of one chlorido ligand (Figure 22, **(56)** and **(57)**). The cytotoxicity of the novel compounds was assessed against the TS/A and HBL-100 cell

lines (72 h). The increased hydrophobicity of  $[\text{Ru}(\eta^6\text{-C}_6\text{H}_5\text{CH}_2\text{CH}_2\text{OH})\text{Cl}(\text{PPh}_3)(\text{PTA})][\text{BF}_4]$  (**57**) resulted in an increase in cytotoxicity towards both the TS/A and HBL-100 cell lines ( $\text{IC}_{50}$  124 and 82  $\mu\text{M}$ , respectively) relative to the inactive  $[\text{Ru}(\eta^6\text{-C}_6\text{H}_5\text{CH}_2\text{CH}_2\text{OH})\text{Cl}_2(\text{PTA})]$  (**10**) analogue ( $\text{IC}_{50} > 300 \mu\text{M}$  in both cell lines). This increase in cytotoxicity was mirrored by increased uptake into TS/A cells relative to  $[\text{Ru}(\eta^6\text{-C}_6\text{H}_5\text{CH}_2\text{CH}_2\text{OH})\text{Cl}_2(\text{PTA})]$ . Relative to RAPTA-C (**1**),  $[\text{Ru}(\eta^6\text{-}i\text{p-cymene})\text{Cl}(\text{PPh}_3)(\text{PTA})][\text{BF}_4]$  (**56**) was more active against the HBL-100 healthy cell line ( $\text{IC}_{50} > 300$  vs. 37  $\mu\text{M}$ , respectively) suggesting that increased hydrophobicity decreases cancer cell selectivity. In protein binding experiments it was observed that  $[\text{Ru}(\eta^6\text{-C}_6\text{H}_5\text{CH}_2\text{CH}_2\text{OH})\text{Cl}(\text{PPh}_3)(\text{PTA})][\text{BF}_4]$  (**57**) was less reactive towards ubiquitin and cytochrome-c than RAPTA-C, and more reactive towards a 14-mer oligonucleotide. The low aqueous solubility of  $[\text{Ru}(\eta^6\text{-}i\text{p-cymene})\text{Cl}(\text{PPh}_3)(\text{PTA})][\text{BF}_4]$  (**56**) prevented a similar analysis. This work exemplified that by tuning the steric bulk and hydrophobicity of the RAPTA complexes selectivity for reactivity towards nucleic acid or protein targets could be modulated, leading to increased cytotoxicity but reduced selectivity. These ideas were subsequently confirmed in binding studies to chromatin that compare RAPTA-C with  $[\text{Ru}(\eta^6\text{-}i\text{p-cymene})(\text{en})\text{Cl}]^+$  (see below) [81].

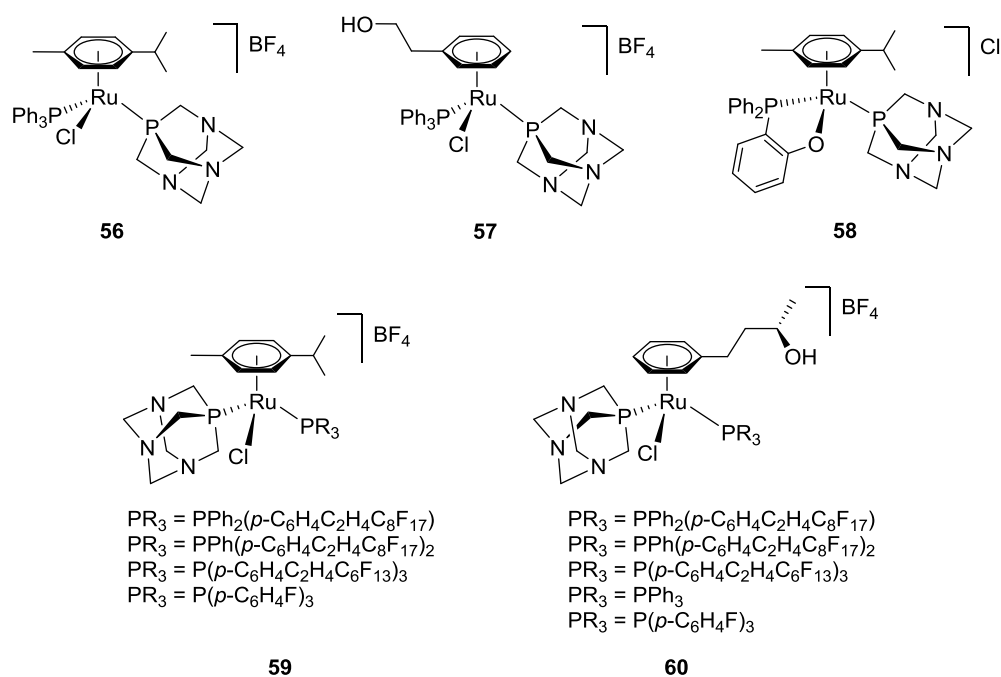


Figure 22. The RAPTA framework modified with additional phosphorus-containing ligands [57, 82, 83].

In contrast, the novel bis-phosphine complex, [Ru( $\eta^6$ -cymene)(PPh<sub>2</sub>(*o*-C<sub>6</sub>H<sub>4</sub>O)- $\kappa^2$ -*P,O*)(PTA)]<sup>+</sup> (Figure 22, **(58)**), containing the chelating phosphine group ortho-oxy-triphenylphosphine, was inert in aqueous solution, essentially unreactive towards a single stranded oligonucleotide and only mildly reactive towards ubiquitin compared to RAPTA-C [82]. Despite being largely inert under physiological conditions, this complex was moderately cytotoxic towards the A2780 cell line (72 h, IC<sub>50</sub> = 138  $\mu$ M). It was postulated that this activity may be due to non-covalent interactions mediated by the chelating phosphine ligand.

A series of RAPTA compounds of the general formula [Ru( $\eta^6$ -arene)Cl(PR<sub>3</sub>)(PTA)] [BF<sub>4</sub>] (arene = *p*-cymene or 4-phenyl-2-butanol; PR<sub>3</sub> = PPh<sub>2</sub>(*p*-C<sub>6</sub>H<sub>4</sub>C<sub>2</sub>H<sub>4</sub>C<sub>8</sub>F<sub>17</sub>), PPh(*p*-C<sub>6</sub>H<sub>4</sub>C<sub>2</sub>H<sub>4</sub>C<sub>8</sub>F<sub>17</sub>)<sub>2</sub>, P(*p*-C<sub>6</sub>H<sub>4</sub>C<sub>2</sub>H<sub>4</sub>C<sub>6</sub>F<sub>13</sub>)<sub>3</sub>, PPh<sub>3</sub> or P(*p*-C<sub>6</sub>H<sub>4</sub>F)<sub>3</sub>, Figure 22, structures **(59)** and **(60)**) were developed to assess the anticancer potential of RAPTA-type complexes in thermotherapy [83]. Thermotherapy (or hyperthermia) is used to



improve drug efficacy by selective heating of the tumor to typically 41–42 °C; however, the small molecule drugs used in this duotherapy are not designed for such an application, *e.g.*, cisplatin is widely used [84]. Phosphine ligands bearing perfluorinated chains were incorporated into the RAPTA structure to endow the complexes with thermomorphic properties since highly fluorinated compounds are known to undergo large changes in solubility with small changes in temperature [85]. The aim of combining the RAPTA structure with perfluorinated substituents was to obtain complexes with increased solubility on raising the temperature, *i.e.*, so that at 37 °C they are insoluble and cannot penetrate cells whereas at 41–42 °C they solubilize and can cross cell membrane (specifically at the heated tumor site). The majority of complexes had no or very limited water solubility, however, the aquation behavior of the water-soluble compound  $[\text{Ru}(\eta^6\text{-4-phenyl-2-butanol})\text{Cl}(\text{PPh}_2(p\text{-C}_6\text{H}_4\text{C}_2\text{H}_4\text{C}_8\text{F}_{17}))(\text{PTA})][\text{BF}_4]$  (Figure 22, bottom) was examined in  $\text{D}_2\text{O}$  by NMR spectroscopy. The complex undergoes ligand exchange over several hours to yield  $[\text{Ru}(\eta^6\text{-4-phenyl-2-butanol})(\text{D}_2\text{O})(\text{PPh}_2(p\text{-C}_6\text{H}_4\text{C}_2\text{H}_4\text{C}_8\text{F}_{17}))(\text{PTA})]^{2+}$ , revealing the lability of the chlorido ligand (addition of 100 mM NaCl displaced the aqua ligand to regenerate the original complex). The solubility of the compounds as a function of temperature was assessed and the solubility of  $[\text{RuCl}(\eta^6\text{-4-phenyl-2-butanol})(\text{PPh}_2(p\text{-C}_6\text{H}_4\text{C}_2\text{H}_4\text{C}_8\text{F}_{17}))(\text{PTA})][\text{BF}_4]$  was found to increase from 2.5 mM at 20 °C to 30 mM at 45 °C, while  $[\text{Ru}(\eta^6\text{-cymene})\text{Cl}(\text{PPh}_2(p\text{-C}_6\text{H}_4\text{C}_2\text{H}_4\text{C}_8\text{F}_{17}))(\text{PTA})]^+$  and  $[\text{Ru}(\eta^6\text{-4-phenyl-2-butanol})\text{Cl}(\text{PPh}_2(p\text{-C}_6\text{H}_4\text{C}_2\text{H}_4\text{C}_8\text{F}_{17}))_2(\text{PTA})]^+$  were essentially insoluble at 37 °C but possessed a solubility in excess of 0.3 mM at 42 °C. The cytotoxicity of the compounds was assessed against the A2780 and A2780cisR cell lines (72 h). Against the A2780 cell line the fluorinated-chain compounds exhibited high to moderate cytotoxicity ( $\text{IC}_{50}$  1.5–97  $\mu\text{M}$ ) and in general only a slight decrease in activity against the A2780cisR cell

line ( $IC_{50}$  5 to  $>200 \mu\text{M}$ ) was observed. Compared to  $[\text{Ru}(\eta^6\text{-4-phenyl-2-butanol})\text{Cl}(\text{PPh}_3)(\text{PTA})]^+$  with  $IC_{50}$  values of  $184 \mu\text{M}$  in A2780 and  $>200 \mu\text{M}$  in A2780cisR, the fluorinated-chain analogues are significantly more cytotoxic. The cytotoxicity of  $[\text{Ru}(\eta^6\text{-4-phenyl-2-butanol})\text{Cl}(\text{PPh}_2(p\text{-C}_6\text{H}_4\text{C}_2\text{H}_4\text{C}_8\text{F}_{17}))(\text{PTA})][\text{BF}_4]$  and  $[\text{Ru}(\eta^6\text{-cymene})\text{Cl}(\text{PPh}_2(p\text{-C}_6\text{H}_4\text{C}_2\text{H}_4\text{C}_8\text{F}_{17}))(\text{PTA})][\text{BF}_4]$ , exhibiting temperature-dependent solubility, were evaluated against the A2780 and A2780cisR cell lines at  $37^\circ\text{C}$  and also under identical conditions except with a 2 h incubation time at  $42^\circ\text{C}$  following addition of the compound. Both compounds were slightly more cytotoxic towards both cell lines after the brief heating period (e.g., the  $IC_{50}$  of  $[\text{Ru}(\eta^6\text{-cymene})\text{Cl}(\text{PPh}_2(p\text{-C}_6\text{H}_4\text{C}_2\text{H}_4\text{C}_8\text{F}_{17}))(\text{PTA})][\text{BF}_4]$  against the A2780 cell line was  $3 \mu\text{M}$  and  $2 \mu\text{M}$  at  $37^\circ\text{C}$  and  $42^\circ\text{C}$ , respectively). A further series of complexes, featuring imidazole ligands functionalized *via* click chemistry with a range of hydrophobic tails (Figure 23, structures **(61)** and **(62)**), was also reported [86]. The *p*-cymene compounds (with the exception of the amine-bearing analogue) were poorly soluble in water. The stability of the soluble compounds in aqueous solution was examined by NMR spectroscopy, showing the complexes to be stable with no changes to the spectra after addition of  $100 \text{ mM NaCl}$  over a period of 72 hours. The cytotoxicity of the compounds was examined in the A2780 and A2780cisR cell lines to yield a range of  $IC_{50}$  values ranging from modestly cytotoxic to essentially inactive ( $34$  to  $>300 \mu\text{M}$ ). In general, compounds with a more positive  $\log P_{\text{ow}}$  coefficient were more active although there are several exceptions. Compounds with the phenyl-2-ethanol arene ligand were also found to exhibit cytotoxic selectivity towards the A2780/A2780cisR cell lines ( $IC_{50} = 50\text{--}144 \mu\text{M}$ ) compared to the healthy HCEC endothelial cell line ( $IC_{50} >500 \mu\text{M}$ ). These results indicated that the increased solubility of the compounds at elevated temperatures may lead to more efficacious compounds and, subsequently,

this concept was extended to a new series of compounds that display remarkable cytotoxic discrimination at 37 °C and 42 °C [87].

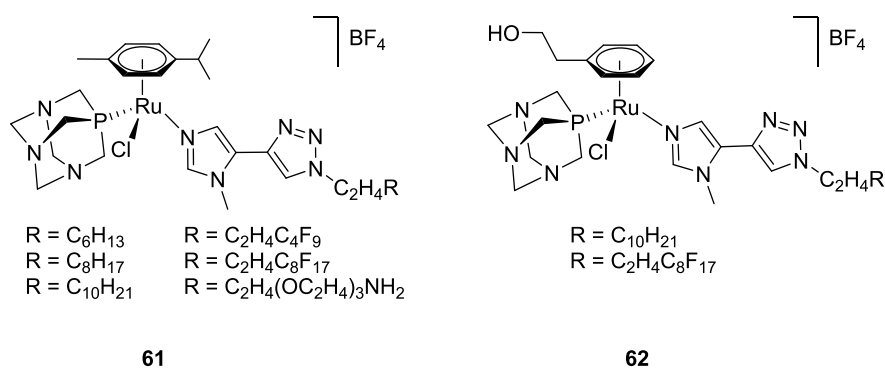


Figure 23. RAPTA-type compounds with imidazole-derived co-ligands modified through click chemistry [86].

#### 4.5. RAPTA-type compounds with $\eta^5$ -coordinated cyclopentadienyl rings

Ruthenium cyclopentadienyl compounds form a growing class of compounds being evaluated for their *in vitro* cytotoxicity. Several examples of these compounds have been developed with a PTA ligand incorporated into the structure forming structures closely related to the early RAPTA compounds (Figure 24, structures **(63)**-**(66)**).

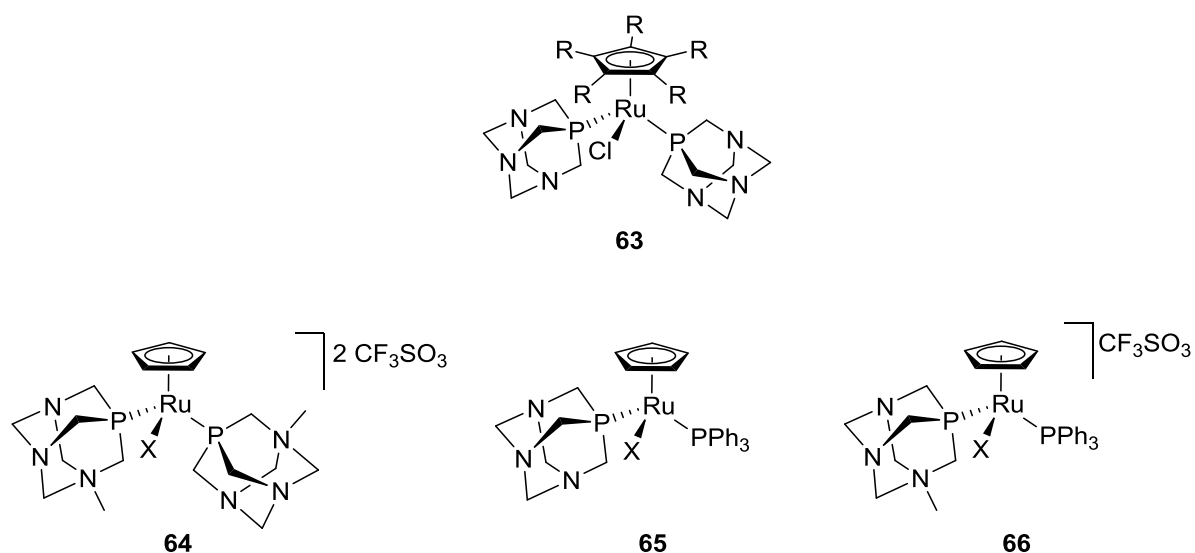


Figure 24. RAPTA-derived cyclopentadienyl-Ru(PTA) complexes (R = H, Me; X = Cl, I) [88, 89].

The antiproliferative activity of piano-stool compounds containing cyclopentadienyl ligands was initially reported for  $[\text{Ru}(\eta^5\text{-C}_5\text{R}_5)\text{Cl}(\text{PTA})_2]$  (R = H, Me) compounds (**63**) [88].  $[\text{Ru}(\eta^5\text{-C}_5\text{H}_5)\text{Cl}(\text{PTA})_2]$  was inactive at any tested concentration against the TS/A murine adenocarcinoma cell line whereas  $[\text{Ru}(\eta^5\text{-C}_5\text{Me}_5)\text{Cl}(\text{PTA})_2]$  exhibits antiproliferative effects starting at a concentration of 10  $\mu\text{M}$  (an  $\text{IC}_{50}$  value was not specified). The interaction of  $[\text{Ru}(\eta^5\text{-C}_5\text{H}_5)\text{Cl}(\text{PTA})_2]$  and the related compounds  $[\text{Ru}(\eta^5\text{-C}_5\text{H}_5)\text{Cl}(\text{mPTA})_2][\text{CF}_3\text{SO}_3]_2$  (**64**),  $[\text{Ru}(\eta^5\text{-C}_5\text{H}_5)\text{Cl}(\text{PPh}_3)(\text{PTA})]$  (**65**) and  $[\text{Ru}(\eta^5\text{-C}_5\text{H}_5)\text{Cl}(\text{mPTA})(\text{PPh}_3)][\text{CF}_3\text{SO}_3]$  (**66**) (mPTA = *N*-methyl-1,3,5-triaza-7-phosphaadamantane; Figure 24) with DNA was probed *via* mobility shift assays [89]. Retardation of scDNA in mobility shift assays was observed in each case when incubated with the complexes, indicative of coordination to the complexes and destabilization of the duplex scDNA. Iodido analogues of the complexes, *i.e.*,  $[\text{Ru}(\eta^5\text{-C}_5\text{H}_5)\text{I}(\text{PTA})_2]$ ,  $[\text{Ru}(\eta^5\text{-C}_5\text{H}_5)\text{I}(\text{PPh}_3)(\text{PTA})]$ ,  $[\text{Ru}(\eta^5\text{-C}_5\text{H}_5)\text{I}(\text{mPTA})_2][\text{CF}_3\text{SO}_3]_2$  and  $[\text{Ru}(\eta^5\text{-C}_5\text{H}_5)\text{I}(\text{mPTA})(\text{PPh}_3)][\text{CF}_3\text{SO}_3]$  (Figure 24), do not interact with DNA indicating

the Ru–I bond is more stable and cannot be displaced by *N*-containing nucleophiles of DNA. Cell-based cytotoxicity assays were not performed with these compounds, but as shown from the earlier report on  $[\text{Ru}(\eta^5\text{-C}_5\text{H}_5)\text{Cl}(\text{PTA})_2]$ , the ability of a complex to coordinate to DNA does not necessarily translate to antiproliferative activity.

The cytotoxicity of two compounds constructed with cyclopentadienyl rings that were heavily functionalised with sterically bulky, lipophilic substituents (Figure 25, **67**) was evaluated on the A2780 and A2780cisR cell lines, 72 h exposure) [90]. Both compounds displayed a similar level of cytotoxicity towards both cell lines ( $\text{IC}_{50} = 4\text{--}10 \mu\text{M}$ ) and are significantly more active than  $[\text{Ru}(\eta^5\text{-C}_5\text{H}_5)\text{Cl}(\text{PTA})_2]$ . The increased activity of these two complexes is likely due to the increased lipophilicity of the complexes as well as facilitated exchange reactions due to the presence of the bulky cyclopentadienyl-type ligands.

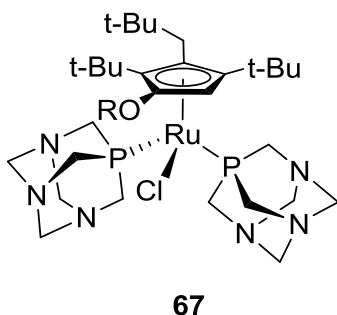


Figure 25. Ru complexes with sterically bulky Cp derivatives (R = Me, Et) [90].

Further studies extended the series of ruthenium(II)-cyclopentadienyl complexes to include examples with three phosphine co-ligands (Figure 26) and examined their interactions with scDNA using the shift mobility assay [91]. The chiral complex  $[\text{Ru}(\eta^5\text{-C}_5\text{H}_5)(\text{mTPPMS})(\text{PTA})(\text{PPH}_3)]$  (**68**) (mTPPMS =  $\text{Ph}_2\text{P}(3\text{-OSO}_2\text{C}_6\text{H}_4)^-$ ) was found to retard scDNA whereas no interactions with scDNA were observed for  $[\text{Ru}(\eta^5\text{-$

$C_5H_5)(mTPPMS)(mPTA)(PPh_3)[CF_3SO_3]$  (**69**),  $[Ru(\eta^5-C_5H_5)(mTPPMS)(PTA)_2]$  (**70**),  $Na[Ru(\eta^5-C_5H_5)(mTPPMS)_2(PTA)]$  (**71**) and  $[Ru(\eta^5-C_5H_5)(mTPPMS)_2(mPTA)]$  (**72**). These complexes do not undergo ligand exchange reactions in water implying that the metal center may not react with the *N*-based nucleophilic groups of DNA. For  $[Ru(\eta^5-C_5H_5)(mTPPMS)(PTA)(PPh_3)]$  (**68**) and other *mTPPMS*-containing triphosphine complexes interacting with DNA [91] it was postulated that the *mTPPMS* ligand may be responsible for the observed interactions. This hypothesis was supported by the observation that *mTPPMS* alone was able to cleave DNA under the incubation conditions.

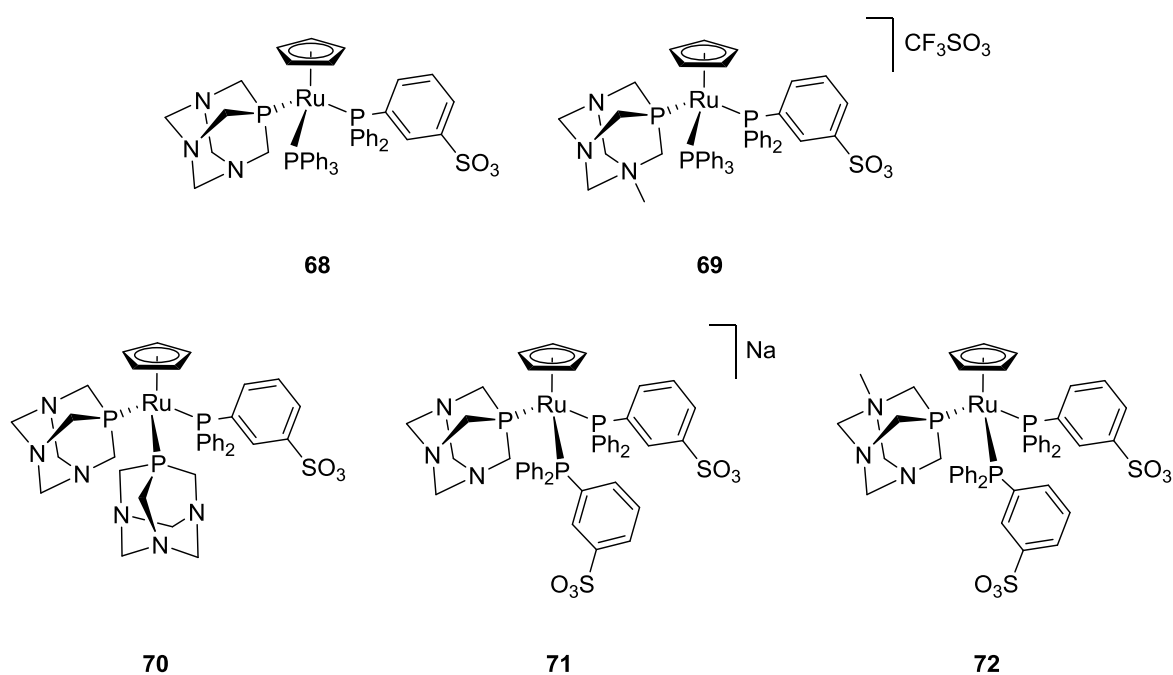


Figure 26. Structures of inert  $RuCp$  compounds featuring three phosphine co-ligands [91].

A series of complexes of formula  $\{[Ru(Cp)(PTA)_2]_xL\}$  and  $\{[Ru(Cp)(PPh_3)(PTA)]_xL\}$  ( $L$  = thiopurine derived ligands,  $x = 1$ ) (**(73)-(76)**) and dinuclear analogues ( $L$  = bis-thiopurine ligands,  $x = 2$ ) (**(77)** and **(78)**) (Figure 27) was reported [92]. The mononuclear ruthenium complexes were stable in solution for more than 2 days. The

measured log  $P_{OW}$  values reflect the nature of the phosphine ligands (2 PTA versus 1 PTA and 1  $PPh_3$ ) and also the lipophilicity of the thiopurine ligand substituents. The mononuclear complexes with two PTA ligands are less cytotoxic ( $IC_{50} >50 \mu M$ ) towards T2 (174 x CEM.T2) cells than those bearing one PTA ligand and one  $PPh_3$  ligand, where the most cytotoxic compound ( $IC_{50} 2-10 \mu M$ ) was the one with the highest log  $P_{OW}$  value (1.54). All complexes were less cytotoxic towards the cisplatin-resistant SKOV3 cell line ( $IC_{50} >50 \mu M$ ) and the dinuclear compounds were all shown to have poor antiproliferative activities.

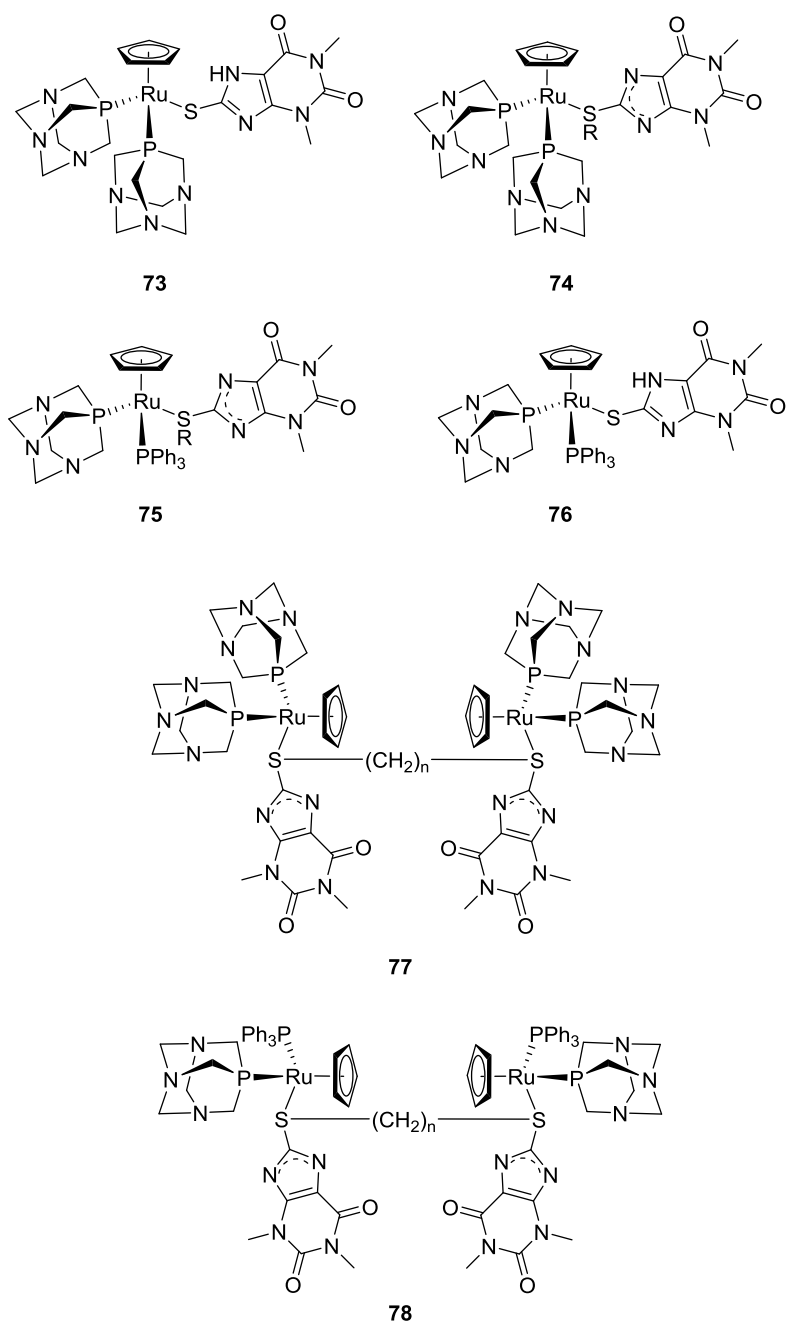


Figure 27. Mono- and dinuclear RuCp complexes with thiopurines (R = Me, CH<sub>2</sub>Ph; n = 1, 2, 3) [92].

Ruthenium cyclopentadienyl complexes with alkylated PTA ligands (Figure 28, structure **(79)**) were evaluated for antiproliferative activity (72 h) against the SKOV3 and SW480 cell lines and compared with [Ru( $\eta^5$ -C<sub>5</sub>H<sub>5</sub>)(PPh<sub>3</sub>)(PTA-Me)Cl]I and [Ru( $\eta^5$ -C<sub>5</sub>H<sub>5</sub>)(PPh<sub>3</sub>)(PTA)Cl] [93]. The ligands (PTA-Me)I and (PTA-C<sub>12</sub>H<sub>25</sub>)PF<sub>6</sub> were



found to have low toxicity against the SKOV3 cell line ( $IC_{50} > 50 \mu M$ ) whereas the PTA- $C_{16}H_{33}^+$  and PTA- $C_{18}H_{37}^+$  ligands were more cytotoxic with  $IC_{50}$  values of 36 and 42  $\mu M$ , respectively. The complexes were more cytotoxic than the ligands with  $IC_{50}$  values of 35, 9.1, 9.6 and 9.5  $\mu M$  for  $[Ru(\eta^5-C_5H_5)(PPh_3)(PTA-Me)Cl]I$ ,  $[Ru(\eta^5-C_5H_5)(PPh_3)(PTA-C_{12}H_{25})Cl]PF_6$ ,  $[Ru(\eta^5-C_5H_5)(PPh_3)(PTA-C_{16}H_{33})Cl]PF_6$  and  $[Ru(\eta^5-C_5H_5)(PPh_3)(PTA-C_{18}H_{37})Cl]PF_6$ , respectively. Similar cytotoxicities were obtained against the SW480 cell line, with the longer chain PTA-bearing complexes being more cytotoxic than the complex with the methylated PTA ligand. In contrast,  $[Ru(\eta^5-C_5H_5)(PPh_3)(PTA)]$  was not cytotoxic ( $IC_{50} > 100 \mu M$  in both cell lines). It is likely that, relative to complexes bearing PTA or PTA-Me ligands, the cellular uptake, localization and biomolecular interactions of those complexes bearing cationic amphiphilic PTA ligands is significantly modulated, leading to the increased cytotoxicity.

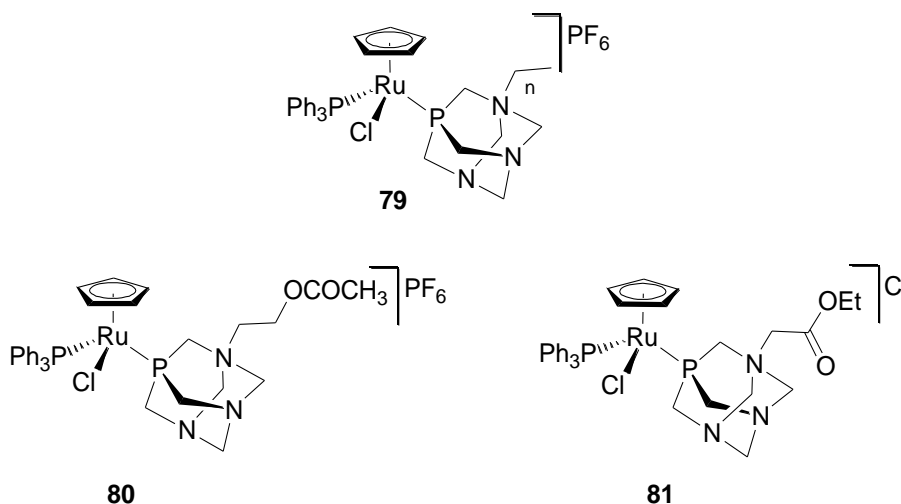


Figure 28. Functionalization of the PTA ligand in RuCp complexes ( $n = 11, 15, 17$ ) [93, 94].

Structurally related PTA analogues of acetylcholine and trimethylglycine, two model compounds containing quaternary ammonium groups [94], were used to generate  $[Ru(\eta^5-C_5H_5)(PPh_3)(PTA-CH_2CH_2CO_2CH_3)Cl][PF_6]$  (**80**) and  $[Ru(\eta^5-$

$C_5H_5)(PPh_3)(PTA-CH_2CO_2Et)Cl]Cl$  (**81**) (Figure 28, bottom), which were evaluated for antiproliferative activity against A2780, SKOV3 and K562 cells (72 h). Both compounds were highly cytotoxic towards all three cancer cell lines with  $IC_{50}$  values in the ranges of 4.7-5.1 and 5.5-8.3  $\mu M$ , respectively. The modified PTA ligands were designed to be structural analogues of naturally occurring quaternary ammonium groups, including the neurotransmitter acetylcholine. Further work is required to determine if there is any specific activity resulting from the structural similarity of the PTA-derived ligands to these naturally occurring ammonium ions or if the high cytotoxicity is simply due to modulation of the amphiphilic nature of the ruthenium complex.

## 5. Mechanistic studies

### 5.1. Plasma protein interaction of RAPTA compounds

Human serum transferrin and human serum albumin are believed to play significant roles in the modes of action of anticancer metallodrugs, both being considered for the transport, delivery and/or storage of various metallodrugs. Albumin binds to a wide range of drugs immediately after their intravenous application [95], and transferrin is an iron-binding blood plasma glycoprotein responsible for controlling the level of free iron in biological fluids [96]. Although the iron affinity of the protein is extremely high other metals can bind to transferrin and due to the overexpression of transferrin receptors on tumor cells, transferrin-drug delivery is an attractive approach for targeted cancer therapy. Mass spectrometric analysis of albumin and transferrin drug adducts is hampered by their high molecular weight (67 and 80 kDa, respectively). To overcome this problem, low molecular weight proteins or peptides mimicking the active sites of albumin and transferrin residues tend to be used. Binding studies of RAPTA-

T (**3**) to apo-Tf and a small peptide which contains His249 involved in iron binding to transferrin indicate the presence of mono-ruthenated  $[\text{Ru}(\eta^6\text{-arene})]$ -apo-Tf species [97]. MS analysis of the RAPTA-bound model peptide adducts demonstrated that a histidine residue is the major binding partner and, as expected, cysteine is also involved in the binding, although to a lesser extent. Notably, the affinity of RAPTA-T for albumin and transferrin is significantly higher than that of cisplatin, possibly because RAPTA compounds can react directly with biomolecular targets without forming aqua adducts (see section 4.3.). It was also shown that RAPTA complexes bind with a higher affinity to holo-transferrin in comparison with apo-transferrin and albumin, whereas cisplatin was non-selective and had a similar affinity to all the proteins used in the study.

## 5.2. Subcellular localization

Once a compound has been taken up by a cancer cell, a knowledge of its subcellular localization helps to provide information on the mode of drug action. In this regard ICP-MS has been used to determine cellular uptake and localization in cells incubated with RAPTA-T [98]. Ruthenium was detected in the cytoskeleton and membranes, which is not unexpected as cytoskeletal proteins are crucial for metastatic processes and RAPTA complexes reduce metastasis. It was found that RAPTA-T uptake into cancer cells is dependent on the cell type, accumulating in cisplatin-resistant cells to a greater extent than in cisplatin-sensitive cells, and indicating that RAPTA-T uptake is not influenced by cisplatin-related resistance mechanisms. RAPTA-T was found to have a high preference for the particulate fraction containing organelles, *i.e.*, mitochondria, endoplasmic reticulum, Golgi apparatus and lysosomes. In the cisplatin-resistant cell line this preference is reduced and shifted towards the nucleus and cytosol [98].

Notably, the amount of RAPTA-T in mitochondria is significantly higher than the amount of cisplatin in both cisplatin-sensitive and resistant cells, where no platinum was detected.

### 5.3. Reactions with potential intracellular targets

#### 5.3.1. DNA as a suggested target

The early report of pH-dependent pBR322 DNA damage mediated by RAPTA-C **(1)** demonstrated the ability of the RAPTA compounds to interact with and distort DNA [29], and led to DNA being considered as a potential intracellular target of the RAPTA compounds. To probe this hypothesis, numerous mechanistic, analytical and theoretical studies were performed. Binding studies with 14-mer DNA oligonucleotides by mass spectrometry showed that RAPTA-C and  $[\text{Ru}(\eta^6\text{-}p\text{-cymene})\text{Cl}_2(\text{PTA-Me})]\text{Cl}$  **(5)** coordinate to DNA *via* the loss of labile chlorido ligands and, following prolonged incubation, loss of the *p*-cymene ligand with retention of the PTA ligand is observed [99]. The loss of *p*-cymene may lead to the formation of  $\pi$ -bound DNA adducts *via* coordination of aromatic rings of nucleobases to the ruthenium center although DFT computations indicated that  $\pi$ -binding is not favored energetically. It is more likely that single-stranded oligomers wrap around the metal center with subsequent formation of multiple coordination bonds, leading to significant distortions of the oligonucleotide. The high reactivity of RAPTA-C to dGMP in acidic conditions was confirmed by CZE-ICP-MS experiments. pH dependent binding of RAPTA-C to dGMP was observed, with a considerably higher reactivity at pH 6.0 compared to pH 7.4, implying that binding would be favoured in the more acidic (hypoxic) environment of tumors and endowing the compound with a built in selectivity mechanism [100].

Computational studies suggest that under acidic conditions RAPTA complexes exist mainly in the mono-aqua form, *i.e.*,  $[\text{Ru}(\eta^6\text{-arene})\text{Cl}(\text{H}_2\text{O})(\text{PTA})]^+$ , and since the aqua ligand is labile the complexes react more efficiently with potential biomolecular targets at low pH values [35]. Adducts of RAPTA-B, RAPTA-C and  $[\text{Ru}(\eta^6\text{-}p\text{-cymene})\text{Cl}_2(\text{PTA-Me})]^+$  with various DNA model compounds (9-methylguanine, 9-methyladenine, guanosine, inosine, hypoxanthine, adenosine, cytidine, thymidine and uridine) in aqueous conditions were characterized by electrospray ionization mass spectrometry (ESI-MS) and  $^1\text{H}$  NMR spectroscopy [101]. The most abundant signals could be attributed to mono-chlorido complexes with purine bases or nucleosides coordinated via *N7*. The *N7* position on guanine appeared to be the preferred coordination site – a conclusion substantiated later by top-down tandem mass spectrometry studies that identified guanine as the preferred coordination site of RAPTA-T with double stranded oligonucleotides [102]. However, it should be noted that adducts with adenine or thymine were also observed, although to a lesser extent.

The DNA binding mechanisms of RAPTA-C, RAPTA-B and  $[\text{Ru}(\eta^6\text{-}p\text{-cymene})(\text{en})\text{Cl}]^+$  were compared using classical and QM/MM molecular dynamics simulations using a 12 base-pair DNA duplex as a model target [103]. It was shown that these compounds bind to the major groove of DNA, with the two different compound families inducing different local and global changes in the DNA structure. The calculations demonstrated that RAPTA-C induced DNA bending towards the major groove without breaking Watson-Crick base pairs or intercalating between them, which is different from  $[\text{Ru}(\eta^6\text{-}p\text{-cymene})(\text{en})\text{Cl}]^+$  for which breakage of a Watson-Crick base-pair was found.

The nature of interactions of RAPTA-C and carbo-RAPTA-C (Figure 19, **(49)**) with the DNA sequence of the human breast cancer suppressor gene 1 (BRCA1) was

investigated using conformational analysis of ruthenated DNA, crosslinking assays and semi-quantitative PCR [104]. In accordance with the results described above, it was shown that ruthenation induced unwinding of the supercoiled DNA. These studies revealed that RAPTA complexes preferentially bind to adenine and guanine.

The ability of four RAPTA complexes (arene = benzene, toluene, *p*-cymene, 1,3,5- $\eta^6$ - $\text{Pr}_3\text{C}_6\text{H}_3$ ) to inhibit transcription in mammalian cells was investigated through transfection of a ruthenated pCMV-GLuc plasmid (encoding the gaussia luciferase (GLuc) reporter gene) followed by quantification of the expressed levels of GLuc in transfected cells [105]. It was found that the RAPTA complexes with the bulkier arene ligands exhibited reduced reactivity towards the plasmid, most likely due to steric repulsion. Ruthenation of the plasmid was found to inhibit transcription effectively in live mammalian cells (HCT-116) only at high Ru-DNA crosslink levels where, perhaps surprisingly, those RAPTA complexes with the more sterically demanding arene ligands were less effective. For example, the reduction of transcription to the level of 50% of non-ruthenated controls required 74, 87, 112 and 302 Ru-DNA crosslinks per plasmid for RAPTA-B, RAPTA-T, RAPTA-C and  $[\text{Ru}(\eta^6\text{-1,3,5-}\eta^6\text{-Pr}_3\text{C}_6\text{H}_3)(\text{PTA})\text{Cl}_2]$ , respectively. It was postulated that the less efficient inhibition by the more bulky complexes is related to more efficient DNA repair of the bulky RAPTA-DNA adducts. This was supported by observation that the transcription recovery rates recovered more rapidly as the steric bulk on the  $\eta^6$ -arene increased, potentially due to enhanced recognition by DNA repair proteins of the DNA distortions induced by the more bulky RAPTA adducts.

### 5.3.2. RAPTA and protein interactions

Although RAPTA complexes can readily react with DNA models under physiologically relevant conditions there is not a strong correlation between this reactivity and cytotoxicity towards cancer cell lines. This limited correlation led to the investigation of proteins as potential targets of RAPTA-based compounds.

Initial studies showed that RAPTA compounds readily bind peptides and proteins such as glutathione [106], lysozyme [107], ubiquitin [108], cytochrome-c [107, 108], superoxide dismutase [108], the human serum proteins albumin and transferrin [97] mentioned in section 5.1, poly(adenosine diphosphate (ADP)-ribose) polymerases (PARPs) [109], and metallothioneins [110]. The wide scope of reactivity is perhaps not unexpected given the number and availability of nucleophilic atoms in protein systems that can coordinate to the ruthenium center through ligand exchange reactions. Indeed, cisplatin can bind to essentially the same range of proteins, but RAPTA-C was more selective and able to discriminate between proteins presumably due to its greater three-dimensional steric bulk.

#### 5.3.2.1. Interactions with model proteins

Ubiquitin (ub) and cytochrome-c (cyt) have been widely used as model proteins in ESI-MS experiments to study protein–metallo drug adduct formation due to their stability and low molecular weight [111]. RAPTA-C reacts with ubiquitin to afford mono-ruthenated adducts, the dominant species being assigned to [ub + Ru( $\eta^6$ -*p*-cymene)] [108]. [Ru( $\eta^6$ -C<sub>6</sub>H<sub>5</sub>CF<sub>3</sub>)(PTA)Cl<sub>2</sub>] (**20**), with a labile arene ligand behaves significantly different from all other members of the RAPTA family [47], forming unusual adducts with ubiquitin. For example, after 1 day of incubation the most abundant signals were assigned to [ub + Ru(PTA)(H<sub>2</sub>O)<sub>x</sub>] (x = 0–2) and ubiquitin adducts with only a ruthenium ion were also observed. As glutathione (GSH) is a high affinity metal binder,

it may induce release of metallodrugs from their conjugates with biological targets through competitive binding. Notably, GSH was shown to slowly displace the RAPTA moiety from RAPTA-ub adducts [106].

The reaction of cyt with RAPTA-C results in extensive protein metallation, whereas only moderate or low ruthenation was observed with carbo-RAPTA-C (**49**) and oxali-RAPTA-C (**48**) (Figure 19) [107], correlating with the ability of the complexes to release their leaving groups upon hydrolysis [112]. For RAPTA-C both mono-ruthenated species, namely [cyt + [Ru( $\eta^6$ -cymene)]] and [cyt + [Ru( $\eta^6$ -*p*-cymene)(PTA)]], and bis-ruthenated species with either two [Ru( $\eta^6$ -*p*-cymene)] fragments or one [Ru( $\eta^6$ -*p*-cymene)] and one [Ru( $\eta^6$ -*p*-cymene)(PTA)] fragment, were detected. In contrast, one adduct with carbo-RAPTA-C did not retain the arene ligand and bis-ruthenated species were not detected. Under the same conditions only one Ru-containing peak with very low intensity was observed with oxali-RAPTA-C (**48**), which was attributed to a mono-ruthenated species with a [Ru( $\eta^6$ -*p*-cymene)] fragment. Under similar conditions cisplatin forms mono-, bis- and tris-adducts with cyt [113], and [Ru( $\eta^6$ -*p*-cymene)(en)Cl]<sup>+</sup> forms exclusively mono-ruthenated species. A bottom-up method (MS analysis of peptides obtained from the enzymatic digestion of the metallated protein) was used to identify the likely RAPTA-C binding sites on cyt [107], identifying His33 as the major interaction site for RAPTA-C (compared to Met65 as the primary binding site for platinum complexes).

In order to study competitive binding to proteins, RAPTA-C was incubated with a mixture of ub, cyt and superoxide dismutase [108] and it was found to coordinate to both ubiquitin and cytochrome-C, which matches well with the data obtained for the binding studies to single proteins [108], with only limited binding to superoxide dismutase.



RAPTA-C binding to metallothioneins was also studied by ESI-MS [110] as this protein is implicated in the homeostasis of essential metals and detoxification of heavy metals [114]. Moreover, the overexpression of metallothioneins serves as a marker for tumor progression and metaldrug resistance [115]. Indeed, metallothionein-2 acts as an effective intracellular scavenger of platinum(II) drugs by forming stable adducts [116]. RAPTA-C formed mono-ruthenated adducts of metallothionein-2 with the concomitant displacement of zinc ions that usually bind to the Cys residues in the protein. In the presence of ubiquitin and glutathione the ruthenium fragment was removed from metallothionein-2 with ubiquitin stripping ruthenium-metallothionein adducts much more efficiently, potentially allowing RAPTA compounds to overcome metallothionein-based drug resistance.

RAPTA complexes were found to inhibit cathepsin B, thioredoxin reductase [117] and poly(adenosine diphosphate (ADP)-ribose) polymerases (PARPs) [109]. The role of thioredoxin reductase in cancer is ambiguous, protecting highly proliferating cells from the immune system, and up-regulation of thioredoxin reductase might contribute towards drug resistance [118]. Several RAPTA compounds were screened towards cytosolic or mitochondrial thioredoxin reductases [117]. None of the RAPTA compounds evaluated were effective inhibitors of mitochondrial thioredoxin reductase although inhibition of cytosolic thioredoxin reductase was more pronounced (45–200  $\mu\text{M}$ ), but probably of little relevance *in vivo*. RAPTA complexes with sterically demanding arenes are less effective inhibitors, presumably as the enzyme cannot easily accommodate the bulky substituents. Interestingly, carbo-RAPTA-C, which does not contain labile chlorido ligands in its structure, was a more effective inhibitor than RAPTA-C. The same series of RAPTA compounds were effective inhibitors of cathepsin B, whose overexpression correlates with metastatic and invasive processes

[117]. Notably, carbo-RAPTA-C was significantly less effective in inhibiting cathepsin B than RAPTA-C, indicating that the release of leaving groups is required to exhibit inhibitory activity. Docking studies indicate that the ruthenium(II) ion binds to cysteine (Cys-29) in the catalytic pocket of the enzyme [119]. The adducts which form between RAPTA-T and apo-ZF-PARP retain both the arene and PTA ligands. The addition of RAPTA-T to the physiological ZF-motif (holo-ZF-PARP) resulted in the standard adduct types without loss of zinc ions, indicating that RAPTA-T coordinates to amino acids that are not involved in the structure of the zinc finger motif.

#### 5.2.3.2. Histone proteins as targets and target identification from cell extracts

A significant percentage of RAPTA-C in cancer cells becomes associated with chromatin, *ca.* 5% in total, thus representing a key target [120]. Moreover, an X-ray structure of a nucleosome core particle (NCP - a double-stranded DNA segment which is wrapped around an octameric histone protein core) co-crystallized with RAPTA-C revealed binding to the histone core rather than DNA (Figure 29) [120]. A previous study of the interactions of a NCP and cisplatin or oxaliplatin revealed that both platinum complexes bound exclusively to DNA despite its lower accessibility in the particle [121]. It has also been shown that  $[\text{Ru}(\eta^6\text{-arene})(\text{en})\text{Cl}]^+$  binds preferentially to DNA in the same model [81]. The study revealed three well-defined histone binding sites for RAPTA-C coordination with the dominate site corresponding to binding *via* two glutamate residues on the exposed, acidic face of the NCP.

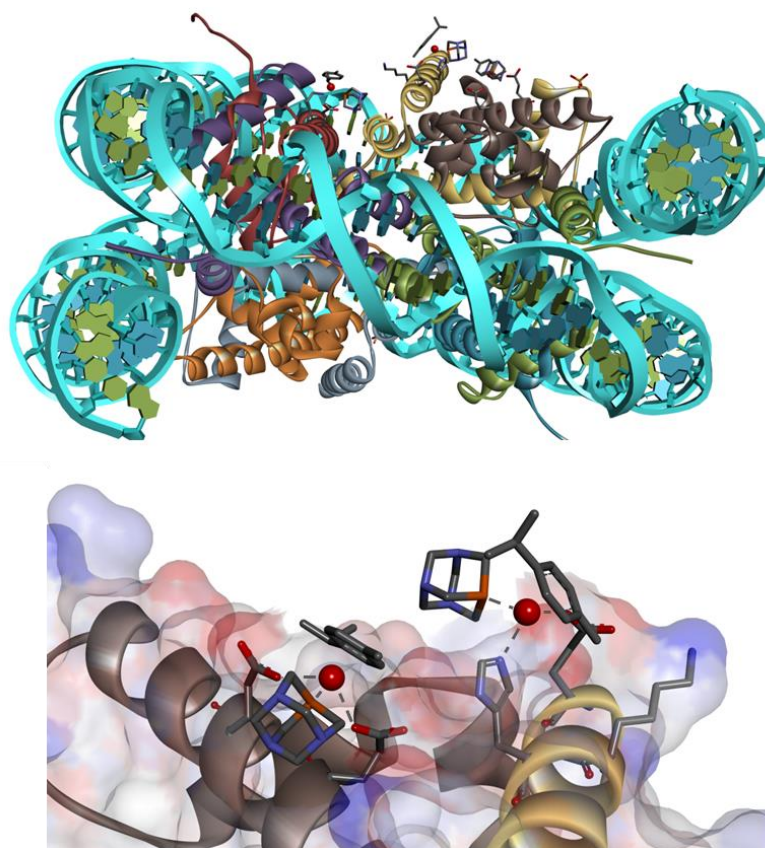


Figure 29. The crystal structure of the nucleosome core particle (top) and a close-up of two of three RAPTA-C binding sites (bottom) (PDB ID: 3MNN) [120].

While interactions with many different biomolecules may be anticipated for a relatively simple metallodrug in addition to the histone target described above, with the exception of histone proteins, interactions with the other biomolecules studied were not established *in cellulo*. In order to profile the molecular targets of RAPTA complexes, a drug pull-down approach based on drug affinity purification of cancer cell lysates with subsequent mass spectrometry and combined bioinformatics was applied [122]. The comparison of data sets obtained for cell lysates from cancer cells before and after pretreatment with a competitive binder suggested that the RAPTA complex interacts with a variety of intracellular proteins including several involved in

antiangiogenic and antimetastatic activity, such as pleiotrophin, midkine and, notably, histone proteins.

Metallomics techniques have also been used to show the downstream effects on cancer cells in response to RAPTA-T treatment. Two-dimensional difference gel electrophoresis (2D-DIGE) was used to monitor changes in the expression of intracellular proteins upon exposure of cancer cells to RAPTA-T [123]. RAPTA-T changes the protein expression profiles of only a few proteins. DNA polymerase epsilon subunit 3 (POLE3), a histone-fold protein which interacts with other histone proteins to bind DNA, was profoundly downregulated, possibly as a direct consequence of RAPTA-binding to the histone core in chromatin. Several proteins were significantly upregulated including acetyl-CoA acetyltransferase, cytosolic (ACAT2), deoxyuridine 5'-triphosphate nucleotidohydrolase, mitochondrial (DUT), ubiquitin-conjugating enzyme E2 G1, omega-amidase (NIT2), thymidylate kinase (TMK), histidine triad nucleotide-binding protein 1 (HINT1) and prefoldin subunit 3 (PFD3). Of these proteins the upregulation of HINT1 is particularly relevant since it is involved in the regulation of apoptotic processes and closely associated with p53 expression. RAPTA-C was shown to induce p53 expression upregulation [124].

Multidimensional protein identification technology (MudPIT) was used to identify protein regulation in various organelles in cells treated with RAPTA-T [98]. Twenty-five proteins demonstrated profound up- or down-regulation found in the endoplasmic reticulum, intermediate filament and mitochondria, nucleus and cytoskeleton. It is worth noting that most identified cytoskeletal proteins serve as constructive elements of cell junctions which might be partly responsible for the antimetastatic activity of RAPTA complexes, since the disruption of cell-cell interactions is related with metastasis [125, 126].

## 6. Concluding remarks

Extensive studies on the anticancer properties of ruthenium(II) compounds have been reported, the main two classes comprising ruthenium(II)-polypyridyl complexes and organometallic ruthenium(II)-arene compounds [19-23, 111, 127, 128]. Of these various compounds the RAPTA-type compounds have been particularly well studied with several encouraging *in vivo* studies reported as well as detailed mechanistic studies. Indeed, the initial identification of RAPTA compounds provided an interesting contrast to the rest of this field – yielding prospective chemotherapeutics that exhibit activity against metastatic tumors and antiangiogenic effects that also leads to activity against primary tumors using appropriate dosing protocols whilst exhibiting low cytotoxicity in cell culture experiments. Such compounds highlight the potential of developing complementary metallotherapeutics that do not necessarily exhibit high cytotoxicity, but instead may be utilized with surgical intervention and complementary chemotherapeutic regimes in combination approaches. Such a strategy has potential in providing a more efficacious clinical outcome of the therapy regime accompanied by a reduction in side-effects. Since the discovery of the prototypical RAPTA compound, RAPTA-C, and the early recognition of its antimetastatic properties, the development of RAPTA compounds has rapidly progressed in the search for more efficacious compounds. This synthetic work has spanned the minor modification of individual ligands of the RAPTA structure to the construction of more targeted structures and complex macromolecular conjugates, and has resulted in a diverse range of compounds designed with a specific biological profile in mind. Alongside these synthetic achievements, efforts have been expended in the application and development of various bioanalytical, biochemical and biophysical techniques to

illuminate the mechanism by which RAPTA compounds exert their biological effects. The unique properties of RAPTA compounds, with respect to the observed biomolecular targets and biological effects, have led to the evaluation of RAPTA-C in several pre-clinical models. The activity of RAPTA-C on these models is highly promising, especially as it is coupled with its fast clearance from organs and the bloodstream and a low general toxicity. Remarkably, when administered during tumor normalization RAPTA-C is more effective in inhibiting tumor growth than the highly cytotoxic compound doxorubicin, even at a lower dose. Since RAPTA-C is reasonably water soluble and tolerates low pH it could potentially be administered orally and currently *in vivo* studies based on oral administration are in progress. Certain newer generation RAPTA-type compounds are also being studied in different pre-clinical models.

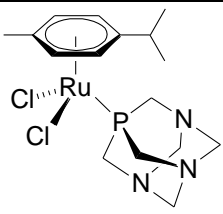
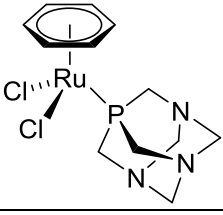
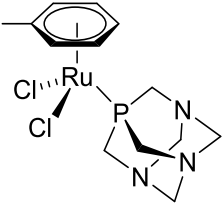
Later RAPTA complexes, in particular those bearing fluorinated arene ligands and those bearing curcuminoid ligands, have shown particularly interesting properties, such as novel binding modes with biomolecular targets and high selective activity towards cancerous cell lines over non-cancerous cell lines, respectively. In addition, the development and evaluation of dinuclear RAPTA complexes is still in its infancy but these complexes display distinct crosslinking binding modes with biomolecular targets and can even be assembled *in vitro*. Rationally designed dinuclear complexes offer a route towards the crosslinking of targeted cellular components and the circumventing of cellular resistance mechanisms. Finally, the utility of macromolecular systems as RAPTA delivery vehicles has briefly been explored in cell-based studies. The continued development of synthetic routes and protocols for the incorporation of RAPTA compounds into well-defined macromolecular/supramolecular delivery and release systems is likely to provide a firm foundation for the future access of

conjugates able to favorably modify the pharmacological profile of these compounds *in vivo*.

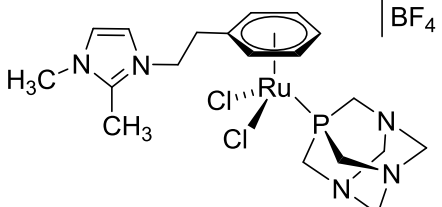
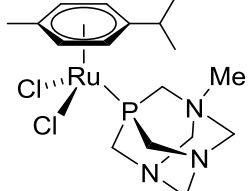
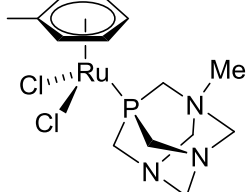
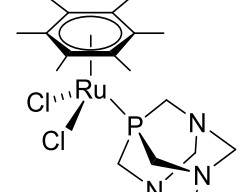
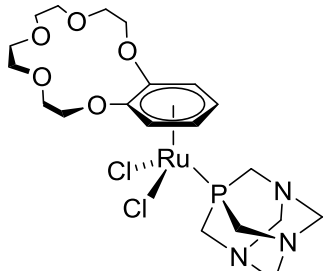
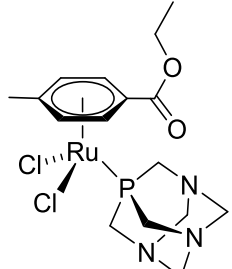
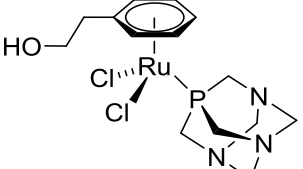
It is clear that for the prototypical RAPTA compounds there is little correlation between their *in vivo* activity and their activity in typical cell-proliferation studies. It is only when more targeted cell-based assays (e.g., those evaluating cell mobility, invasion and adhesion) were used in conjunction with appropriate cell lines that correlations could be drawn between *in cellulo* and *in vivo* activity. Given this paradigm, it is likely that there are examples of recently developed RAPTAs that warrant further evaluation in more appropriate assays and that a wider range of relevant pharmacological activity will be uncovered. As the application of proteomic techniques within this field becomes more routine it may be envisaged that the decision of which are the most appropriate cell-based assays in which to screen a compound will be led by results from proteomics studies. These results will indicate the essential targets *in cellulo* and from this the likely chemotherapeutic effects may be predictable. However, the progress made to date with the RAPTA compounds is extremely encouraging and the future combination of rational design with advanced proteomics should lead to the identification of more efficacious chemotherapeutics with promising anticancer properties.

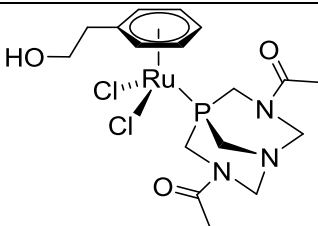
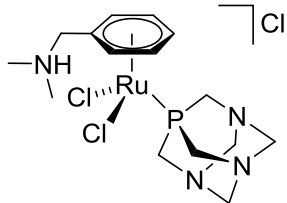
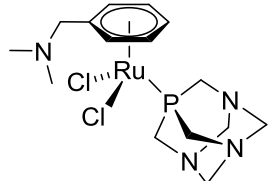
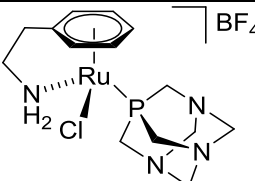
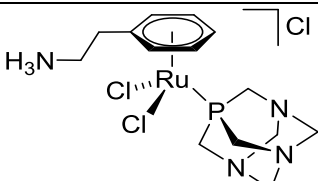
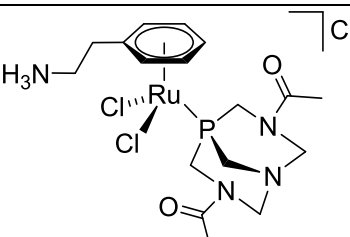
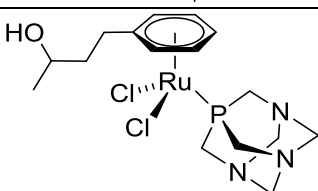
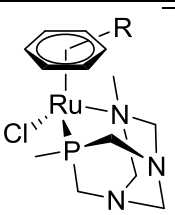
Table 1. A summary of available *in vitro* and *in vivo* activity for all compounds discussed.

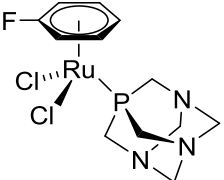
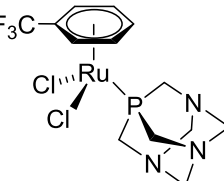
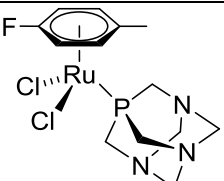
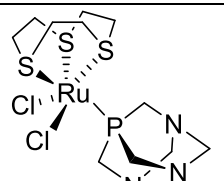
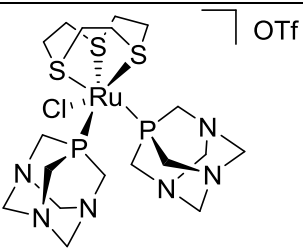
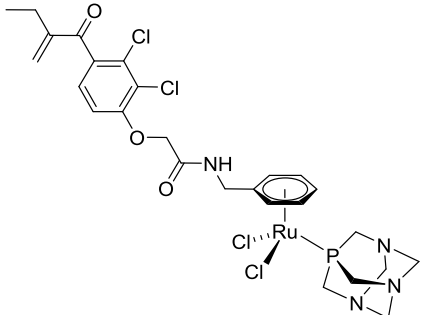
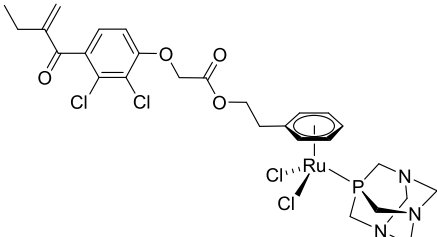
#	Structure	Activity <i>in vitro</i>	Activity <i>in vivo</i>	Refs.
---	-----------	--------------------------	-------------------------	-------

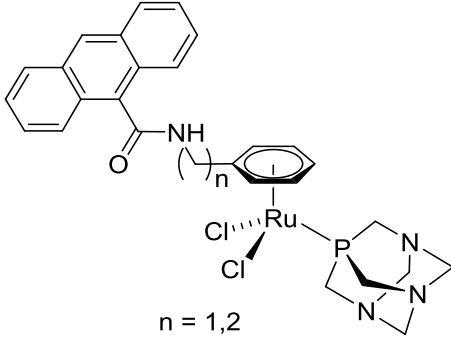
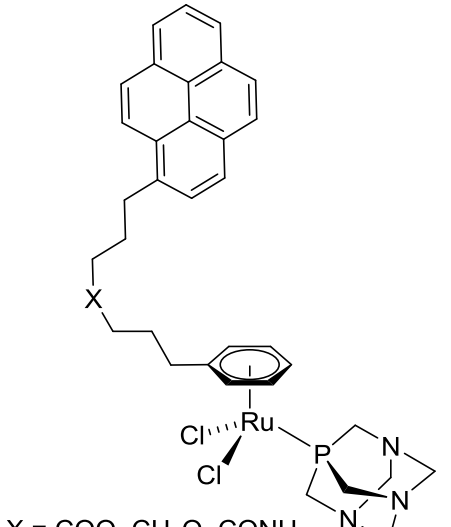
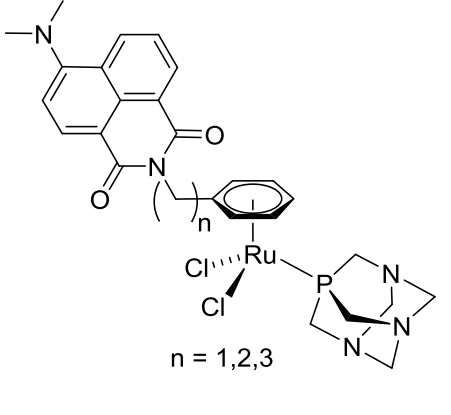
		<b>(IC<sub>50</sub>, 72 h, MTT assay unless stated otherwise)</b>		
<b>(1)</b>		TS/A: >300 μM HBL-100: >300 μM  A2780: 353±12 μM	CAM model (A2780 ovarian carcinoma): inhibition of tumour growth by approx. 75% (0.2 mg kg <sup>-1</sup> per day for 5 days, starting 4 days after tumour inoculation).  Athymic mice (LS174T colorectal adenocarcinoma): 50% inhibition of tumour growth (100 mg kg <sup>-1</sup> per day for 11 days). Antiangiogenic activity observed in tumour tissue.  Athymic mice (LS174T colorectal adenocarcinoma): Approx. 80% reduction in tumour growth when used in combination with erlotinib and BEZ-235 (single RAPTA-C dose of 40 mg kg <sup>-1</sup> ).  CAM model (A2780 ovarian carcinoma): 90% inhibition in tumour growth (400 μg kg <sup>-1</sup> ) following pre-treatment with axitinib.	[30] [37] [38] [39] [43] [45]
<b>(2)</b>		TS/A: >231 μM HBL-100: >300 μM		[30]
<b>(3)</b>		TS/A: >74 μM HBL-100: >300 μM  MDA-MB-231: reduction in ability to adhere, migrate, detach and reduced invasive ability following treatment with RAPTA-T	CBA mouse model (murine mammary carcinoma): reduction in weight of lung metastases and reduction in metastases of large dimensions (80 mg kg <sup>-1</sup> per day on days 8,9,12 following implanting of tumour).	[30] [36]

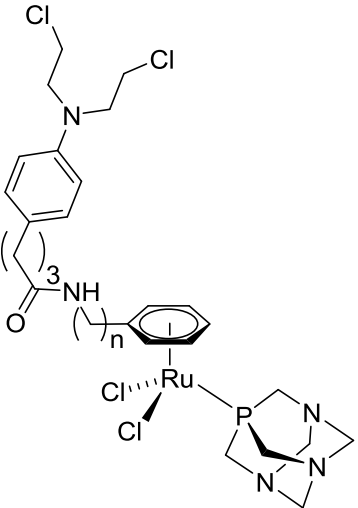
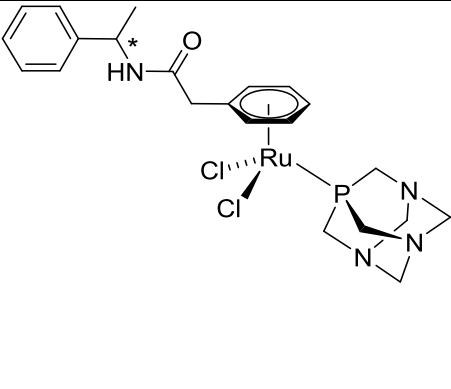
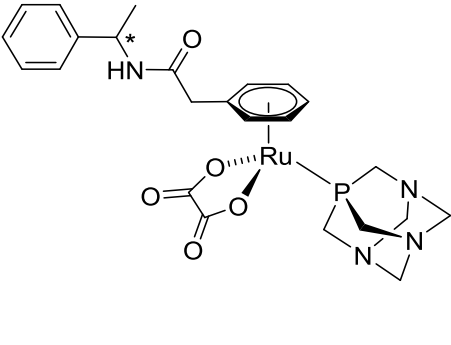


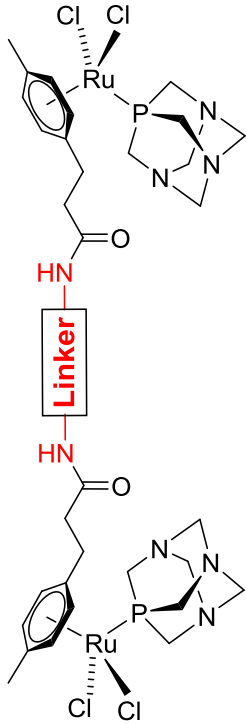
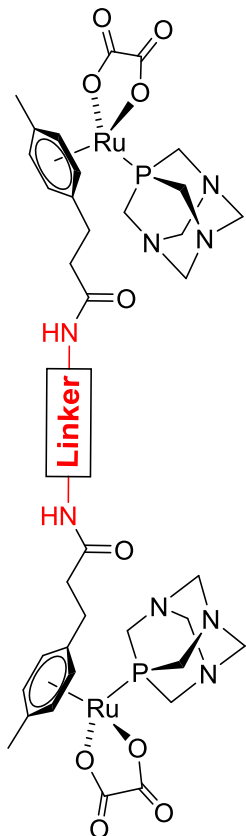
(4)		TS/A: >66 $\mu\text{M}$ HBL-100: >300 $\mu\text{M}$		[30]
(5)		TS/A: >300 $\mu\text{M}$ HBL-100: >246 $\mu\text{M}$		[30]
(6)		TS/A: >110 $\mu\text{M}$ HBL-100: >77 $\mu\text{M}$		[30]
(7)		TS/A: >199 $\mu\text{M}$ HBL-100: >300 $\mu\text{M}$		[30]
(8)		TS/A: >159 $\mu\text{M}$ HBL-100: >300 $\mu\text{M}$		[30]
(9)		TS/A: >103 $\mu\text{M}$ HBL-100: >300 $\mu\text{M}$		[30]
(10)		TS/A: >570 $\mu\text{M}$ HBL-100: >778 $\mu\text{M}$		[44]

(11)		TS/A: >538 $\mu\text{M}$ HBL-100: >715 $\mu\text{M}$	[44]
(12)		TS/A: >449 $\mu\text{M}$ HBL-100: >603 $\mu\text{M}$	[44]
(13)		TS/A: >458 $\mu\text{M}$ HBL-100: >813 $\mu\text{M}$	[44]
(14)		TS/A: >1000 $\mu\text{M}$ HBL-100: >612 $\mu\text{M}$	[44]
(15)		TS/A: >820 $\mu\text{M}$ HBL-100: >666 $\mu\text{M}$	[44]
(16)		TS/A: >1000 $\mu\text{M}$ HBL-100: >1000 $\mu\text{M}$	[44]
(17)		TS/A: >505 $\mu\text{M}$ HBL-100: >891 $\mu\text{M}$	[44]
(18)	 Arene <i>p</i> -cymene benzene toluene hexamethylbenzene	A2780: 154-278 $\mu\text{M}$	[45]

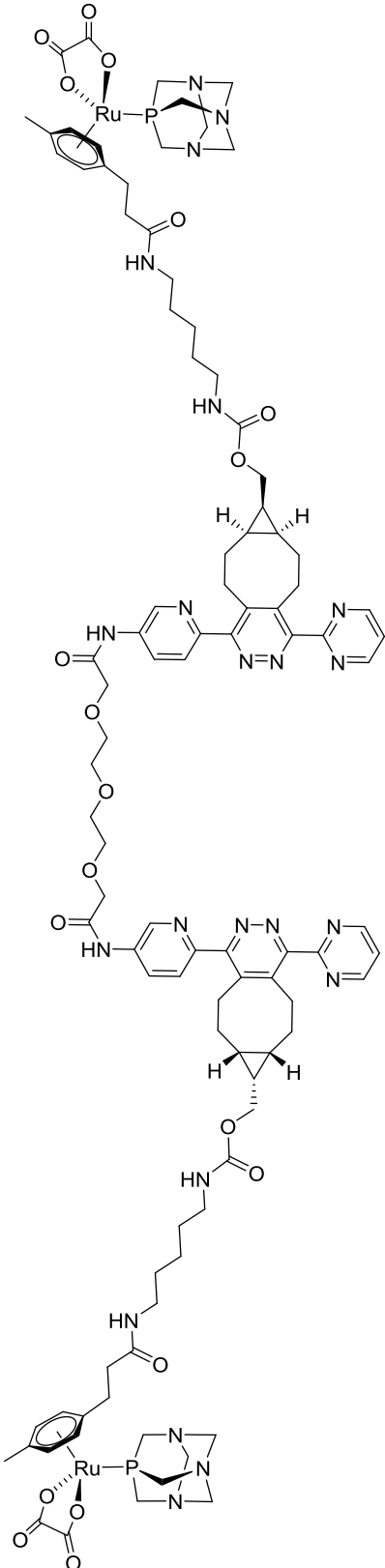
(19)		A2780: 507 $\mu\text{M}$		[46]
(20)		A2780: 38 $\mu\text{M}$		[46]
(21)		A2780: 78 $\mu\text{M}$		[46]
(22)		TS/A: >650 $\mu\text{M}$ HBL-100: >738 $\mu\text{M}$		[48]
(23)		TS/A: >388 $\mu\text{M}$ HBL-100: >1000 $\mu\text{M}$		[48]
(24)		(MTT assay, 48 h) MCF-7: 20 $\mu\text{M}$ HT-29: 50 $\mu\text{M}$  Inhibition of activity of GST P1-1: $\text{IC}_{50} = 13.7 \mu\text{M}$		[49] [54]
(25)		Inhibition of activity of GST P1-1: $\text{IC}_{50} = 5.9 \mu\text{M}$		[49]

(26)	 <p style="text-align: center;"><math>n = 1, 2</math></p>	<p>LN18, LN229, LNZ308, SW480, HT29, CaCo2, A549, MDA-MB231, MCF-7, HCEC, A2780, A2780cisR: <math>IC_{50} &gt; 200 \mu M</math> in all cases for <math>n = 1, 2</math>.</p>		[52]
(27)	 <p style="text-align: center;"><math>X = COO, CH_2O, CONH</math></p>	<p>When <math>X = COO, CONH</math>: A549, A2780, A2780cisR, Me300, HeLa: <math>IC_{50} &gt; 25 \mu M</math>.</p> <p>When <math>X = CH_2O</math>: A549, HeLa: <math>IC_{50} &gt; 25 \mu M</math>. A2780: <math>IC_{50} = 19.7 \pm 6.5 \mu M</math>. A2780cisR: <math>IC_{50} = 15.8 \pm 6.0 \mu M</math>. Me300: <math>IC_{50} = 17.7 \pm 7.0 \mu M</math>.</p> <p>When compounds encapsulated in <math>[Ru_6(\eta^6-p\text{-cymene})_6(tpt)_2(donq)_3]^{6+}</math> cage <math>IC_{50}</math> values ranged between 2.0 – 7.7 <math>\mu M</math> for all cell lines.</p>		[53]
(28)	 <p style="text-align: center;"><math>n = 1, 2, 3</math></p>	<p>When <math>n = 1</math> A2780: <math>IC_{50} 8.5 \pm 1.4 \mu M</math>. A2780cisR: <math>IC_{50} 6.9 \pm 1.5 \mu M</math>. HEK: <math>IC_{50} 16.6 \pm 1.1 \mu M</math>.</p> <p>When <math>n = 2</math> A2780: <math>IC_{50} 2.3 \pm 0.1 \mu M</math>. A2780cisR: <math>IC_{50} 2.3 \pm 0.25 \mu M</math>. HEK: <math>IC_{50} 6.6 \pm 0.2 \mu M</math>.</p> <p>When <math>n = 3</math> A2780: <math>IC_{50} 6.5 \pm 0.5 \mu M</math>. A2780cisR: <math>IC_{50} 9.1 \pm 1.7 \mu M</math>. HEK: <math>IC_{50} 17.4 \pm 0.3 \mu M</math>.</p>		[56]

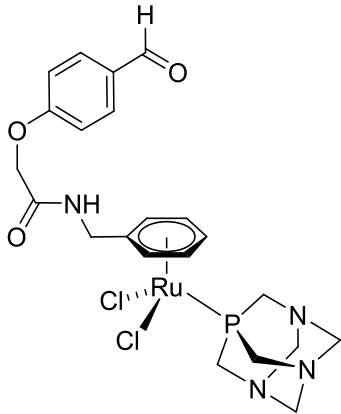
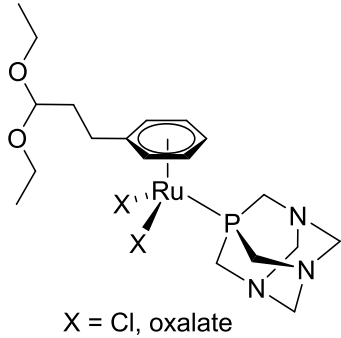
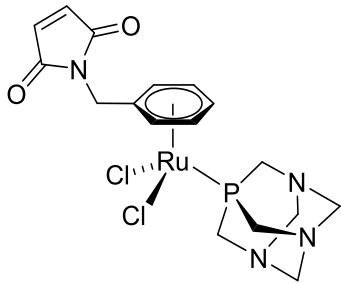
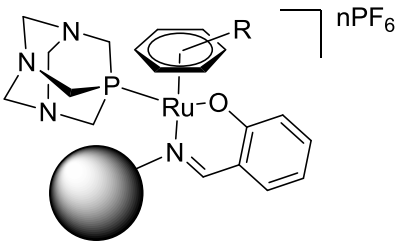
(29)		<p>When <math>n = 1</math>  A2780: <math>IC_{50} = 8.3 \pm 1.3 \mu\text{M}</math>.  A2780cisR: <math>IC_{50} = 10 \pm 3 \mu\text{M}</math>.  MCF7: <math>IC_{50} = 12 \pm 4 \mu\text{M}</math>.</p> <p>When <math>n = 2</math>  A2780: <math>IC_{50} = 12 \pm 4 \mu\text{M}</math>.  A2780cisR: <math>IC_{50} = 45 \pm 17 \mu\text{M}</math>.  MCF7: <math>IC_{50} = 37 \pm 9 \mu\text{M}</math>.</p>	[58]
(30)		<p>When * = <i>R</i> configuration  A2780: <math>IC_{50} = 44 \pm 1 \mu\text{M}</math>.  A2780cisR: <math>IC_{50} = 396 \pm 3 \mu\text{M}</math>.  HEK: <math>IC_{50} &gt; 1000 \mu\text{M}</math>.</p> <p>When * = <i>S</i> configuration  A2780: <math>IC_{50} = 30 \pm 0.5 \mu\text{M}</math>.  A2780cisR: <math>IC_{50} = 228 \pm 16 \mu\text{M}</math>.  HEK: <math>IC_{50} = 255 \pm 13 \mu\text{M}</math>.</p>	[59]
(31)		<p>When * = <i>R</i> configuration  A2780: <math>IC_{50} = 34 \pm 1 \mu\text{M}</math>.  A2780cisR: <math>IC_{50} = 33 \pm 1 \mu\text{M}</math>.  HEK: <math>IC_{50} = 32 \pm 1 \mu\text{M}</math>.</p> <p>When * = <i>S</i> configuration  A2780: <math>IC_{50} = 8.7 \pm 0.1 \mu\text{M}</math>.  A2780cisR: <math>IC_{50} = 21 \pm 2.5 \mu\text{M}</math>.  HEK: <math>IC_{50} = 32 \pm 5 \mu\text{M}</math>.</p>	[59]

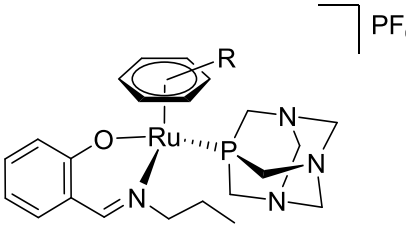
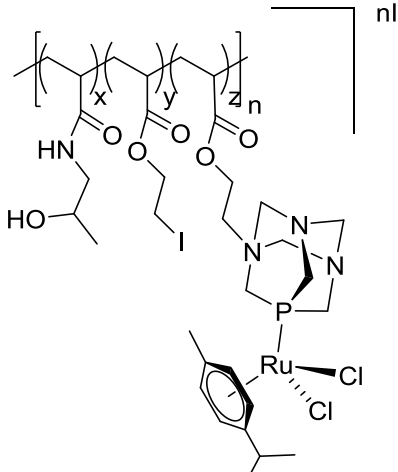
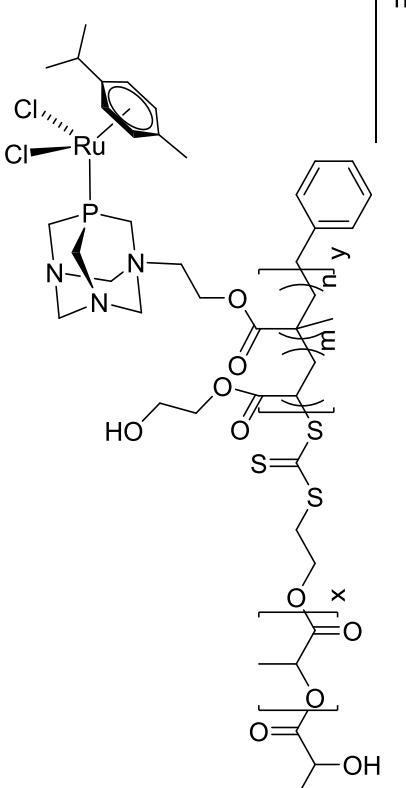
(32)	 <p>The structure shows a central Ru atom coordinated to two chlorine atoms and two chiral ferrocenyl phosphine ligands. Two amide groups are attached to the Ru center, with a linker connecting the nitrogen atoms of these amide groups. The linker is highlighted in a red box.</p>	<p>Linker = ethylenediamine:  A2780: <math>IC_{50} = 64 \pm 9.5 \mu M</math>.  A2780cisR: <math>IC_{50} &gt; 300 \mu M</math>.  HEK: <math>IC_{50} = 35 \pm 5 \mu M</math>.</p> <p>Linker = <i>meso</i>-1,2-diphenylethylenediamine:  A2780: <math>IC_{50} = 20 \pm 0.5 \mu M</math>.  A2780cisR: <math>IC_{50} = 95 \pm 6.5 \mu M</math>.  HEK: <math>IC_{50} = 24 \pm 3.5 \mu M</math>.</p> <p>Linker = (1<i>S</i>,2<i>S</i>)-(-)-1,2-diphenylethylenediamine:  A2780: <math>IC_{50} = 3.7 \pm 0.6 \mu M</math>.  A2780cisR: <math>IC_{50} = 4.5 \pm 0.2 \mu M</math>.  HEK: <math>IC_{50} = 8.0 \pm 0.5 \mu M</math>.</p> <p>Linker = (1<i>R</i>,2<i>R</i>)-(+)-1,2-diphenylethylenediamine:  A2780: <math>IC_{50} = 3.7 \pm 0.6 \mu M</math>.  A2780cisR: <math>IC_{50} = 7.0 \pm 0.5 \mu M</math>.  HEK: <math>IC_{50} = 5.9 \pm 0.2 \mu M</math>.</p> <p><math>IC_{50}</math> values are complex concentrations.</p>		[60]
(33)	 <p>The structure is similar to (32), but the Ru center is also coordinated to a chiral auxiliary group (a cyclic carbonate derivative) in addition to the two chlorine atoms and the two phosphine ligands. The linker is highlighted in a red box.</p>	<p>Linker = ethylenediamine:  A2780: <math>IC_{50} = 23 \pm 0.5 \mu M</math>.  A2780cisR: <math>IC_{50} = 88 \pm 10 \mu M</math>.  HEK: <math>IC_{50} = 29 \pm 2.5 \mu M</math>.</p> <p>Linker = <i>meso</i>-1,2-diphenylethylenediamine:  A2780: <math>IC_{50} = 25 \pm 2.5 \mu M</math>.  A2780cisR: <math>IC_{50} = 74 \pm 6.0 \mu M</math>.  HEK: <math>IC_{50} = 19 \pm 4.0 \mu M</math>.</p> <p>Linker = (1<i>S</i>,2<i>S</i>)-(-)-1,2-diphenylethylenediamine:  A2780: <math>IC_{50} = 10 \pm 0.5 \mu M</math>.  A2780cisR: <math>IC_{50} = 10 \pm 1 \mu M</math>.  HEK: <math>IC_{50} = 6.0 \pm 1.0 \mu M</math>.</p> <p>Linker = (1<i>R</i>,2<i>R</i>)-(+)-1,2-diphenylethylenediamine:  A2780: <math>IC_{50} = 8.5 \pm 0.5 \mu M</math>.  A2780cisR: <math>IC_{50} = 15 \pm 0.5 \mu M</math>.  HEK: <math>IC_{50} = 6.0 \pm 0.5 \mu M</math>.</p>		[60]

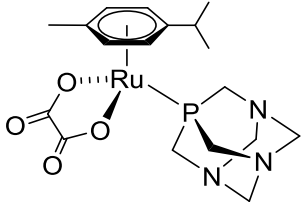
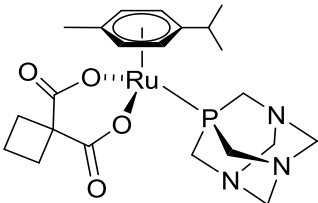
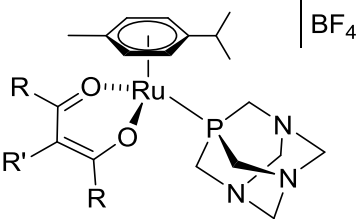
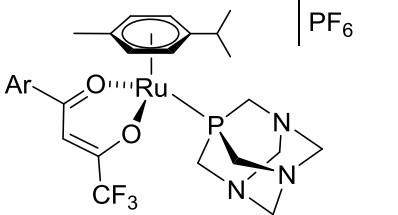
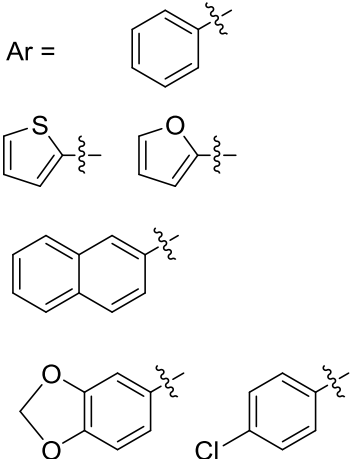
		IC <sub>50</sub> values are complex concentrations.		
(34)		<p>A2780: IC<sub>50</sub> &gt;300 μM.  A2780cisR: IC<sub>50</sub> &gt;300 μM.  HEK: IC<sub>50</sub> &gt;300 μM.</p>		[60]
(35)		<p>A2780: IC<sub>50</sub> &gt;400 μM.  A2780cisR: IC<sub>50</sub> &gt;400 μM.  HEK: IC<sub>50</sub> &gt;400 μM.</p>		[60]
(36)		<p>A2780: IC<sub>50</sub> = 12±1 μM.</p>		[61]

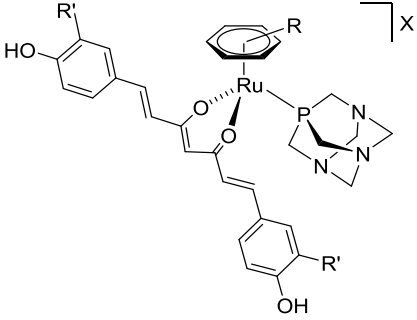
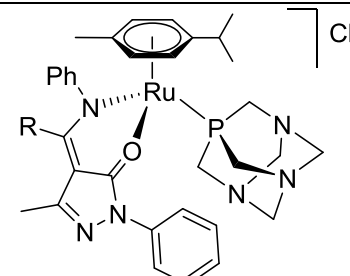
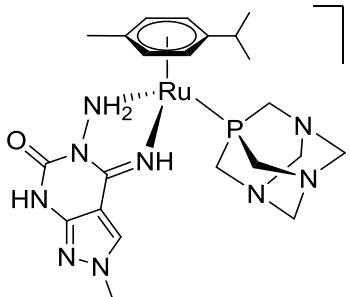
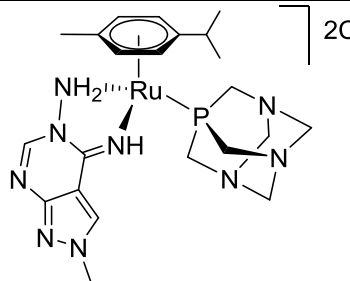
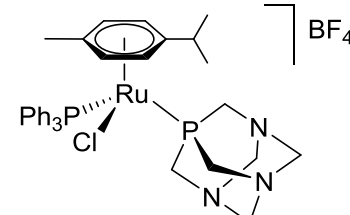
(38)	 <p>The structure shows a ruthenium (Ru) center coordinated to a chiral ferrocene-based phosphine ligand. The ferrocene backbone is substituted with a long aliphatic chain that includes a secondary amine (HN) and a carbonyl group (C=O). This chain is further linked to a complex heterocyclic moiety. This moiety consists of a central diazole ring (N=N) fused to a bicyclic system, with additional nitrogen-containing rings and a long aliphatic chain ending in another secondary amine and carbonyl group.</p>	<p>A2780: <math>IC_{50} = 2.5 \pm 0.4 \mu M</math>        (preformed sample not isolated, <math>IC_{50}</math> given is complex concentration).</p>		[61]
------	---	---	--	------

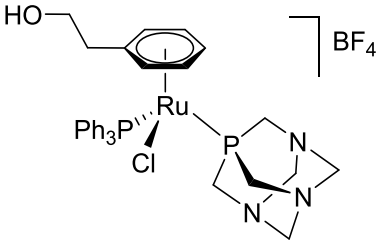
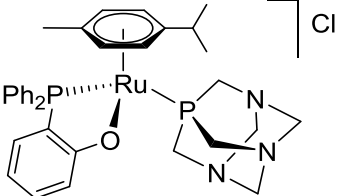
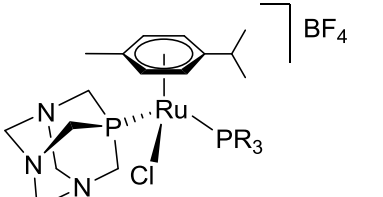
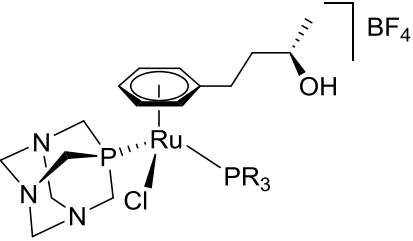
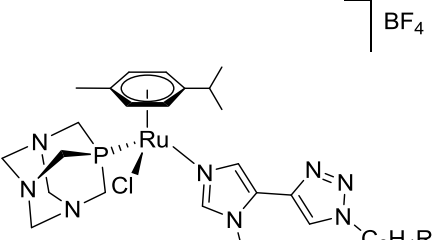


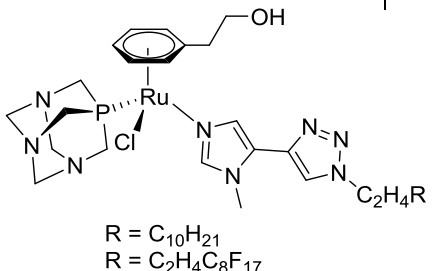
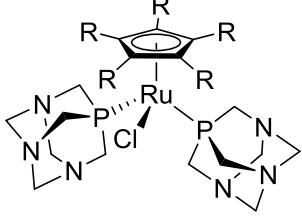
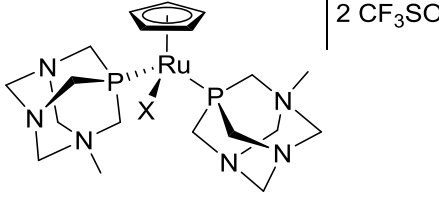
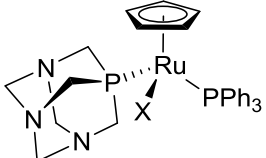
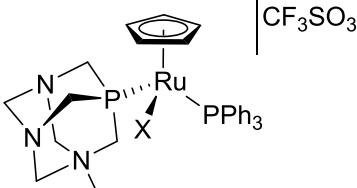
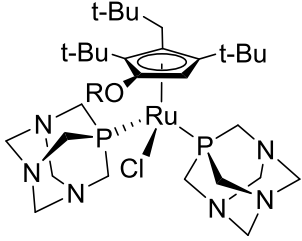
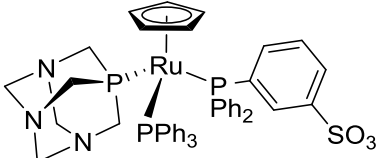
(39)		<p>A2780: <math>IC_{50} = 288 \mu M</math></p> <p>When utilised to construct a rHSA-RAPTA conjugate <math>IC_{50} = 11 \mu M</math> (rHSA concentration used, 3-4 RAPTA molecules per rHSA protein)</p>		[63]
(40)	 <p>X = Cl, oxalate</p>	<p>Utilised in labelling experiments with HEK cells.</p>		[68]
(42)		<p>(MTT assay, 96 h)</p> <p>CH1: <math>IC_{50} = 26 \pm 1 \mu M</math>.</p> <p>SW480: <math>IC_{50} = 191 \pm 49 \mu M</math>.</p> <p>A549: <math>IC_{50} &gt; 640 \mu M</math>.</p>		[69]
(43)		<p>A2780: For dendrimers with 4, 8, 16 or 32 RAPTA moieties the <math>IC_{50}</math> values when arene = <i>p</i>-cymene are <math>IC_{50} = 174 \pm 40, 9.3 \pm 0.4, 1.4 \pm 0.4, 0.8 \pm 0.1 \mu M</math> respectively.</p> <p>When arene = hexamethylbenzene <math>IC_{50} = 8.9 \pm 2.8, 6.2 \pm 0.3, 2.9 \pm 0.1, 2.0 \pm 0.1 \mu M</math> respectively.</p> <p>A2780cisR: For dendrimers with 4, 8, 16 or 32 RAPTA moieties the <math>IC_{50}</math> values when arene = <i>p</i>-cymene are <math>IC_{50} = 72.8 \pm 1.6, 19.3 \pm 0.2, 3.6 \pm 0.2, 2.7 \pm 0.1 \mu M</math> respectively.</p> <p>When arene = hexamethylbenzene <math>IC_{50} = 25 \pm 5.0, 11.8 \pm 1.1, 2.0 \pm 0.1, 1.1 \pm 0.1 \mu M</math> respectively.</p>		[71]

		(IC <sub>50</sub> concentrations are dendrimer concentrations)		
(44)		<p>When arene = <i>p</i>-cymene  A2780: IC<sub>50</sub> = &gt;200 μM  A2780cisR: IC<sub>50</sub> = 82.0±6.0 μM</p> <p>When arene = hexamethylbenzene  A2780: IC<sub>50</sub> = 38.0±3.4 μM  A2780cisR: IC<sub>50</sub> = 93.0±7.0 μM</p>		[74]
(45)		<p>Sulforhodamine B assay, 72 h.  OVCAR-3 cell line.</p> <p>P(HPMA<sub>172</sub>-IEMA<sub>44</sub>-(RAPTA-C-EMA)<sub>44</sub>) - IC<sub>50</sub> concentration &gt;IC<sub>50</sub> for RAPTA-C at equivalent Ru concentrations.</p>		[72]
(46)		<p>WST-1 assay, 72h.</p> <p>Micelles formed from PLA<sub>347</sub>-<i>b</i>-P(HEA<sub>74</sub>-(RAPTA-C-EMA)<sub>25</sub>)  A2780: IC<sub>50</sub> = 15 μM  A2780cisR: IC<sub>50</sub> = 24 μM  OVCAR-3: 46 μM</p> <p>Micelles formed from PLA<sub>347</sub>-<i>b</i>-P(HEA<sub>140</sub>-(RAPTA-C-EMA)<sub>45</sub>)  A2780: IC<sub>50</sub> = 51 μM  A2780cisR: IC<sub>50</sub> = 101 μM  OVCAR-3: 61 μM</p>		[73]
(47)	<p>RAPTA-C covalently attached to [CP-p(HEA<sub>58</sub>-co-CEMA<sub>10</sub>)<sub>2</sub>] that then self-assembled into nanotubes.</p>	<p>WST-1 assay, 72 h.  A2780: IC<sub>50</sub> = 15 μM  A2780cisR: IC<sub>50</sub> = 22 μM</p>		[74]

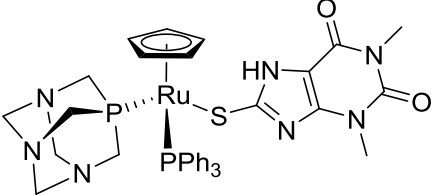
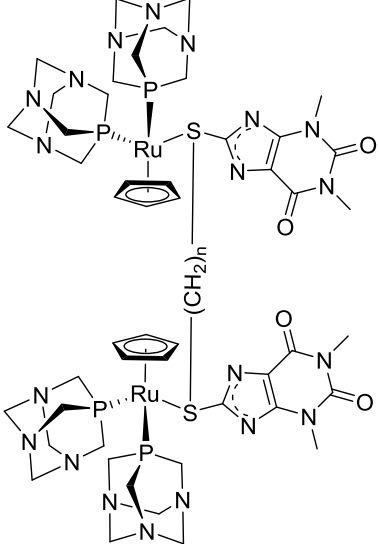
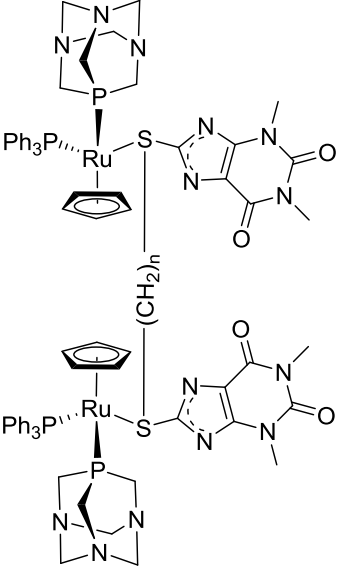
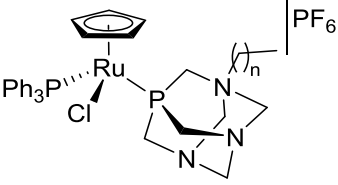
(48)		<p>HT29: IC<sub>50</sub> = 267 μM  A549: IC<sub>50</sub> = 1130 μM  T47D: IC<sub>50</sub> = 1174 μM  MCF7: IC<sub>50</sub> = &gt;1600 μM</p>	[75]
(49)		<p>HT29: IC<sub>50</sub> = 265 μM  A549: IC<sub>50</sub> = 1567 μM  T47D: IC<sub>50</sub> = 1088 μM  MCF7: IC<sub>50</sub> = &gt;1600 μM</p>	[78]
(50)	 <p>R = Me, R' = H    R = Ph, R' = H  R = tBu, R' = H    R = Me, R' = Cl</p>	<p>A549: IC<sub>50</sub> = 51-97 μM except  when R=Me, R'=H IC<sub>50</sub> = &gt;2000  μM.  A2780: IC<sub>50</sub> = 7-15 μM.</p>	[76]
(51)	 <p>Ar =</p> 	<p>CH1: IC<sub>50</sub> = 8-46 μM.  MG63: IC<sub>50</sub> = 17-41 μM.  HaCaT: IC<sub>50</sub> = &gt;100 μM except  the 4-chlorophenyl-acac  complex (72 μM).</p>	[77]

(52)	 <p>arene = <i>p</i>-cymene, R' = -OCH<sub>3</sub>, X = SO<sub>3</sub>CF<sub>3</sub><sup>-</sup>  arene = <i>p</i>-cymene, R' = -OCH<sub>3</sub>, X = PF<sub>6</sub><sup>-</sup>  arene = hmb, R' = -OCH<sub>3</sub>, X = SO<sub>3</sub>CF<sub>3</sub><sup>-</sup>  arene = <i>p</i>-cymene, R' = H, X = SO<sub>3</sub>CF<sub>3</sub><sup>-</sup>  arene = <i>p</i>-cymene, R' = H, X = PF<sub>6</sub><sup>-</sup>  arene = hmb, R' = H, X = SO<sub>3</sub>CF<sub>3</sub><sup>-</sup></p>	A2780: IC <sub>50</sub> = 0.14-1.15 μM. A2780cisR: IC <sub>50</sub> = 0.27-1.18 μM. HEK293: IC <sub>50</sub> = 4.5-30 μM		[78]
(53)		When R = Ph: A2780: IC <sub>50</sub> = 18.9±0.8 μM. A2780cisR: IC <sub>50</sub> = 19.5±0.3 μM. When R = Naph: A2780: IC <sub>50</sub> = 6.0±0.5 μM. A2780cisR: IC <sub>50</sub> = 6.1±0.5 μM.		[79]
(54)		Assessed as a RAPTA-based inhibitor of human hA1, hA2 and hA3 adenosine receptors expressed in Chinese hamster ovary (CHO) cells.		[80]
(55)		Assessed as a RAPTA-based inhibitor of human hA1, hA2 and hA3 adenosine receptors expressed in Chinese hamster ovary (CHO) cells.		[80]
(56)		TS/A: IC <sub>50</sub> = >300 μM. HBL-100: IC <sub>50</sub> = 37±3 μM.		[57]

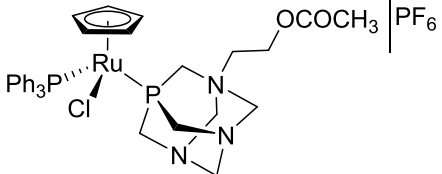
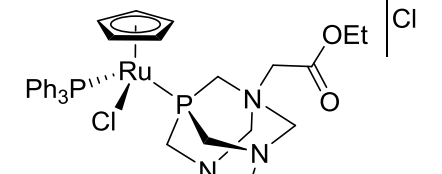
(57)		<p>TS/A: IC<sub>50</sub> = 124±13 μM. HBL-100: IC<sub>50</sub> = 82±9 μM.</p>		[57]
(58)		<p>A2780: IC<sub>50</sub> = 138 μM.</p>		[82]
(59)	 <p>PR<sub>3</sub> = PPh<sub>2</sub>(<i>p</i>-C<sub>6</sub>H<sub>4</sub>C<sub>2</sub>H<sub>4</sub>C<sub>8</sub>F<sub>17</sub>)  PR<sub>3</sub> = PPh(<i>p</i>-C<sub>6</sub>H<sub>4</sub>C<sub>2</sub>H<sub>4</sub>C<sub>8</sub>F<sub>17</sub>)<sub>2</sub>  PR<sub>3</sub> = P(<i>p</i>-C<sub>6</sub>H<sub>4</sub>C<sub>2</sub>H<sub>4</sub>C<sub>6</sub>F<sub>13</sub>)<sub>3</sub>  PR<sub>3</sub> = P(<i>p</i>-C<sub>6</sub>H<sub>4</sub>F)<sub>3</sub></p>	<p>A2780: IC<sub>50</sub> = 1.5 - 87 μM. A2780cisR: IC<sub>50</sub> = 5 - 172 μM.</p>		[83]
(60)	 <p>PR<sub>3</sub> = PPh<sub>2</sub>(<i>p</i>-C<sub>6</sub>H<sub>4</sub>C<sub>2</sub>H<sub>4</sub>C<sub>8</sub>F<sub>17</sub>)  PR<sub>3</sub> = PPh(<i>p</i>-C<sub>6</sub>H<sub>4</sub>C<sub>2</sub>H<sub>4</sub>C<sub>8</sub>F<sub>17</sub>)<sub>2</sub>  PR<sub>3</sub> = P(<i>p</i>-C<sub>6</sub>H<sub>4</sub>C<sub>2</sub>H<sub>4</sub>C<sub>6</sub>F<sub>13</sub>)<sub>3</sub>  PR<sub>3</sub> = PPh<sub>3</sub>  PR<sub>3</sub> = P(<i>p</i>-C<sub>6</sub>H<sub>4</sub>F)<sub>3</sub></p>	<p>When PR<sub>3</sub>=PPh<sub>3</sub>  A2780: IC<sub>50</sub> = 184±12 μM.  A2780cisR: IC<sub>50</sub> = &gt;200 μM.</p> <p>Otherwise:</p> <p>A2780: IC<sub>50</sub> = 6 - 97 μM.  A2780cisR: IC<sub>50</sub> = 13 - &gt;200 μM.</p>		[83]
(61)	 <p>R = C<sub>6</sub>H<sub>13</sub>  R = C<sub>8</sub>H<sub>17</sub>  R = C<sub>10</sub>H<sub>21</sub>  R = C<sub>2</sub>H<sub>4</sub>C<sub>4</sub>F<sub>9</sub>  R = C<sub>2</sub>H<sub>4</sub>C<sub>8</sub>F<sub>17</sub>  R = C<sub>2</sub>H<sub>4</sub>(OC<sub>2</sub>H<sub>4</sub>)<sub>3</sub>NH<sub>2</sub></p>	<p>A2780: IC<sub>50</sub> = 43 - &gt;300 μM.  A2780cisR: IC<sub>50</sub> = 34 - &gt;300 μM.</p>		[86]

(62)	 <p>R = C<sub>10</sub>H<sub>21</sub> R = C<sub>2</sub>H<sub>4</sub>C<sub>8</sub>F<sub>17</sub></p>	Interaction with DNA probed. Cell-based cytotoxicity assays were not reported.		[86]
(63)		When R = H: TS/A: Reported as inactive.  When R = Me: Antiproliferative effects observed starting at 10 μM (IC <sub>50</sub> not specified)		[88]
(64)		Interaction with DNA probed. Cell-based cytotoxicity assays were not reported.		[89]
(65)		Interaction with DNA probed. Cell-based cytotoxicity assays were not reported.		[89]
(66)		Interaction with DNA probed. Cell-based cytotoxicity assays were not reported.		[89]
(67)		When R = Me A2780: IC <sub>50</sub> = 5 μM. A2780cisR: IC <sub>50</sub> = 6 μM.  When R = Et A2780: IC <sub>50</sub> = 4 μM. A2780cisR: IC <sub>50</sub> = 10 μM.		[90] [90]
(68)		Interaction with DNA probed. Cell-based cytotoxicity assays were not reported.		[91]

(69)		Interaction with DNA probed. Cell-based cytotoxicity assays were not reported.	[91]
(70)		Interaction with DNA probed. Cell-based cytotoxicity assays were not reported.	[91]
(71)		Interaction with DNA probed. Cell-based cytotoxicity assays were not reported.	[91]
(72)		Interaction with DNA probed. Cell-based cytotoxicity assays were not reported.	[91]
(73)		T2: $IC_{50} = >50 \mu M$ . SKOV3: $IC_{50} = >50 \mu M$ .	[92]
(74)		When R = Me T2: $IC_{50} = >50 \mu M$ . SKOV3: $IC_{50} = >50 \mu M$ . When R = $CH_2Ph$ T2: $IC_{50} = >50 \mu M$ . SKOV3: $IC_{50} = >50 \mu M$ .	[92]
(75)		When R = Me T2: $IC_{50} = \sim 50 \mu M$ . SKOV3: $IC_{50} = >50 \mu M$ . When R = $CH_2Ph$ T2: $IC_{50} = 2-10 \mu M$ . SKOV3: $IC_{50} = >50 \mu M$ .	[92]

(76)		<p>T2: IC<sub>50</sub> = ~50 μM. SKOV3: IC<sub>50</sub> = &gt;50 μM.</p>		[92]
(77)		<p>Poor activity reported – no IC<sub>50</sub> given.</p>		[92]
(78)		<p>Poor activity reported – no IC<sub>50</sub> given.</p>		[92]
(79)		<p>When n = 12 SKOV3: IC<sub>50</sub> = 9.1±0.2 μM. SW480: IC<sub>50</sub> = 9.7±0.15 μM.</p> <p>When n = 16 SKOV3: IC<sub>50</sub> = 9.6±0.2 μM. SW480: IC<sub>50</sub> = 9.7±0.1 μM.</p> <p>When n = 18 SKOV3: IC<sub>50</sub> = 9.5±1.2 μM. SW480: IC<sub>50</sub> = 9.1±1.3 μM.</p>		[93]



(80)		SKOV3: IC <sub>50</sub> = 6.0±0.5 μM. A2780: IC <sub>50</sub> = 4.7±1 μM. K562: IC <sub>50</sub> = 5.1±0.3 μM.		[94]
(81)		SKOV3: IC <sub>50</sub> = 8.3±0.8 μM. A2780: IC <sub>50</sub> = 5.8±0.5 μM. K562: IC <sub>50</sub> = 5.5±0.2 μM.		[94]

## 7. Acknowledgements

Over the years many organizations, foundations and companies have supported our research, and many excellent co-workers and collaborators have contributed to this exciting area of research, we thank them all. Their names are found in the references and the acknowledgements of the original articles.

## 8. References

- [1] A.S. Abu-Surrah, M. Kettunen, *Curr. Med. Chem.*, 13 (2006) 1337-1357.
- [2] C.A. Rabik, M.E. Dolan, *Cancer Treat. Rev.*, 33 (2007) 9-23.
- [3] T. Boulikas, G.P. Stathopoulos, N. Volakakis, M. Vougiouka, *Anticancer Res.*, 25 (2005) 3031-3039.
- [4] G.P. Stathopoulos, J. Stathopoulos, J. Dimitroulis, *Oncol. Lett.*, 4 (2012) 1013-1016.
- [5] M. Callari, J.R. Aldrich-Wright, P.L. de Souza, M.H. Stenzel, *Prog. Polym. Sci.*, 39 (2014) 1614-1643.
- [6] X. Wang, Z. Guo, *Chem. Soc. Rev.*, 42 (2013) 202-224.
- [7] I. Ott, R. Gust, *Arch. Pharm.*, 340 (2007) 117-126.
- [8] N. Muhammad, Z. Guo, *Curr. Opin. Chem. Biol.*, 19 (2014) 144-153.
- [9] A. Bergamo, G. Sava, *Dalton Trans.*, (2007) 1267-1272.
- [10] J.M. Rademaker-Lakhai, D. Van Den Bongard, D. Pluim, J.H. Beijnen, J.H.M. Schellens, *Clin. Cancer Res.*, 10 (2004) 3717-3727.
- [11] S. Leijen, S. Burgers, P. Baas, D. Pluim, M. Tibben, E. van Werkhoven, E. Alessio, G. Sava, J. Beijnen, J.M. Schellens, *Invest. New Drugs*, 33 (2015) 201-214.

- [12] C.G. Hartinger, S. Zorbas-Seifried, M.A. Jakupec, B. Kynast, H. Zorbas, B.K. Keppler, *J. Inorg. Biochem.*, 100 (2006) 891-904.
- [13] R. Trondl, P. Heffeter, C.R. Kowol, M.A. Jakupec, W. Berger, B.K. Keppler, *Chem. Sci.*, 5 (2014) 2925-2932.
- [14] M. Pongratz, P. Schluga, M.A. Jakupec, V.B. Arion, C.G. Hartinger, G. Allmaier, B.K. Keppler, *J. Anal. At. Spectrom.*, 19 (2004) 46-51.
- [15] C.G. Hartinger, M.A. Jakupec, S. Zorbas-Seifried, M. Groessl, A. Egger, W. Berger, H. Zorbas, P.J. Dyson, B.K. Keppler, *Chem. Biodiversity*, 5 (2008) 2140-2155.
- [16] A. Habtemariam, M. Melchart, R. Fernandez, S. Parsons, I.D.H. Oswald, A. Parkin, F.P.A. Fabbiani, J.E. Davidson, A. Dawson, R.E. Aird, D.I. Jodrell, P.J. Sadler, *J. Med. Chem.*, 49 (2006) 6858-6868.
- [17] R.E. Morris, R.E. Aird, P.d.S. Murdoch, H. Chen, J. Cummings, N.D. Hughes, S. Parsons, A. Parkin, G. Boyd, D.I. Jodrell, P.J. Sadler, *J. Med. Chem.*, 44 (2001) 3616-3621.
- [18] A. Bergamo, A. Masi, A.F.A. Peacock, A. Habtemariam, P.J. Sadler, G. Sava, *J. Inorg. Biochem.*, 104 (2010) 79-86.
- [19] C.G. Hartinger, P.J. Dyson, *Chem. Soc. Rev.*, 38 (2009) 391-401.
- [20] G.S. Smith, B. Therrien, *Dalton Trans.*, 40 (2011) 10793-10800.
- [21] C.G. Hartinger, N. Metzler-Nolte, P.J. Dyson, *Organometallics*, 31 (2012) 5677-5685.
- [22] A.K. Singh, D.S. Pandey, Q. Xu, P. Braunstein, *Coord. Chem. Rev.*, 270-271 (2014) 31-56.
- [23] G. Süss-Fink, *J. Organomet. Chem.*, 751 (2014) 2-19.
- [24] A.A. Nazarov, C.G. Hartinger, P.J. Dyson, *J. Organomet. Chem.*, 751 (2014) 251-260.
- [25] A. Levina, A. Mitra, P.A. Lay, *Metallomics*, 1 (2009) 458-470.
- [26] C.G. Hartinger, A.D. Phillips, A.A. Nazarov, *Curr. Top. Med. Chem.*, 11 (2011) 2688-2702.
- [27] G. Gasser, I. Ott, N. Metzler-Nolte, *J. Med. Chem.*, 54 (2011) 3-25.
- [28] A.K. Singh, D.S. Pandey, Q. Xu, P. Braunstein, *Coord. Chem. Rev.*, 270-271 (2014) 31-56.
- [29] C.S. Allardyce, P.J. Dyson, D.J. Ellis, S.L. Heath, *Chem. Commun.*, (2001) 1396-1397.

- [30] C. Scolaro, A. Bergamo, L. Brescacin, R. Delfino, M. Cocchietto, G. Laurency, T.J. Geldbach, G. Sava, P.J. Dyson, *J. Med. Chem.*, 48 (2005) 4161-4171.
- [31] A.D. Phillips, L. Gonsalvi, A. Romerosa, F. Vizza, M. Peruzzini, *Coord. Chem. Rev.*, 248 (2004) 955-993.
- [32] C.S. Allardyce, P.J. Dyson, D.J. Ellis, P.A. Salter, R. Scopelliti, *J. Organomet. Chem.*, 668 (2003) 35-42.
- [33] A. Dorcier, W.H. Ang, S. Bolano, L. Gonsalvi, L. Juillerat-Jeannerat, G. Laurency, M. Peruzzini, A.D. Phillips, F. Zanobini, P.J. Dyson, *Organometallics*, 25 (2006) 4090-4096.
- [34] C. Scolaro, C.G. Hartinger, C.S. Allardyce, B.K. Keppler, P.J. Dyson, *J. Inorg. Biochem.*, 102 (2008) 1743-1748.
- [35] C. Gossens, A. Dorcier, P.J. Dyson, U. Rothlisberger, *Organometallics*, 26 (2007) 3969-3975.
- [36] A. Bergamo, A. Masi, P.J. Dyson, G. Sava, *Int. J. Oncol.*, 33 (2008) 1281-1289.
- [37] A. Weiss, R.H. Berndsen, M. Dubois, C. Muller, R. Schibli, A.W. Griffioen, P.J. Dyson, P. Nowak-Sliwinska, *Chem. Sci.*, 5 (2014) 4742-4748.
- [38] P. Nowak-Sliwinska, B.J.R. van, A. Casini, A.A. Nazarov, G. Wagnieres, d.B.H. van, P.J. Dyson, A.W. Griffioen, *J. Med. Chem.*, 54 (2011) 3895-3902.
- [39] A. Weiss, X. Ding, J.R. van Beijnum, L. Wong, T.J. Wong, R.H. Berndsen, O. Dormond, M. Dallinga, L. Shen, R.O. Schlingemann, R. Pili, C.-M. Ho, P.J. Dyson, H. van den Bergh, A.W. Griffioen, P. Nowak-Sliwinska, *Angiogenesis*, 18 (2015) 233-244.
- [40] J. Marshall, *Cancer*, 107 (2006) 1207-1218.
- [41] K. Garber, *J. Natl. Cancer Inst.*, 101 (2009) 288-290.
- [42] A. Weiss, D. Bonvin, R.H. Berndsen, E. Scherrer, T.J. Wong, P.J. Dyson, A.W. Griffioen, P. Nowak-Sliwinska, *Sci. Rep.*, 5 (2015).
- [43] O. Tacar, P. Sriamornsak, C.R. Dass, *J. Pharm. Pharmacol.*, 65 (2013) 157-170.
- [44] C. Scolaro, T.J. Geldbach, S. Rochat, A. Dorcier, C. Gossens, A. Bergamo, M. Cocchietto, I. Tavernelli, G. Sava, U. Rothlisberger, P.J. Dyson, *Organometallics*, 25 (2006) 756-765.
- [45] A.K. Renfrew, A.D. Phillips, A.E. Egger, C.G. Hartinger, S.S. Bosquain, A.A. Nazarov, B.K. Keppler, L. Gonsalvi, M. Peruzzini, P.J. Dyson, *Organometallics*, 28 (2009) 1165-1172.
- [46] A.K. Renfrew, A.D. Phillips, E. Tapavicza, R. Scopelliti, U. Rothlisberger, P.J. Dyson, *Organometallics*, 28 (2009) 5061-5071.

- [47] A.E. Egger, C.G. Hartinger, A.K. Renfrew, P.J. Dyson, *J. Biol. Inorg. Chem.*, 15 (2010) 919-927.
- [48] B. Serli, E. Zangrando, T. Gianferrara, C. Scolaro, P.J. Dyson, A. Bergamo, E. Alessio, *Eur. J. Inorg. Chem.*, (2005) 3423-3434.
- [49] W.H. Ang, L.J. Parker, L.A. De, L. Juillerat-Jeanneret, C.J. Morton, B.M. Lo, M.W. Parker, P.J. Dyson, *Angew. Chem., Int. Ed. Engl.*, 48 (2009) 3854-3857.
- [50] S. Chatterjee, I. Biondi, P.J. Dyson, A. Bhattacharyya, *J. Biol. Inorg. Chem.*, 16 (2011) 715-724.
- [51] K. Chakree, C. Ovatlarnporn, P.J. Dyson, A. Ratanaphan, *Int. J. Mol. Sci.*, 13 (2012) 13183-13202.
- [52] A.A. Nazarov, J. Risse, W.H. Ang, F. Schmitt, O. Zava, A. Ruggi, M. Groessl, R. Scopelitti, L. Juillerat-Jeanneret, C.G. Hartinger, P.J. Dyson, *Inorg. Chem.*, 51 (2012) 3633-3639.
- [53] M.A. Furrer, F. Schmitt, M. Wiederkehr, L. Juillerat-Jeanneret, B. Therrien, *Dalton Trans.*, 41 (2012) 7201-7211.
- [54] K.J. Kilpin, C.M. Clavel, F. Edefe, P.J. Dyson, *Organometallics*, 31 (2012) 7031-7039.
- [55] A. Wolfe, G.H. Shimer Jr., T. Meehan, *Biochemistry*, 26 (1987) 6392-6396.
- [56] C. Bailly, M. Braña, M.J. Waring, *Eur. J. Biochem.*, 240 (1996) 195-208.
- [57] C. Scolaro, A.B. Chaplin, C.G. Hartinger, A. Bergamo, M. Cocchietto, B.K. Keppler, G. Sava, P.J. Dyson, *Dalton Trans.*, (2007) 5065-5072.
- [58] A.A. Nazarov, S.M. Meier, O. Zava, Y.N. Nosova, E.R. Milaeva, C.G. Hartinger, P.J. Dyson, *Dalton Trans.*, 44 (2014) 3614-3623.
- [59] K.J. Kilpin, S.M. Cammack, C.M. Clavel, P.J. Dyson, *Dalton Trans.*, 42 (2013) 2008-2014.
- [60] B.S. Murray, L. Menin, R. Scopelliti, P.J. Dyson, *Chem. Sci.*, 5 (2014) 2536-2545.
- [61] B.S. Murray, S. Crot, S. Siankevich, P.J. Dyson, *Inorg. Chem.*, 53 (2014) 9315-9321.
- [62] K. Lang, L. Davis, S. Wallace, M. Mahesh, D.J. Cox, M.L. Blackman, J.M. Fox, J.W. Chin, *J. Am. Chem. Soc.*, 134 (2012) 10317-10320.
- [63] W.H. Ang, E. Daldini, L. Juillerat-Jeanneret, P.J. Dyson, *Inorg. Chem.*, 46 (2007) 9048-9050.
- [64] H. Maeda, J. Wu, T. Sawa, Y. Matsumura, K. Hori, *J. Controlled Release*, 65 (2000) 271-284.

- [65] F. Kratz, U. Beyer, T. Roth, M.T. Schütte, A. Unold, H.H. Fiebig, C. Unger, *Archiv der Pharmazie*, 331 (1998) 47-53.
- [66] F. Dosio, P. Brusa, P. Crosasso, S. Arpicco, L. Cattel, *J. Controlled Release*, 47 (1997) 293-304.
- [67] M. Chaves-Ferreira, I.S. Albuquerque, D. Matak-Vinkovic, A.C. Coelho, S.M. Carvalho, L.M. Saraiva, C.C. Romão, G.J.L. Bernardes, *Angew. Chem., Int. Ed. Engl.*, 54 (2015) 1172-1175.
- [68] Y.Q. Tan, P.J. Dyson, W.H. Ang, *Organometallics*, 30 (2011) 5965-5971.
- [69] M. Hanif, A.A. Nazarov, A. Legin, M. Groessl, V.B. Arion, M.A. Jakupec, Y.O. Tsybin, P.J. Dyson, B.K. Keppler, C.G. Hartinger, *Chem. Commun.*, 48 (2012) 1475-1477.
- [70] H. Kobayashi, R. Watanabe, P.L. Choyke, *Theranostics*, 4 (2014) 81-89.
- [71] P. Govender, L.C. Sudding, C.M. Clavel, P.J. Dyson, B. Therrien, G.S. Smith, *Dalton Trans.*, 42 (2013) 1267-1277.
- [72] B.M. Blunden, D.S. Thomas, M.H. Stenzel, *Polym. Chem.*, 3 (2012) 2964-2975.
- [73] B.M. Blunden, H. Lu, M.H. Stenzel, *Biomacromolecules*, 14 (2013) 4177-4188.
- [74] B.M. Blunden, R. Chapman, M. Danial, H. Lu, K.A. Jolliffe, S. Perrier, M.H. Stenzel, *Chem. Eur. J.*, 20 (2014) 12745-12749.
- [75] W.H. Ang, E. Daldini, C. Scolaro, R. Scopelliti, L. Juillerat-Jeannerat, P.J. Dyson, *Inorg. Chem.*, 45 (2006) 9006-9013.
- [76] C.A. Vock, A.K. Renfrew, R. Scopelliti, L. Juillerat-Jeanneret, P.J. Dyson, *Eur. J. Inorg. Chem.*, (2008) 1661-1671.
- [77] S. Seršen, J. Kljun, K. Kryeziu, R. Panchuk, B. Alte, W. Körner, P. Heffeter, W. Berger, I. Turel, *J. Med. Chem.*, 58 (2015) 3984-3996.
- [78] R. Pettinari, F. Marchetti, F. Condello, C. Pettinari, G. Lupidi, R. Scopelliti, S. Mukhopadhyay, T. Riedel, P.J. Dyson, *Organometallics*, 33 (2014) 3709-3715.
- [79] R. Pettinari, C. Pettinari, F. Marchetti, C.M. Clavel, R. Scopelliti, P.J. Dyson, *Organometallics*, 32 (2013) 309-316.
- [80] P. Paira, M.J. Chow, G. Venkatesan, V.K. Kosaraju, S.L. Cheong, K.-N. Klotz, W.H. Ang, G. Pastorin, *Chem. Eur. J.*, 19 (2013) 8321-8330.
- [81] Z. Adhireksan, G.E. Davey, P. Campomanes, M. Groessl, C.M. Clavel, U. Rothlisberger, P.J. Dyson, H. Yu, P. Droge, A.A. Nazarov, C.H.F. Yeo, W.H. Ang, C.A. Davey, *Nat. Commun.*, 5 (2014) 3462.

- [82] A.K. Renfrew, A.E. Egger, R. Scopelliti, C.G. Hartinger, P.J. Dyson, C. R. Chim., 13 (2010) 1144-1150.
- [83] A.K. Renfrew, R. Scopelliti, P.J. Dyson, Inorg. Chem., 49 (2010) 2239-2246.
- [84] R.D. Issels, Eur. J. Cancer, 44 (2008) 2546-2554.
- [85] T. Soos, B.L. Bennett, D. Rutherford, L.P. Barthel-Rosa, J.A. Gladysz, Organometallics, 20 (2001) 3079-3086.
- [86] A.K. Renfrew, L. Juillerat-Jeanneret, P.J. Dyson, J. Organomet. Chem., 696 (2011) 772-779.
- [87] C.M. Clavel, E. Paunescu, P. Nowak-Sliwinska, P.J. Dyson, Chem. Sci., 5 (2014) 1097-1101.
- [88] D.N. Akbayeva, L. Gonsalvi, W. Oberhauser, M. Peruzzini, F. Vizza, P. Brueggeller, A. Romerosa, G. Sava, A. Bergamo, Chem. Commun., (2003) 264-265.
- [89] A. Romerosa, T. Campos-Malpartida, C. Lidrissi, M. Saoud, M. Serrano-Ruiz, M. Peruzzini, J.A. Garrido-Cardenas, F. Garcia-Maroto, Inorg. Chem., 45 (2006) 1289-1298.
- [90] B. Dutta, C. Scolaro, R. Scopelliti, P.J. Dyson, K. Severin, Organometallics, 27 (2008) 1355-1357.
- [91] A. Romerosa, M. Saoud, T. Campos-Malpartida, C. Lidrissi, M. Serrano-Ruiz, M. Peruzzini, J.A. Garrido, F. Garcia-Maroto, Eur. J. Inorg. Chem., (2007) 2803-2812.
- [92] L. Hajji, C. Saraiba-Bello, A. Romerosa, G. Segovia-Torrente, M. Serrano-Ruiz, P. Bergamini, A. Cannella, Inorg. Chem., 50 (2011) 873-882.
- [93] P. Bergamini, L. Marvelli, A. Marchi, F. Vassanelli, M. Fogagnolo, P. Formaglio, T. Bernardi, R. Gavioli, F. Sforza, Inorg. Chim. Acta, 391 (2012) 162-170.
- [94] V. Ferretti, M. Fogagnolo, A. Marchi, L. Marvelli, F. Sforza, P. Bergamini, Inorg. Chem., 53 (2014) 4881-4890.
- [95] J. Ghuman, P.A. Zunszain, I. Petitpas, A.A. Bhattacharya, M. Otagiri, S. Curry, J. Mol. Biol., 353 (2005) 38-52.
- [96] M.C.M. Chung, Biochem. Educ., 12 (1984) 146-154.
- [97] M. Groessl, M. Terenghi, A. Casini, L. Elviri, R. Lobinski, P.J. Dyson, J. Anal. At. Spectrom., 25 (2010) 305-313.
- [98] D.A. Wolters, M. Stefanopoulou, P.J. Dyson, M. Groessl, Metallomics, 4 (2012) 1185-1196.
- [99] A. Dorcier, P.J. Dyson, C. Gossens, U. Rothlisberger, R. Scopelliti, I. Tavernelli, Organometallics, 24 (2005) 2114-2123.

- [100] M. Groessl, C.G. Hartinger, P.J. Dyson, B.K. Keppler, J. Inorg. Biochem., 102 (2008) 1060-1065.
- [101] A. Dorcier, C.G. Hartinger, R. Scopelliti, R.H. Fish, B.K. Keppler, P.J. Dyson, J. Inorg. Biochem., 102 (2008) 1066-1076.
- [102] M. Groessl, Y.O. Tsybin, C.G. Hartinger, B.K. Keppler, P.J. Dyson, J. Biol. Inorg. Chem., 15 (2010) 677-688.
- [103] C. Gossens, I. Tavernelli, U. Rothlisberger, J. Am. Chem. Soc., 130 (2008) 10921-10928.
- [104] A. Ratanaphan, P. Temboot, P.J. Dyson, Chem. Biodiversity, 7 (2010) 1290-1302.
- [105] A. Astarina, M.J. Chow, W.H. Ang, Aust. J. Chem., 65 (2012) 1271-1276.
- [106] C.G. Hartinger, A. Casini, C. Duhot, Y.O. Tsybin, L. Messori, P.J. Dyson, J. Inorg. Biochem., 102 (2008) 2136-2141.
- [107] A. Casini, G. Mastrobuoni, W.H. Ang, C. Gabbiani, G. Pieraccini, G. Moneti, P.J. Dyson, L. Messori, ChemMedChem, 2 (2007) 631-635.
- [108] A. Casini, C. Gabbiani, E. Michelucci, G. Pieraccini, G. Moneti, P.J. Dyson, L. Messori, J. Biol. Inorg. Chem., 14 (2009) 761-770.
- [109] F. Mendes, M. Groessl, A.A. Nazarov, Y.O. Tsybin, G. Sava, I. Santos, P.J. Dyson, A. Casini, J. Med. Chem., 54 (2011) 2196-2206.
- [110] A. Casini, A. Karotki, C. Gabbiani, F. Rugi, M. Vasak, L. Messori, P.J. Dyson, Metallomics, 1 (2009) 434-441.
- [111] C.G. Hartinger, M. Groessl, S.M. Meier, A. Casini, P.J. Dyson, Chem. Soc. Rev., 42 (2013) 6186-6199.
- [112] W.H. Ang, E. Daldini, C. Scolaro, R. Scopelliti, L. Juillerat-Jeannerat, P.J. Dyson, Inorg. Chem., 45 (2006) 9006-9013.
- [113] A. Casini, C. Gabbiani, G. Mastrobuoni, L. Messori, G. Moneti, G. Pieraccini, ChemMedChem, 1 (2006) 413-417.
- [114] A.T. Miles, G.M. Hawksworth, J.H. Beattie, V. Rodilla, Crit. Rev. Biochem. Mol. Biol., 35 (2000) 35-70.
- [115] M. Knipp, Curr. Med. Chem., 16 (2009) 522-537.
- [116] M. Knipp, A.V. Karotki, S. Chesnov, G. Natile, P.J. Sadler, V. Brabec, M. Vasak, J. Med. Chem., 50 (2007) 4075-4086.

- [117] A. Casini, C. Gabbiani, F. Sorrentino, M.P. Rigobello, A. Bindoli, T.J. Geldbach, A. Marrone, N. Re, C.G. Hartinger, P.J. Dyson, L. Messori, *J. Med. Chem.*, 51 (2008) 6773-6781.
- [118] S. Gromer, S. Urig, K. Becker, *Med. Res. Rev.*, 24 (2004) 40-89.
- [119] A. Casini, F. Edafe, M. Erlandsson, L. Gonsalvi, A. Ciancetta, N. Re, A. Ienco, L. Messori, M. Peruzzini, P.J. Dyson, *Dalton Trans.*, 39 (2010) 5556-5563.
- [120] B. Wu, M.S. Ong, M. Groessl, Z. Adhireksan, C.G. Hartinger, P.J. Dyson, C.A. Davey, *Chem. Eur. J.*, 17 (2011) 3562-3566.
- [121] B. Wu, C.A. Davey, *Chem. Biol.*, 15 (2008) 1023-1028.
- [122] M.V. Babak, S.M. Meier, K. Huber, J. Reynisson, A.A. Legin, M.A. Jakupec, A. Roller, A. Stukalov, M. Gridling, K.L. Bennett, J. Colinge, W. Berger, P.J. Dyson, G. Superti-Furga, B.K. Keppler, C.G. Hartinger, *Chem. Sci.*, 6 (2015) 2449-2456.
- [123] F. Guidi, A. Modesti, I. Landini, S. Nobili, E. Mini, L. Bini, M. Puglia, A. Casini, P.J. Dyson, C. Gabbiani, L. Messori, *J. Inorg. Biochem.*, 118 (2013) 94-99.
- [124] S. Chatterjee, S. Kundu, A. Bhattacharyya, C.G. Hartinger, P.J. Dyson, *J. Biol. Inorg. Chem.*, 13 (2008) 1149-1155.
- [125] D. Li, R.J. Mrsny, *J. Cell. Biol.*, 148 (2000) 791-800.
- [126] A.P. Soler, R.D. Miller, K.V. Laughlin, N.Z. Carp, D.M. Klurfeld, J.M. Mullin, *Carcinogenesis*, 20 (1999) 1425-1432.
- [127] S.J. Dougan, P.J. Sadler, *Chimia*, 61 (2007) 704-715.
- [128] M.R. Gill, J.A. Thomas, *Chem. Soc. Rev.*, 41 (2012) 3179-3192.



# TOC

